Charles University
Second Faculty of Medicine

Doctoral study programme: Biochemistry and Pathobiochemistry

M.Sc. Oleh Durydivka

Selective regulation of presynaptic receptors by SGIP1

Dissertation Thesis

Supervisor: doc. MUDr. Jaroslav Blahoš, Ph.D.

Prague, 2023

Declaration

I declare hereby that I made this dissertation thesis by myself and that I mentioned and cited properly all the sources and literature. At the same time, I declare that this thesis was not used to obtain another or the same title.

I agree with permanent deposition of an electronic version of my thesis in the system database of interuniversity project Thesis.cz for a permanent control of similarities of theses.

In Prague on 16.10.2023

Oleh Durydivka

…….

Acknowledgements

I would like to express my gratitude to my supervisor, Dr. Jaroslav Blahoš, for making it possible to pursue doctoral studies to work on the project on cannabinoid receptor 1 and for guidance during the project and to my internship supervisor, Dr. Michel Bouvier, for the opportunity to join one of the leading laboratories on GPCR signaling at the Institute for Research in Immunology and Cancer, Université de Montréal, where I learnt approaches in biosensor design and drug testing. I would also like to thank my colleagues Matej Gazdarica, Irina Cheveleva, Michaela Dvořáková, Judith Noda-Mayor, Lucie Pejšková, Pedro H. Scarpelli Pereira, Supriya Gaitonde, Sajjad Ahrari, Charlotte Avet, Monique Lagacé for their support and willingness to help during my doctoral studies.

This work has been supported by the grants of the Czech Science Foundation (GACR) 19-24172S and GACR 21-02371S and by the project of the Ministry of Education, Youth and Sports of the Czech Republic entitled "International mobility of IMG researchers II, No. CZ.02.2.69/0.0/0.0/18_053/0016981 Support of Professional Development". We acknowledge the Light Microscopy Core Facility, IMG, Prague, Czech Republic, supported by MEYS – LM2023050 and RVO – 68378050-KAV-NPUI, for their support with the confocal imaging presented herein. The authors used services of the Czech Centre for Phenogenomics at the Institute of Molecular Genetics supported by the Czech Academy of Sciences RVO 68378050, by the project LM2023036 Czech Centre for Phenogenomics provided by the Ministry of Education, Youth and Sports of the Czech Republic, and by CZ.02.1.01/0.0/0.0/18_046/0015861 CCP Infrastructure Upgrade II by MEYS and ESIF.

Selective regulation of presynaptic receptors by SGIP1

Abstract

Cannabinoid receptor 1 (CB1R) is involved in a plethora of physiological processes, such as memory formation, motor coordination, anxiety, pain perception, and immune response. The properties of many minor cannabinoid receptor ligands remain unknown. The activity of CB1R is regulated by Src homology 3-domain growth factor receptor-bound 2-like endophilin interacting protein 1 (SGIP1). Several splice variants of SGIP1 have been described in the literature, but their specific functional roles are unknown. SGIP1 inhibits CB1R internalization and enhances β-arrestin and G protein-coupled receptor kinase 3 (GRK3) interactions with the receptor. In mice, deletion of *Sgip1* results in altered mood-related behavior, decreased anxiety-like behavior, and decreased acute nociception. In this work, we tested the effect of *Sgip1* deletion on chronic nociception. We further explored the pattern of alternative splicing of *Sgip1* in the brain. In addition, we tested the effect of the minor cannabinoid hexahydrocannabinol (HHC) on CB1R signaling. We found that *Sgip1* deletion results in an increase in chronic nociception in male but not in female mice. We detected 15 *Sgip1* splice variants in the mouse brain. The *Sgip1* exons that undergo alternative splicing encode portions of the MP domain and proline-rich region of the Sgip1 protein. We found that the pharmacological activity of (9R)-HHC epimer is higher than that of (9S)-HHC epimer, and the activity of (9R)-HHC epimer is similar to that of Δ^9-tetrahydrocannabinol (THC). These results demonstrate that SGIP1 is an important player in pain sensitivity and other functions controlled by CB1R, that multiple *Sgip1* splice variants are expressed in the brain, and that cannabinoid HHC has similar properties to the common cannabinoid THC.

Keywords

alternative splicing, cannabinoid receptor 1, endocytosis, hexahydrocannabinol, nociception

LIST OF ABBREVIATIONS

(9R)-HHC	(9R)-hexahydrocannabinol
(9S)-HHC	(9S)-hexahydrocannabinol
µHD	µ homology domain
2-AG	2-arachidonoylglycerol
aa	amino acid
AEA	N-arachidonoylethanolamine
AMPA	α-amino-3-hydroxyl-5-methyl-4-isoxazole-propionate
ANOVA	analysis of variance
AP-2	adaptor protein 2
AP-3	adaptor protein 3
APA	AP2 activator
ART	aligned rank transformation
BAR	Bin/amphiphysin/Rvs
BARR2	β-arrestin 2
BCA	bicinchoninic acid
bp	base pair
BRET	bioluminescence resonance energy transfer
BSA	bovine serum albumin
cAMP	cyclic adenosine monophosphate
CB	cerebellum
CB1R	cannabinoid receptor 1
CB2R	cannabinoid receptor 2
CBD	cannabidiol
cDNA	complementary DNA
CHAPS	(3-[(3-cholamidopropyl) dimethylammonio]-1- propanesulfonate)
CRIP1a	cannabinoid receptor-interacting protein 1a
DAG	diacylglycerol
DAGL	diacylglycerol lipase
DAPI	4',6-diamidin-2-fenylindol
DMEM	Dulbecco's Modified Eagle's Medium
DMSO	dimethyl sulfoxide

DSE	depolarization-induced suppression of excitation
DSI	depolarization-induced suppression of inhibition
DTT	dithiothreitol
ebBRET	enhanced bystander BRET
EC50	half maximal effective concentration
EMCDDA	European Monitoring Centre for Drugs and Drug Addiction
Eps15	epidermal growth factor receptor pathway substrate 15
ERK1/2	extracellular signal-regulated kinase 1/2
EWS	European Union Early Warning System
Ex	exon
EYFP	enhanced yellow fluorescent protein
FAAH	fatty acid amino hydrolase
F-BAR	FER-CIP4 homology-BAR
FBS	fetal bovine serum
FCH	FER and CIP4 homology
FCHO1/2	FER and CIP4 homology domain only proteins 1 and 2
GABA	gamma-aminobutyric acid
GASP1	G protein-associated sorting protein 1
GPCR	G protein-coupled receptors
GRK	G protein-coupled receptor kinase
HC	hippocampus
HEK293	human embryonic kidney 293
HHC	hexahydrocannabinol
HRP	horseradish peroxidase
HyD	hybrid detector
IP	immunoprecipitation
IP_3	inositol 1,4,5-trisphosphate
IPTG	Isopropyl β-d-1-thiogalactopyranoside
JNK1/2/3	c-Jun N-terminal kinase 1/2/3
kDa	kilodalton
K_{ir}	inwardly-rectifying potassium channels
KO	knock-out

LB	Luria-Bertani
MGL	monoacylglycerol lipase
mGluR	metabotropic glutamate receptors
MOR	μ-opioid receptor
MP	membrane phospholipid-binding
MS	mass spectrometry
NAPE-PLD	N-acetylphosphatidylethanolamine-hydrolysing phospholipase D
NMDA	*N*-methyl-d-aspartate
p38 MAPK	p38 mitogen-activated protein kinase
p42/p44 MAPK	p42/p44 mitogen-activated protein kinase
PBS	phosphate-buffered saline
PCR	polymerase chain reaction
PEI	polyethylenimine
PFA	paraformaldehyde
PFC	prefrontal cortex
PIP_2	phosphatidylinositol 4,5-bisphosphate
PKA	protein kinase A
PLCβ	phospholipase C β
PR	proline-rich region
RIPA	radioimmunoprecipitation assay
Rluc	Renilla luciferase
RT-PCR	reverse transcription polymerase chain reaction
SAP	shrimp alkaline phosphatase
SDC	sodium deoxycholate
SDS	sodium dodecyl sulfate
SDS-PAGE	SDS-polyacrylamide gel
SEM	standard error of the mean
SGIP1	Src homology 3-domain growth factor receptor-bound 2-like endophilin interacting protein 1
SH3	SRC homology 3
SV	splice variant
Syp1	suppressor of yeast profilin deletion 1

TCEP	tris(2-carboxyethyl)phosphine
TEAB	triethylamonium bicarbonate
TFA	trifluoroacetic acid
THC	Δ^9-tetrahydrocannabinol
TRPM8	transient receptor potential cation channel subfamily M member 8
TRPV1	transient receptor potential cation channel subfamily V member 1
U	unit
VEH	vehicle
VGCC	voltage-gated calcium channels
WIN	WIN 55,212-2
WT	wild-type
WW	tryptophan-tryptophan-proline
X-Gal	5-bromo-4-chloro-3-indolyl-β-D-galactopyranoside
Δ^8-THC	Δ^8-tetrahydrocannabinol

TABLE OF CONTENTS

1. INTRODUCTION

The endocannabinoid system is an elaborate system comprising cannabinoid receptors, their endogenous ligands (endocannabinoids), and enzymes that synthesize or degrade endocannabinoids. Cannabinoid receptor 1 (CB1R) is a G-protein coupled receptor (GPCR) that is the central molecule of the neuronal endocannabinoid system. In the central nervous system, CB1R is predominantly found presynaptically. It is located at the highest density on many GABAergic terminals but is also targeted to glutamatergic, cholinergic, serotonergic, and noradrenergic terminals (Kano et al., 2009). Thus, CB1R is a regulator of synaptic transmission. Endocannabinoids are synthesized on demand, meaning they are released in an activity-dependent synaptic state. Signaling via CB1R affects higher-order behaviors, such as anxiety, mood, fear extinction, addiction, or adaptive handling of stressful situations (Mechoulam et al., 2013; Micale et al., 2013; Lutz et al., 2015; Morena et al., 2016). The endocannabinoid system is a promising target for chronic pain treatment (Finn et al., 2021). However, only a few ligands that target the endocannabinoid system are currently available to the patients (dronabinol, nabilone, and nabiximols).

Several proteins associate with CB1R and alter its signaling, as reviewed in (Fletcher-Jones et al., 2020). For example, CB1R interacting protein (CRIP1a) modulates the CB1R signaling and endocytosis (Blume et al., 2015; Smith et al., 2015; Mascia et al., 2017), Adaptor protein 3 (AP-3) controls sorting and signaling of the intracellular CB1R (Rozenfeld et al., 2008), and G protein-associated sorting protein 1 (GASP1) is involved in lysosomal trafficking of the phosphorylated and internalized CB1R (Martini et al., 2007). Finally, SGIP1 hinders CB1R endocytosis and considerably enhances the receptor's cell surface stability. This association extensively regulates CB1R endocytosis, resulting in functional consequences in transfected cells (Hajkova et al., 2016; Gazdarica et al., 2021) and *in vivo* (Dvorakova et al., 2021).

Control of synaptic transmission by presynaptic G protein-coupled receptors

Information in the nervous system is encoded as a change in the membrane potential. Membrane potential is determined by the electrochemical gradient of ions, mainly Na^+, K^+, and Cl^-, across the plasma membrane. Non-excitable cells maintain a constant membrane potential, and the intracellular side of the plasma membrane of the cells has a negative charge. Neurons are excitable cells and thus can undergo rapid changes in their membrane potential. The main

factor contributing to the excitability of neurons is the influx of Na^+ into the cell, caused by the opened Na^+ channels upon neurotransmitter release. The depolarization of the plasma membrane due to Na^+ influx reverses the membrane potential so that the intracellular side of the plasma membrane becomes positively charged. The local depolarization of the plasma membrane opens the neighboring voltage-sensitive (or voltage-gated) Na^+ channels, which depolarize the adjacent regions of the membrane. The depolarization, and therefore excitation, propagates through dendrites, the soma, and the axon by the turn of activation of ion channels.

When the depolarization wave reaches the presynaptic terminal of the axon, neurotransmitters are released into the synaptic cleft. Neurotransmitters, such as glutamate or gamma-aminobutyric acid (GABA), are stored in the presynaptic terminal in vesicles (Figure 1). Depolarization of the presynaptic membrane activates voltage-gated calcium channels (VGCC), which allow extracellular Ca^{2+} inside the presynaptic terminal. An increase in Ca^{2+} concentration in the presynapse stimulates the fusion of the vesicles with the plasma membrane by exocytosis and the release of the vesicle's content into the synaptic cleft. The released neurotransmitters, such as glutamate, activate ionotropic glutamate receptors located on the postsynaptic membrane. The activated ionotropic glutamate receptors pass Na^+ inside the postsynaptic terminal so that the Na^+ influx depolarizes the postsynaptic membrane, thus resulting in the excitation of the postsynaptic neuron (Ribrault et al., 2011; Niciu et al., 2012; Ashery et al., 2014).

Therefore, three main factors are involved in the neurotransmitter release:

1) the synaptic vesicle exocytosis;
2) the flow of Ca^{2+} through VGCC;
3) the ability of the presynaptic membrane to be depolarized.

These three factors are subject to regulation, discussed further below.

While glutamate is the main excitatory neurotransmitter that activates Na^+ channels (*N*-methyl-d-aspartate (NMDA) receptors, α-amino-3-hydroxyl-5-methyl-4-isoxazole-propionate (AMPA) receptors, and kainate receptors), GABA is the main inhibitory neuromodulator that activates Cl^- channels (GABA receptors). The Cl^- influx into the postsynaptic terminal makes the membrane potential more negative, a phenomenon known as hyperpolarization. Hyperpolarization decreases the probability of depolarization of the postsynaptic neuron. One neuron receives synaptic inputs from different types of excitatory and inhibitory neurons. In

sum, neurons integrate all of the incoming excitatory and inhibitory stimuli, and their net sum decides if the signal propagates further.

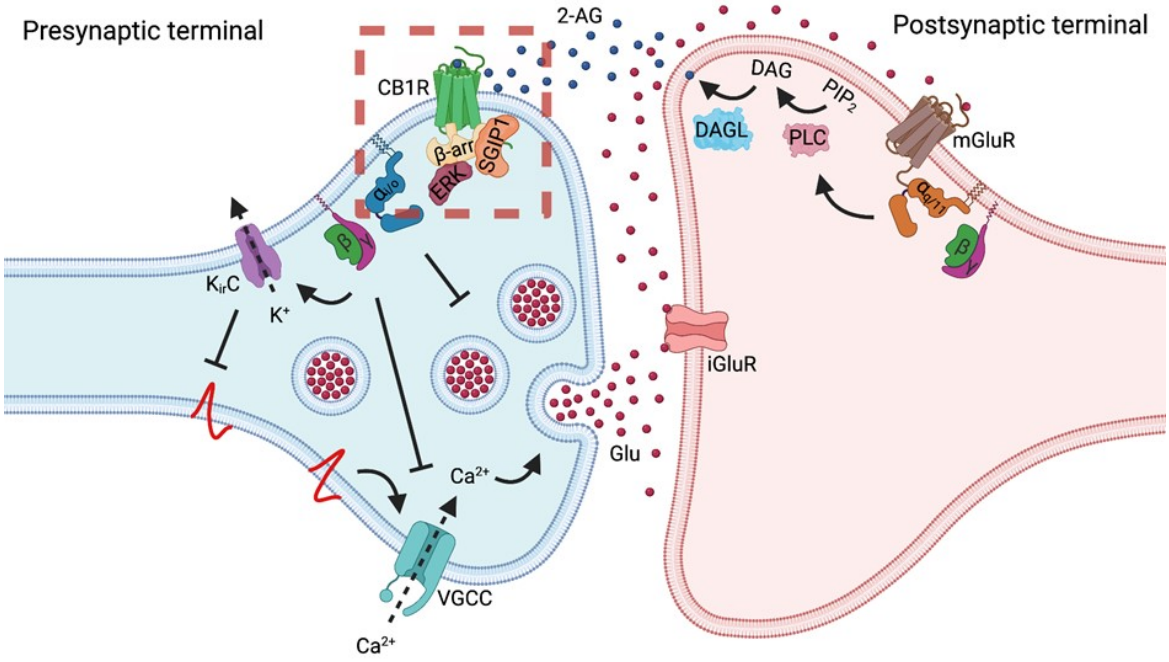

Figure 1. Signal transmission at a glutamatergic synapse and its regulation by cannabinoid receptor 1. Depolarization of the presynaptic membrane activates voltage-gated calcium channels (VGCC). The influx of Ca^{2+} stimulates exocytosis of glutamate-filled vesicles. Glutamate (Glu) activates ionotropic glutamate receptors (iGluR), which allow Na^{+} inside the postsynaptic terminal and stimulate depolarization of the postsynaptic membrane and activation of the postsynaptic neuron. At the same time, glutamate stimulates metabotropic glutamate receptors 1 and 5 (mGluR). These receptors are coupled to G_q protein and activate phospholipase C β (PLCβ)-mediated pathway. PLCβ converts membrane phospholipid phosphatidylinositol 4,5-bisphosphate (PIP_2) into second messengers diacylglycerol (DAG) and inositol 1,4,5-trisphosphate (IP_3, not shown). Diacylglycerol lipase (DAGL), located at the postsynapse, converts DAG into endocannabinoid 2-arachidonoylglycerol (2-AG). 2-AG diffuses into the synaptic cleft and the presynaptic membrane, activating cannabinoid receptor 1 (CB1R). The 2-AG synthesis cascade is referred to as the on-demand production of endocannabinoids. Another endocannabinoid, N-arachidonoylethanolamine (AEA), also known as anandamide, is produced tonically from its precursor by N-acetylphosphatidylethanolamine-hydrolysing phospholipase D (NAPE-PLD, not shown). CB1R activity decreases synaptic vesicle exocytosis by multiple mechanisms. These mechanisms include $G_{\alpha i/o}$ protein-mediated decrease in intracellular cAMP

and protein kinase A activity and $G_{\beta\gamma}$ protein-mediated inhibition of voltage-gated calcium channels (VGCC) and activation of inwardly-rectifying potassium channels (K_{ir}). VGCC inhibition decreases presynaptic Ca^{2+} levels, thus inhibiting synaptic vesicle fusion with the plasma membrane. K_{ir} activation results in the hyperpolarization of the presynaptic membrane, thus preventing activation of VGCC. Therefore, CB1R plays the role of retrograde signaling regulator by fine-tuning the synaptic transmission. In cultured neurons, CB1R located in axons and the presynapse exhibits a high degree of membrane stability compared to the receptor located in the somatodendritic compartment. This stabilization can be mediated by the effect of Src homology 3-domain growth factor receptor-bound 2-like endophilin interacting protein 1 (SGIP1). SGIP1 inhibits CB1R endocytosis and alters its signaling. The red dashed square illustrates the aspects of the CB1R-SGIP1 relationship tested in heterologous systems shown in Figure 3 (Durydivka et al., 2023b).

While one means of regulating neuronal excitability is the integration of excitatory and inhibitory stimuli from different synapses, another means involves controlling neurotransmitter release at each synapse. Receptors that, upon activation, inhibit or facilitate neurotransmitter release are located on the presynaptic membrane and include neuromodulator receptors cannabinoid receptor 1 (CB1R) and μ-opioid receptor (MOR), among others (Schlicker et al., 2017).

CB1R is typically expressed in presynaptic terminals of glutamatergic and GABAergic neurons (Katona et al., 1999; Kawamura et al., 2006). Unlike most neurotransmitters, endocannabinoids (CB1R endogenous ligands) are synthesized on demand at postsynaptic sites (Dimarzo et al., 1994; Stella et al., 1997).

Glutamate that is released into the synaptic cleft, in addition to ionotropic glutamate receptors, activates post-synaptic metabotropic glutamate receptors (mGluR), namely mGluR1 and mGluR5 (Figure 1). These receptors are G_q-coupled and activate phospholipase C β (PLCβ) that cleaves membrane phospholipid phosphatidylinositol 4,5-bisphosphate (PIP_2) into diacylglycerol (DAG) and inositol 1,4,5-trisphosphate (IP_3), which serve as second messengers. DAG is further converted by diacylglycerol lipase (DAGL) to endocannabinoid 2-arachidonoylglycerol (2-AG) (Murataeva et al., 2014). Another endocannabinoid, N-arachidonoylethanolamine (AEA), also known as anandamide, is synthesized from its precursor by N-acetylphosphatidylethanolamine-hydrolysing phospholipase D (NAPE-PLD). AEA is

produced at steady levels (Wettschureck et al., 2006), and its production increases in a Ca^{2+}-dependent manner (Dimarzo et al., 1994). The newly-synthesized endocannabinoids diffuse into the synaptic cleft, bind to, and activate presynaptic CB1R (Castillo et al., 2012).

CB1R is coupled predominantly to $G_{i/o}$ protein, so CB1R inhibits the activity of adenylate cyclase and modulates ion channels. While adenylate cyclase is regulated by the G_{α} subunit of $G_{i/o}$, ion channels are modulated by the $G_{\beta\gamma}$ subunit of the G protein. The cumulative effect of CB1R activation centers on the inhibition of the synaptic transmission by:

1) the inhibition of the synaptic vesicle exocytosis due to decreased levels of cyclic adenosine monophosphate (cAMP);
2) the inhibition of VGCC, resulting in decreased presynaptic Ca^{2+} levels;
3) the activation of inwardly-rectifying potassium channels (K_{ir}), resulting in hyperpolarization of the presynaptic plasma membrane.

These processes ensure rapid and precise inhibition of the synaptic transmission. Therefore, CB1R is an effective "circuit breaker" in the nervous system (Katona et al., 2008; Di Marzo, 2011). Inhibition of the synaptic currents after depolarization is a distinctive feature of CB1R-expressing synapses. This inhibition phenomenon is known as depolarization-induced suppression of excitation (DSE) for excitatory neurons and depolarization-induced suppression of inhibition (DSI) for inhibitory neurons (Kreitzer et al., 2001b, 2001a; Straiker et al., 2005). DSE and DSI are the forms of short-term synaptic plasticity. CB1R is also involved in long-term synaptic plasticity, which may mediate long-term changes to neural circuits and behavior (Chevaleyre et al., 2007; Heifets et al., 2009).

Another type of presynaptic receptors that modulate synaptic activity is opioid receptors, and MOR is among them. MOR is expressed primarily on glutamatergic and GABAergic neurons in brain pathways that modulate pain perception, and it is involved in pain signaling and antinociception (Corder et al., 2018; Reeves et al., 2022). MOR is $G_{i/o}$ protein-coupled, and its effect on synaptic transmission is similar to that of CB1R, including a decrease in cAMP levels, inhibition of VGCC, and activation of potassium channels (Sobczak et al., 2014). Unlike endocannabinoids, MOR agonists such as β-endorphins are packed into vesicles in neuronal soma and are transported down to axon terminals. These opioids are released tonically or upon presynaptic depolarization (Corder et al., 2018; Reeves et al., 2022).

Molecular mechanisms of CB1R signaling and regulation

CB1R is one of the most abundant G protein-coupled receptors (GPCR) in the brain (Zou et al., 2018). CB1R is expressed at high levels in the neocortex, hippocampus, basal ganglia, cerebellum, and brainstem, as well as in the neurons of dorsal root ganglia (Herkenham et al., 1990; Howlett et al., 1990; Herkenham et al., 1991; Bridges et al., 2003; Mackie, 2005). The CB1R signaling in the brain has been linked to a plethora of physiological functions, such as memory formation, motor coordination, appetite and metabolic control, thermoregulation, immune response, neurogenesis, anxiety, and analgesia, as well as pathological conditions (Chaperon et al., 1999; Viveros et al., 2005; Zou et al., 2018).

The endocannabinoid system

The activity of CB1R in the brain is a complex process that is finely tuned by the interplay of various enzymes and proteins that fall into the endocannabinoid system. This intricate system plays a crucial role in regulating various physiological processes in the body (Castillo et al., 2012; Lu et al., 2016; Zou et al., 2018). The key components of the endocannabinoid system include:

1) cannabinoid receptors 1 and 2. While CB1R is primarily found in the central nervous system, particularly in the brain, cannabinoid receptor 2 (CB2R) is mainly located in immune cells and peripheral tissues, where it influences immune responses and inflammation. Expression of CB2R in the brain has been associated with some pathological conditions, such as addiction, inflammation, and anxiety, or with non-neuronal cells (Miller et al., 2011; Mecha et al., 2015). Additional receptors, such as transient receptor potential cation channel subfamily V member 1 (TRPV1), transient receptor potential cation channel subfamily M member 8 (TRPM8), G protein-coupled receptor (GPR) 18, GPR55 and GPR119, have been recently linked to the endocannabinoid system (van der Stelt et al., 2004; Brown, 2007; De Petrocellis et al., 2007; Johns et al., 2007; Pertwee, 2008; Chavez et al., 2010; McHugh et al., 2010);
2) endogenous cannabinoid receptor ligands 2-AG and AEA (also known as anandamide). These endocannabinoids are produced by the body in response to the depolarization of the postsynaptic plasma membrane. The levels of 2-AG in the brain are approximately 1000 times higher than the levels of AEA, and altered metabolism of 2-AG, but not AEA, has prominent effects on endocannabinoid-mediated retrograde signaling. Therefore, 2-AG was

proposed as the primary endogenous ligand for CB1R in the central nervous system (Katona et al., 2008; Di Marzo et al., 2012; Murataeva et al., 2014). While 2-AG specifically binds to and activates CB1R and CB2R, AEA can also activate other receptors, such as TRPV1 and TRPM8 (van der Stelt et al., 2004; De Petrocellis et al., 2007; Pertwee, 2008; Chavez et al., 2010);

3) endocannabinoid synthesis enzymes NAPE-PLD and DAGL. The enzymes involved in the synthesis of endocannabinoids are located in the postsynaptic terminal and produce 2-AG or AEA in response to depolarization of the postsynaptic membrane or tonically;
4) endocannabinoid degradation enzymes fatty acid amino hydrolase (FAAH) and monoacylglycerol lipase (MGL). These enzymes are located at presynaptic terminals, where they are optimally positioned to break down 2-AG and AEA that have engaged presynaptic CB1R. Thus, FAAH and MGL ensure tight regulation of the endocannabinoid system activity.

The orchestration of these components is critical for fine-tuning the endocannabinoid system's activity. The impairments in the endocannabinoid system result in various psychiatric, neurological, and neurodegenerative disorders, such as obesity, dementia, and epilepsy (Soltesz et al., 2015; Lu et al., 2016; Busquets-Garcia et al., 2018).

Signaling pathways activated by CB1R

CB1R shares common structural features of Class A GPCR: seven transmembrane helices joined by extracellular and intracellular loops, the extracellular N-terminus medium, and the cytoplasmic C-terminus. The C-terminus begins with a short helical segment (helix 8), which is crucial for the receptor's trafficking (Ahn et al., 2010). The CB1R C-terminal tail also contains helix 9 that separates two clusters of serine/threonine residues (Figure 2). Phosphorylation of the serine/threonine residues is crucial for the regulation of the receptor's signaling. Helix 9 has been shown to control the intracellular distribution of CB1R and its stability on the plasma membrane (Fletcher-Jones et al., 2019). For Class A GPCR, the extracellular surface of the transmembrane domain is involved in ligand binding. The intracellular surface, including the intracellular loops and the C-terminus, are involved in interactions with G proteins and other regulatory proteins (Al-Zoubi et al., 2019).

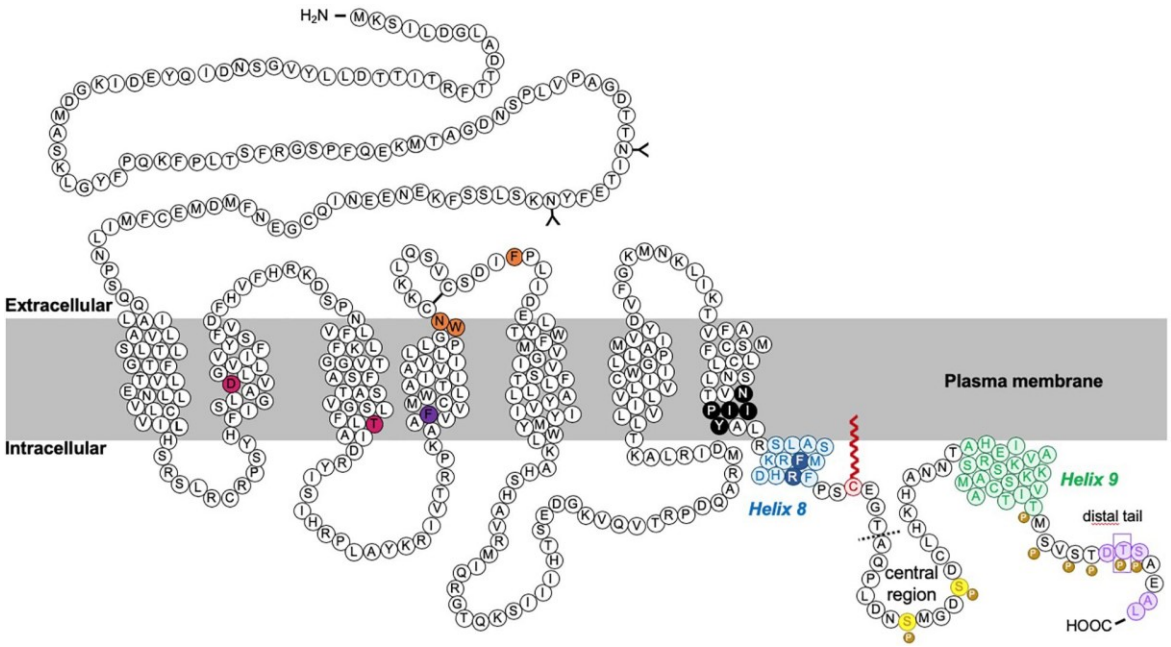

Figure 2. Schematic representation of CB1R structure and its post-translational modifications. The C-terminal tail of CB1R contains two helical structures, helix 8 and 9 (highlighted in blue and green). Helix 8 is crucial for the trafficking of CB1R, and helix 9 controls the delivery of the receptor to neuronal compartments and the stability of the receptor in the plasma membrane. The phosphorylation of amino acid residues within the central region and distal tail, corresponding to clusters ^{425}SMGDS^{429} and ^{460}TMSVSTDTS^{468}, regulates the activity of the receptor. Sites of glycosylation or palmitoylation are represented by "Y" and a red zigzag line. Residues required for constitutive internalization are shown in pink. The orange residues mark amino acids required for proper receptor maturation and surface expression. The purple residue represents F238 residue modulating localization to lipid rafts. The black residues indicate NPXXY motif, critical for β-arrestin recruitment. F409/R410 motif in H8 is likely the binding site of GASP1, while CRIP1a requires DTSXXAL motif at the C-terminus of CB1R. SGIP1 likely interacts with helix 9 of CB1R, but the intracellular loops might also be involved (Fletcher-Jones et al., 2020; Fletcher-Jones et al., 2023).

CB1R couples to heterotrimeric G proteins when activated by agonists. Agonist binding increases the intrahelical cavity within the intracellular side of the transmembrane helices of CB1R, allowing the cavity to accommodate α subunit of G protein. This coupling facilitates GDP-to-GTP exchange in the G_{α} subunit and results in its activation and dissociation from $G_{\beta\gamma}$ dimer (Figure 3A). Active G_{α} modulates the activity of effector proteins, such as adenylyl

cyclase, phospholipase C, or monomeric GTPases, while active $G_{\beta\gamma}$ modulates the activity of ion channels. As stated above, CB1R couples predominantly to $G_{i/o}$ family of G proteins, which results in inhibition of adenylyl cyclase activity and in subsequent fall in cAMP levels, contributing to the inhibition of synaptic vesicle exocytosis. The $G_{i/o}$ activity results in inactivation of the protein kinase A (PKA) phosphorylation pathway and activation of extracellular signal-regulated kinase 1/2 (ERK1/2), c-Jun N-terminal kinase 1/2/3 (JNK1/2/3), p38 and p42/p44 mitogen-activated protein kinase (p38 and p42/p44 MAPK) (Howlett, 2005; Turu et al., 2010). CB1R signaling modulates the activity of ion channels: increases K^+ conductance of G protein-coupled inward rectifying K^+ channels (K_{ir}) and decreases Ca^{2+} conductance of N- and P/Q-type voltage-gated calcium channels (VGCC) (Pan et al., 1996; Twitchell et al., 1997).

Structural alterations resulting from the activation of CB1R are sensed by G protein-coupled receptor kinase (GRK). GRK binds to the activated CB1R and phosphorylates its C-terminal tail at two clusters containing serine/threonine residues: ^{425}SMGDS^{429} and ^{460}TMSVSTDTS^{468} (human CB1R numbering). GRK3 was shown to be the major GRK isoform involved in CB1R phosphorylation, and phosphorylation of the residues within ^{425}SMGDS^{429} cluster is necessary for the recruitment of β-arrestins (Jin et al., 1999; Delgado-Peraza et al., 2016). B-arrestins bind to the phosphorylated CB1R's C-terminal tail and to the intracellular surface of the receptor's transmembrane core. This association prevents CB1R from coupling to and activating G proteins; such a decrease in the receptor's signaling efficiency is known as desensitization of the receptor.

Both ^{425}SMGDS^{429} and ^{460}TMSVSTDTS^{468} clusters are involved in β-arrestin binding, and inhibition of GRK3 abrogates β-arrestin association to CB1R (Straiker et al., 2012; Morgan et al., 2014; Ibsen et al., 2019; Gazdarica et al., 2021). GRK3-mediated phosphorylation of these clusters has an opposing effect on the dynamics of GRK3-CB1R association. On the one hand, phosphorylation of the residues within ^{460}TMSVSTDTS^{468} favors this association. On the other hand, phosphorylation of the residues within ^{425}SMGDS^{429} disfavors it (Gazdarica et al., 2021). By phosphorylating the ^{425}SMGDS^{429} cluster, GRK3 manifests a steric effect on its interaction with CB1R. This spatial hindrance due to GRK3-mediated phosphorylation may be the factor responsible for the dissociation of GRK3 from CB1R. CB1R, freed of GRK3, can now interact with β-arrestin.

Along with the role in desensitization, β-arrestins act as scaffolds bringing components of signaling cascades such as ERK1/2, JNK1/2/3, or p38 MAPK to the desensitized receptor, thus facilitating their activation (Rueda et al., 2000; Shenoy et al., 2011; Flores-Otero et al., 2014). These signaling cascades are considered G protein-independent, but they may also be activated in a G protein-depended manner (Wartmann et al., 1995; Liu et al., 2000; Rueda et al., 2000; Derkinderen et al., 2003).

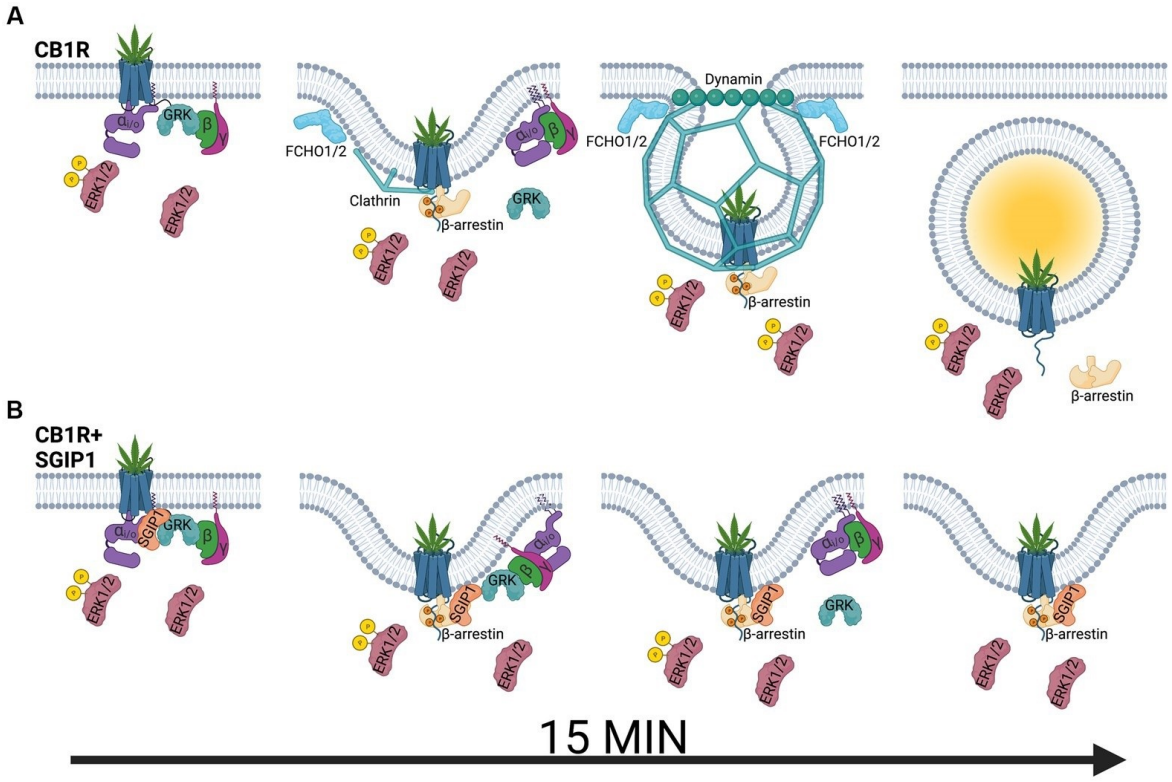

Figure 3. Signaling and internalization of cannabinoid receptor 1 and its modulation by SGIP1. (A) Agonist-induced activation of cannabinoid receptor 1 (CB1R) stimulates GDP-to-GTP exchange in α subunit of $G_{i/o}$ protein and dissociation of α and βγ subunits of the G protein. The activity of α and βγ subunits modulates various intracellular signaling cascades, such as adenylyl cyclase-protein kinase A cascade, phospholipase C-protein kinase C cascade, extracellular signal-regulated kinase 1/2 (ERK1/2) mitogen-activated protein kinase cascade, or the activity of ion channels. Phosphorylation of CB1R by G protein-coupled receptor kinase (GRK) mediates β-arrestin binding to the receptor, resulting in desensitization of the receptor, promotion of clathrin-mediated internalization, and facilitation of β-arrestin-mediated pathways, including ERK1/2 and c-Jun N-terminal kinase 1/2/3 (JNK1/2/3). The key proteins involved in clathrin-mediated internalization include FER and CIP4 homology domain only

proteins 1 and 2 (FCHO1/2), which initiate membrane invaginations, clathrin and adaptor protein 2 (AP-2, not shown), which stabilize the endocytic pits and link the receptor to them, and dynamin, which is involved in the scission of newly formed clathrin-coated vesicles from the plasma membrane. (B) SGIP1 inhibits the internalization of CB1R. The retention of the receptor in the plasma membrane results in increased GRK and β-arrestin association with CB1R, but $G_{i/o}$ protein activity is not affected. SGIP1 interaction with CB1R inhibits the activity of the ERK1/2 pathway, which may be explained by the lack of signaling from the endocytosed pool of CB1R or by a different β-arrestin conformation that impedes ERK1/2 activation. SGIP1 is an endocytic protein that interferes with CB1R endocytosis by an undescribed mechanism. It is not known if the CB1R-containing endocytic pits preserve the clathrin coating or other endocytic proteins (Durydivka et al., 2023b).

The important function of β-arrestins is to mediate the internalization of the desensitized receptor. Internalization was shown to depend on the phosphorylation of residues within cluster ^{460}TMSVSTDTS^{468} of the CB1R C-terminal tail (Hsieh et al., 1999; Jin et al., 1999). B-arrestin binding to the phosphorylated CB1R directs it toward internalization by clathrin-mediated endocytosis (Hsieh et al., 1999).

Clathrin-mediated endocytosis comprises several consecutive steps, resulting in the translocation of a plasma membrane cardo into the intracellular compartments (Figure 3A). Invagination of the plasma membrane is crucial for the progression of endocytosis. Multiple proteins can sense or induce membrane invaginations. These proteins contain Bin/amphiphysin/Rvs (BAR) domain, which binds preferentially to curved membranes (Stanishneva-Konovalova et al., 2016). Important initiators of clathrin-mediated endocytosis are FER and CIP4 homology domain only proteins 1 and 2 (FCHO1/2). FCHO1/2 contain Fes/Cip4 homology BAR (F-BAR) domain, which is involved in membrane binding and bending. Dimerization of the F-BAR domain creates a positively-charged interaction surface that interacts with the negatively-charged phospholipids in the plasma membrane. Therefore, positively-charged lysine, arginine, or histidine amino acid residues are crucial for membrane binding (Henne et al., 2007; Frost et al., 2008; Henne et al., 2010).

Plasma membrane invaginations, induced by FCHO1/2, are further stabilized by the central protein of clathrin-mediated endocytosis – clathrin. Clathrin is composed of three heavy and three light chains, which assemble into a triskelion structure. Polymerization of multiple clathrin

triskelia forms a basket that stabilizes invaginations of the plasma membrane (Fotin et al., 2004; McMahon et al., 2011). The clathrin's association with the plasma membrane is mediated by clathrin adaptor protein 2 (AP-2). AP-2 is a heterotetrameric protein that links the endocytic machinery together. Apart from interacting with clathrin, AP-2 also interacts with β-arrestin, the endocytic cargo, other accessory endocytic proteins, and the plasma membrane, thus ensuring proper positioning of the endocytic cargo (the desensitized receptor) to the sites of clathrin-coated pit nucleation and maturation (Kelly et al., 2014; Smith et al., 2017; Beacham et al., 2019; Kovtun et al., 2020).

Clathrin-stabilized membrane invaginations containing the cargo are removed from the plasma membrane by dynamin. Dynamin is a GTPase that polymerizes at the neck of the membrane invagination resulting in the scission of the clathrin-coated vesicles (Faelber et al., 2011; Antonny et al., 2016). In the cytoplasm, clathrin-coated vesicles containing the cargo undergo uncoating and are further sorted within the endosomal compartments. Internalization regulates the number of receptors on the plasma membrane and, therefore, controls the signaling output of receptors.

Subcellular distribution of CB1R in neurons

In the brain, CB1R is principally located at the presynaptic terminals of glutamatergic and GABAergic neurons (Hoffman et al., 2000; Domenici et al., 2006), but it is also found presynaptically on cholinergic, serotonergic, dopaminergic and noradrenergic neurons (Lau et al., 2008; Goonawardena et al., 2010; Haring et al., 2015; Busquets-Garcia et al., 2016). CB1R is expressed in the soma and is transported through the axon to the presynaptic terminals by adaptor protein 3 (AP-3)- and kinesin-1-mediated axonal transport (Rozenfeld et al., 2008; Saez et al., 2020). Subpopulations of CB1R have been observed on the somatic and dendritic plasma membrane and in various intracellular organelles, such as endosomes, lysosomes, and mitochondria (McIntosh et al., 1998; Brailoiu et al., 2011; Benard et al., 2012; Hebert-Chatelain et al., 2016).

In neurons, the expression of CB1R on the surface of the plasma membrane is highly polarized towards the axons and synapses, displaying an increasing gradient towards the presynaptic compartments (Irving et al., 2000; Coutts et al., 2001). The precise mechanisms of delivery of CB1R from the trans-Golgi network to the axonal and presynaptic compartments are not well defined; however, three models of the CB1R trafficking pathways have been proposed

(Fletcher-Jones et al., 2020). These models are based on previous studies assessing the CB1R localization, internalization rates, and the trafficking of newly synthesized receptors.

Compartmentalization of the neuronal plasma membrane plays an essential role in the polarization of protein distribution. Several barriers in the plasma membrane ensure the directionality of information flow and concentration gradients of proteins and other molecules. The axon initial segment limits the lateral diffusion of proteins and lipids between the somatodendritic and the axonal membrane. Synaptic protein machinery and receptors are localized and anchored to the synaptic active zone proteins and the postsynaptic density proteins (Leterrier, 2018; Guzikowski et al., 2021). Plasma membrane compartmentalization is also achieved by different chemical composition of its subdomains. The axonal and dendritic plasma membrane contains a high proportion of ceramides, which decrease membrane fluidity (Calderon et al., 1995; Saeedimasine et al., 2019; Fitzner et al., 2020). Synaptic membranes have lipid raft properties due to a high proportion of cholesterol and sphingolipids (Westra et al., 2021). Decreased membrane fluidity restricts the lateral diffusion of proteins and obstructs their internalization. These physical and chemical barriers regulate protein localization and trafficking.

Most of the CB1R-positive staining is associated with the presynaptic sites in the brain tissue processed by immunohistochemical methods (Katona et al., 1999); however, in cultured neurons, CB1R is distributed within the axonal and somatodendritic compartments (Coutts et al., 2001). CB1R in these compartments displays different properties towards its removal from the plasma membrane by endocytosis.

In transfected non-neuronal cells, CB1R internalization is rapid and is characterized by the rate constant 0.28 min^{-1} for agonist WIN55,212-2, while the constitutive internalization (in the absence of agonists) rate constant is 0.0032 min^{-1} (Zhu et al., 2019). Most of the surface CB1R internalizes within 30 min to 1 h (Rinaldi-Carmona et al., 1998; Jin et al., 1999). In contrast, in neuronal cultures, CB1R exhibits low levels of internalization when located on axons, and the removal of the majority of the surface CB1R was achieved only upon prolonged agonist exposure for 5-16 h (Coutts et al., 2001). Unlike CB1R located on axons, CB1R on the soma and dendrites has a high rate of internalization, comparable to the CB1R expressed in transfected non-neuronal cells (Leterrier et al., 2006). This high internalization rate is caused by a significant endocannabinoid tone in the brain or cultured cells, which constantly stimulates the receptor, causing its internalization (Howlett et al., 2011). Constitutive internalization has been

proposed as a mechanism for the polarized surface distribution of CB1R in neurons. Low rates of CB1R internalization from the axonal plasma membrane contrasts with high rates of internalization from the somatodendritic compartments. This difference results in the accumulation of CB1R on the axonal plasma membrane, maintaining the polarized distribution of the receptor (Leterrier et al., 2006; Bohn, 2007; McDonald et al., 2007; Simon et al., 2013).

The membrane stability of CB1R has been closely evaluated with regard to its location at the synapses of cultured neurons (Mikasova et al., 2008). The study evaluated the lateral mobility of the surface CB1R and correlated its localization to synaptic or extrasynaptic compartments. After the application of the agonist, a fraction of CB1R had restricted mobility. This fraction of the receptor was located in the vicinity of synapses. These results suggest that CB1R located in presynaptic compartments of axons is resistant to internalization and has low surface mobility.

Early research on the sorting of CB1R from the trans-Golgi network reported that CB1R is delivered to the somatodendritic and axonal membrane without discrimination. Polarized distribution is achieved by a high rate of CB1R internalization from the somatodendritic membrane and a low rate of internalization from the axonal membrane (Leterrier et al., 2006).

Another model suggests that CB1R does not reach the somatodendritic surface and is directly targeted to late endosomes or lysosomes and delivered to the axonal compartment. This is supported by reports showing that newly synthesized CB1R is rapidly degraded without reaching the plasma membrane in the N18TG2 neuroblastoma cell line (McIntosh et al., 1998) and that CB1R colocalizes with the late endosomal/lysosomal markers in primary neurons and interacts with adaptor protein 3 (AP-3) complex, involved in trafficking between the trans-Golgi network and lysosomes (Rozenfeld et al., 2008; Guardia et al., 2018).

A recent, more specific approach testing the CB1R targeting found that CB1R is preferentially delivered to the axonal membrane from the trans-Golgi network (Fletcher-Jones et al., 2019). This approach found that newly-synthesized CB1R was detected in the axonal membrane earlier than in the somatodendritic membrane. This preferential delivery depended on the helix 9 of the CB1R C-terminal tail. This helix was also involved in the increased stability of CB1R on the axonal membrane, which maintains the polarization.

Thus, an emerging consensus in the field reconciles that while newly-synthesized CB1R is preferentially driven to the axon by the trafficking machinery, endocytosis from the soma and dendrites maintains and enhances the polarized distribution of CB1R. Specific factors

controlling the subcellular distribution of CB1R have been proposed. Identification of the region of CB1R that is responsible for the polarized distribution (the helix 9 of the CB1R C-terminal tail) provides experimental approaches for testing these polarization factors.

Regardless of the intracellular sorting, polarized distribution of CB1R may be maintained by physical or chemical anchors, as stated above, or by the protein environment. Several proteins have been shown to interact with CB1R and alter its signaling and trafficking. These proteins include cannabinoid receptor-interacting protein 1a (CRIP1a), which modulates CB1R signaling and endocytosis (Niehaus et al., 2007; Blume et al., 2015; Blume et al., 2016; Guggenhuber et al., 2016); adaptor protein 3 (AP-3), which plays a role in the processing and signaling of intracellular CB1R (Rozenfeld et al., 2008); G protein-associated sorting protein 1 (GASP1), which controls lysosomal trafficking of phosphorylated and internalized CB1R (Martini et al., 2007; Martini et al., 2010); and Src homology 3-domain growth factor receptor-bound 2-like endophilin interacting protein 1 (SGIP1), which inhibits CB1R endocytosis and alters its signaling (Hajkova et al., 2016; Dvorakova et al., 2021; Gazdarica et al., 2021).

CB1R association with SGIP1

SGIP1 was identified as a CB1R-interacting partner using a yeast two-hybrid approach in our laboratory. SGIP1 associates with the C-terminal tail of CB1R (Hajkova et al., 2016; Fletcher-Jones et al., 2023). This association was verified by coimmunoprecipitation and bioluminescence resonance energy transfer (BRET) assay, and SGIP1 and CB1R colocalize in cultured neurons. When SGIP1 is co-expressed with CB1R in a heterologous system, such as HEK293 cells, this results in the inhibition of agonist-promoted endocytosis of CB1R (Figure 3B). However, the interaction of GRK3 and β-arrestin with the activated CB1R is not inhibited; instead, it is enhanced and prolonged (Hajkova et al., 2016; Gazdarica et al., 2021). Hypothetically, the enhanced GRK3 and β-arrestin interactions with the receptor may be explained by the retention of activated CB1R at the plasma membrane due to SGIP1-mediated inhibition of internalization. The enhanced GRK3 and β-arrestin interactions also indicate no competition for the CB1R C-terminus between SGIP1 and GRK3 or β-arrestin. At the same time, CB1R-dependent $G_{i/o}$ protein signaling was unaltered in the presence of SGIP1. On the other hand, the activity of the ERK1/2 pathway was inhibited in the presence of SGIP1 (Hajkova et al., 2016). Thus, the effect of SGIP1 on the CB1R signaling is specific towards certain

pathways. This preference of the receptor towards one signaling pathway over the others is known as biased signaling (Kenakin, 1995; Ibsen et al., 2017; Leo et al., 2021).

A recent study showed that helix 9 of the CB1R C-terminal tail binds to SGIP1 and is involved in the increased expression of the receptor on the axonal membrane (Fletcher-Jones et al., 2023). The helix 9 lies between ^{425}SMGDS^{429} and ^{460}TMSVSTDTS^{468} clusters. We previously showed that mutations of serine and threonine residues in these clusters do not influence the effects of SGIP1 on CB1R signaling. Deletion of helix 9 distorts the polarized distribution of CB1R, but overexpression of SGIP1 promotes the CB1R polarization in neurons (Fletcher-Jones et al., 2023). Therefore, helix 9 of the CB1R C-terminal tail is involved in the preferential delivery of CB1R to axons and stabilization of CB1R on the axonal membrane. By binding to helix 9 of CB1R, SGIP1 is likely the factor that stabilizes CB1R in the axonal membrane and decreases the internalization rate of CB1R from the axonal membrane.

SGIP1 interferes with CB1R endocytosis

SGIP1 is the adaptor protein involved in the internalization of several cargo molecules, such as transferrin and epidermal growth factor receptors (Uezu et al., 2007), synaptotagmin 1 (Lee et al., 2019), and cannabinoid receptor 1 (Hajkova et al., 2016). SGIP1 has also been shown to interact with endophilin (Trevaskis et al., 2005), epidermal growth factor receptor pathway substrate 15 (Eps15) (Uezu et al., 2007), intersectin (Dergai et al., 2010), calnexin (Li et al., 2011), and AP-2 (Hollopeter et al., 2014).

SGIP1 belongs to the muniscin family of adaptor proteins. Muniscins are involved in clathrin-mediated endocytosis and are known as cargo adaptors because they participate in selecting which cargo molecules internalize from the plasma membrane (Robinson, 2015). Muniscin family includes SGIP1, FCHO1/2, and yeast suppressor of yeast profilin deletion 1 (Syp1) (Reider et al., 2009) (Figure 4). Muniscins have a high degree of homology between their C-termini, represented by the μ homology domain (μHD), which evolved from a part of an ancient cargo adaptor protein complex TSET (Hirst et al., 2014). The μHD domain is involved in dimerization and interaction with other proteins, such as endophilin, intersectin, and Eps15 (Trevaskis et al., 2005; Uezu et al., 2007; Dergai et al., 2010).

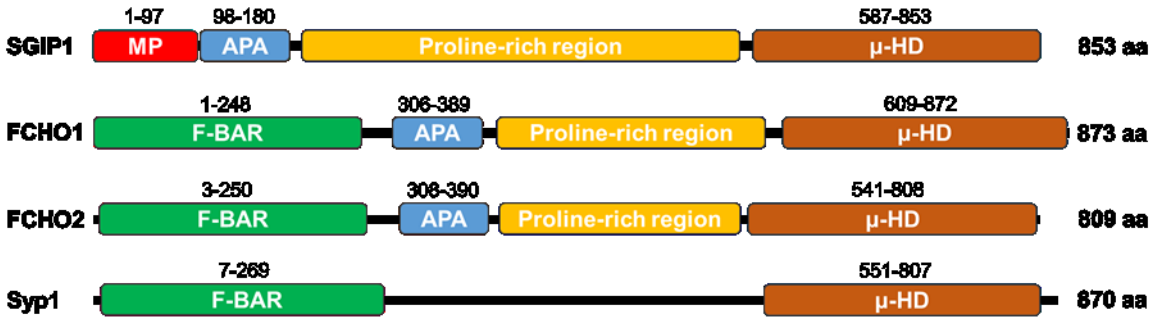

Figure 4. Schematic domain structure of the proteins of the muniscin family. Muniscins share the C-terminal μ homology domain (μHD), and SGIP1 and FCHO1/2 have a high degree of homology between their AP2 activator (APA) domain and proline-rich region. Muniscins differ in their N-terminal domain. FCHO1/2 and Syp1 contain the Fer-CIP4 homology-BAR (F-BAR) domain on their N-termini, but SGIP1 lacks the F-BAR domain and instead contains the membrane phospholipid-binding (MP) domain. The amino acid ranges corresponding to particular domains are provided above the domain, and the total lengths of the proteins are provided in amino acids (aa).

Muniscins differ in the composition of their N-termini. FCHO1/2 contain the Fer-CIP4 homology-BAR (F-BAR) domain at their N-termini. The F-BAR domain was shown to be necessary for the initiation of clathrin-mediated internalization during the early stages of nascent pit formation. The F-BAR domain mediates membrane curvature-sensing/inducing by FCHO1/2 (Henne et al., 2007; Henne et al., 2010; Uezu et al., 2011). SGIP1 lacks the F-BAR domain and instead contains the membrane phospholipid-binding (MP) domain, which is unique to SGIP1 because it has little homology to the F-BAR or other protein domains. Similar to the F-BAR domain, the MP domain was shown to bind to and deform membranes, but the mechanisms of its action are less well understood (Uezu et al., 2007).

The central region of muniscins is unstructured and is represented by the AP2 activator (APA) domain and the proline-rich region. The APA domain was shown to interact with and activate the AP-2 complex (Hollopeter et al., 2014). Therefore, both SGIP1 and FCHO1/2 contain the domain that is involved in the activation of the AP-2 complex, which is necessary for clathrin recruitment and clathrin-coated pit maturation (Mishra et al., 2021; Partlow et al., 2022). The proline-rich region is a long unstructured region of the muniscins' sequence that contains many putative phosphorylation sites (Craft et al., 2008; Edbauer et al., 2009) and binding sites to proteins containing SRC homology 3 (SH3) and tryptophan-tryptophan-proline

(WW) domains (Zarrinpar et al., 2003). The proline-rich region may be involved in interaction with other proteins or in dimerization; however, the precise role of the proline-rich region remains unknown.

Both SGIP1 and FCHO1/2 contain the APA domain that stimulates clathrin-mediated endocytosis, but these proteins have an opposing effect on CB1R endocytosis: SGIP1 inhibits CB1R endocytosis, but FCHO1/2 promotes it. Because most of the sequence of these proteins has a high degree of homology, the difference in the effect on CB1R internalization may be attributed to the absence of the F-BAR domain and the presence of the MP domain in SGIP1 (Figure 4).

Expression pattern of SGIP1

SGIP1 is expressed primarily in the brain (Trevaskis et al., 2005; Uezu et al., 2007). SGIP1 is present throughout all neuronal compartments and was determined to constitute 0.431% of synaptosome protein content (Wilhelm et al., 2014). The expression of SGIP1 and CB1R considerably overlaps in many brain regions involved in mood control, regulation of energy balance, addiction, and pain sensitivity (Lein et al., 2007).

SGIP1 was discovered as an overexpressed transcript in the hypothalamus of Israeli sand rats (*Psammomys obesus*) that developed obesity due to free access to food in captivity (Trevaskis et al., 2005). Further studies identified rat and mouse homologs of SGIP1. Several variants of SGIP1 protein were described in the literature; these variants include proteins comprising 806 amino acids (aa), 854 aa (termed SGIP1α), 826 aa, and 660 aa (termed SGIP1β). These isoforms have been suggested to result from alternative splicing of SGIP1 pre-mRNA transcripts. To avoid misidentification, we specify SGIP1 splice variants based on their amino acid length. Therefore, the known SGIP1 isoforms are SGIP1 806, SGIP1 854, SGIP1 826, and SGIP1 660.

Due to alternative splicing, different variants of a protein can be synthesized from a single gene. In this process, different exons of the same gene are taken together in different combinations, and introns are removed. Alternative splicing modes include (a) cassette alternative exon, (b) alternative 5′ splice site, (c) alternative 3′ splice site, (d) intron retention, (e) mutually exclusive exons (Figure 5). In addition, alternative start codons and polyadenylation sites can be included in a nascent mRNA transcript during splicing (Wang et al., 2015; Liu et al., 2022). Gene transcripts in the brain are more likely to undergo alternative

splicing, which provides an example of the versatility of the regulation of gene expression and signaling in the brain (Yeo et al., 2004; Vuong et al., 2016).

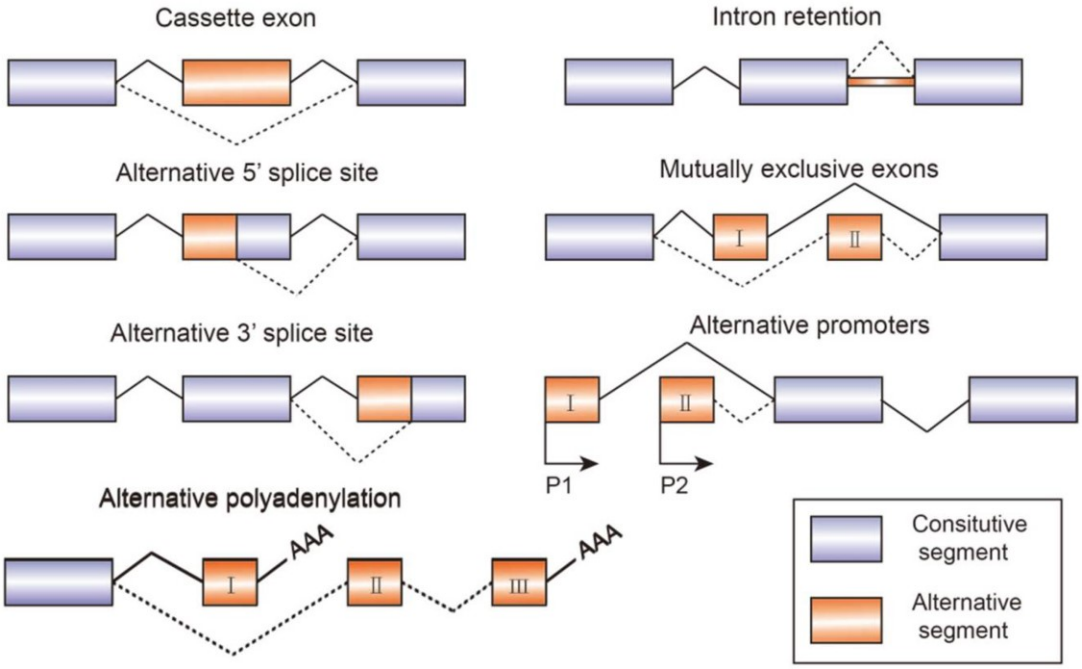

Figure 5. Different modes of alternative splicing of pre-mRNA: cassette alternative exon, alternative 5′ splice site, alternative 3′ splice site, intron retention, mutually exclusive exons, alternative promoters, and alternative polyadenylation sites. Exons are represented by boxes, and introns are represented by lines. Dashed lines connect alternative splicing sites (Liu et al., 2022).

The isoforms of SGIP1, resulting from the alternative splicing of SGIP1 pre-mRNA, may differ in characteristics or functions. However, the available experimental works have focused on only one of the SGIP1 isoforms in regard to a particular function. For example, the 806 aa isoform inhibits CB1R endocytosis (Hajkova et al., 2016), 854 aa isoform controls the endocytosis and recycling of synaptotagmin 1 (Lee et al., 2019), 826 aa isoform binds calnexin (Li et al., 2011), and 660 aa isoform increases CB1R expression in axons (Fletcher-Jones et al., 2023). It is not known if these properties are specific to any isoform or if they are common for all SGIP1 isoforms. To date, only one study has attempted to compare two known SGIP1 isoforms (Lee et al., 2021), and no study has studied the splicing of SGIP1. The NCBI Gene database predicts that 20 *Sgip1* splice variants can be transcribed in mice. This prediction includes the four known variants but also provides 16 more variants. These variants, if

experimentally detected, may provide new insights into SGIP1's functions, characteristics, and evolutional history.

The *in vivo* impact of the CB1R-SGIP1 association

The modulation of CB1R activity exerts various physiological effects, often influencing higher-order behaviors such as mood control, fear extinction, addiction, and adaptive handling of stressful situations. Activation of CB1R in animal models induces hypolocomotion (decreased movement), hypothermia (decreased body temperature), antinociception (decreased sensitivity to pain), and catalepsy (the state of immobility). These behavioral effects are evaluated in the cannabinoid tetrad test and are used in the characterization of cannabinoid ligands. Additional tests assessing cognition, working memory, anxiety-related behavior, and immune response evaluate the effect of cannabinoids on an organism's function (Chaperon et al., 1999; Howlett, 2002; Bosier et al., 2010; Lutz et al., 2015; Morena et al., 2016).

The widespread effects of CB1R on the organism have been demonstrated by genetic and pharmacological targeting of the receptor. Genetic deletion of CB1R in mice results in hypoactivity, antinociception, and increased mortality. CB1R knock-out mice also display lean phenotype and are more resistant to obesity (Zimmer et al., 1999; Trillou et al., 2004). The ability of CB1R to regulate metabolism and body mass was exploited in the development of anti-obesity drugs, such as CB1R antagonist rimonabant. By blocking the function of CB1R to stimulate appetite (Foltin et al., 1986), it was expected that rimonabant would help to treat obesity. Clinical trials showed that rimonabant markedly reduces body weight and improves cardiometabolic risk (Van Gaal et al., 2005; Curioni et al., 2006), and rimonabant was approved as an anti-obesity drug. However, rimonabant was withdrawn from the market because of its reported severe side effects, such as increased anxiety, depression, and suicidal intentions. Therefore, inhibition of CB1R might have deleterious effects on an organism; however, novel strategies can be employed to overcome this limitation and develop a safe CB1R antagonist (Di Marzo et al., 2009). These strategies include weak CB1R agonists, which may be more appropriate anti-obesity drugs rather than the CB1R inverse agonist rimonabant.

The endocannabinoid tone in the brain can be affected by targeting endocannabinoid degradation and synthesis pathways. Chemical inhibition and genetic deletion of FAAH, the enzyme of the synthetic pathway of AEA, results in decreased anxiety-like behavior. On the opposite, genetic deletion of DAG, involved in 2-AG synthesis, results in increased anxiety-like

behavior (Kathuria et al., 2003; Moreira et al., 2008; Shonesy et al., 2014; Jenniches et al., 2016). Therefore, targeting the enzymes of the endocannabinoid system provides indirect approaches to the modulation of CB1R activity.

Another functional outcome of CB1R signaling in the brain is the modulation of pain perception. Pain perception is mediated by ascending and descending neuronal pathways. Neurons in the ascending pathway receive input from peripheral primary afferent fibers and project from the dorsal horn of the spinal cord to the thalamus and parabrachial nucleus, which in turn relays the information to cortical and amygdalar regions, where the information is processed and decoded as a painful stimulus. The first synapse in the pain pathway is located in the dorsal horn of the spinal cord. The descending pathways modulate pain sensation. The most studied regions that contribute to pain modulation are the midbrain periaqueductal gray and rostral ventromedial medulla. The periaqueductal gray receives inputs from the midbrain and is heavily interconnected to the hypothalamus and limbic forebrain structures, including the amygdala. The periaqueductal gray projects to the rostral ventromedial medulla, which in turn sends its output to dorsal horn laminae, which is important for nociception (Neubert et al., 2004; Heinricher et al., 2009; Starowicz et al., 2013; Woodhams et al., 2017).

CB1R and other components of the endocannabinoid system are found in regions involved in the transmission and modulation of nociceptive signaling. Behavioral tests assessing acute and chronic nociception confirm that the endocannabinoid system, and especially CB1R, mediates nociception (Pertwee, 2001). The CB1R-mediated antinociceptive effects were confirmed by behavioral tests, such as the tail-flick test, hot-plate test, formalin test, and in nerve injury or inflammatory models.

Acute pain often functions as an indicator of a disease or harm to the body, and it usually disappears when the underlying cause is treated or healed. Chronic pain often results from impaired neuronal circuits in the nervous system or from the sensitization of the nervous system during inflammation, and this pain persists past the healing time for more than 12 weeks (Treede et al., 2015). Acute pain is usually efficiently treated with non-steroidal anti-inflammatory drugs and opioids, but chronic pain is often difficult to treat (Vanegas et al., 2010; Gatchel et al., 2014; Vuckovic et al., 2018). Accumulating data suggest that CB1R has a substantial role in modulating acute and chronic pain (Milligan et al., 2020). The endocannabinoid system has a vast potential for pain treatment, but few drugs (dronabinol, nabilone, and nabiximols) targeting the endocannabinoid system are approved and available on the market (Finn et al., 2021). It

remains unclear how the modulation of cell signaling by CB1R affects pain pathways in the nervous system and what the role of CB1R-interacting proteins in these processes is.

SGIP1 was initially described as an overexpressed transcript in obese Israeli sand rats (*Psammomys obesus*), which can be used as a model of diet-induced obesity and type 2 diabetes (Trevaskis et al., 2005). These findings linked SGIP1 functions to the regulation of energy balance. Consequent studies showed that the polymorphisms in the *SGIP1* gene are associated with various measures of obesity and the risk of complex psychiatric diseases, such as alcoholism, schizophrenia, and anxiety disorders in humans (Hodgkinson et al., 2010; Cummings et al., 2012; Yako et al., 2015; Chwedorowicz et al., 2016). The precise mechanisms of the SGIP1's effect on energy homeostasis and the progression of psychiatric disorders remain unknown. However, the possible mechanisms of these effects may depend on the SGIP1's link to CB1R signaling.

The effect of SGIP1 on CB1R and the endocannabinoid system has been evaluated *in vivo* by behavioral testing of *Sgip1* knock-out mice. These *Sgip1* knock-out mice had intact cognition and motor skills but exhibited altered mood-related behavior, decreased anxiety-like behavior, and decreased acute pain nociception (Dvorakova et al., 2021). *Sgip1* deletion did not affect the body weight of the mice, in contrast to the association of *Sgip1* overexpression with the obese phenotype. The altered responses of the *Sgip1* knock-out mice to the cannabinoid tetrad tests demonstrate that *Sgip1* deletion affects the endocannabinoid system in the brain. These altered responses include anti-nociception, catalepsy, and body temperature. In addition, the *Sgip1* knock-out mice exhibited pronounced THC withdrawal signs manifested as intense jumping, which is characteristic of morphine withdrawal (Francis et al., 1971; Dvorakova et al., 2021). Moreover, the antinociceptive effect of morphine was enhanced in *Sgip1* knock-out mice as well. These observations suggest a crosstalk of the endocannabinoid and opioid systems in the brain (Robledo et al., 2008).

Deletion of *Sgip1* in mice results in an antinociceptive effect in both naïve mice and mice treated with cannabinoid drugs in the tail-flick test (Dvorakova et al., 2021). The tail-flick test measures acute nociception and assesses short-term stimulation of the pain pathways, including CB1R-controlled pathways. In chronic pain, the relationships between pain pathways and associated mechanisms can undergo significant changes over time, and the role of CB1R may become more complex due to neuroplasticity, sensitization of pain pathways, and adaptive changes in endocannabinoid signaling. Because *Sgip1* deletion makes the mice more sensitive

to analgesics, the role of SGIP1 in chronic pain perception should be considered as well. Extensive exploration of the SGIP1-CB1R relationship may widen the understanding of pain processing and offer new approaches for pharmaceutical targeting of the endocannabinoid system. These insights may help to reduce the adverse effects of the currently available drugs acting on CB1R.

Classification of CB1R ligands

Ligands acting on CB1R (cannabinoids) can be classified according to their origin into endocannabinoids, phytocannabinoids, synthetic cannabinoids, or semi-synthetic cannabinoids. Endocannabinoids are endogenously produced in the brain and include 2-AG and AEA; phytocannabinoids are naturally occurring cannabinoids that are produced by the *Cannabis sativa* plant and include Δ^9-tetrahydrocannabinol (THC) and cannabidiol (CBD) among other components; synthetic cannabinoids include various ligands, such as WIN 55,212-2 (WIN), CP 55,940, HU-210, SR-141716A, and AM251 (Figure 6). CB1R ligands can be further classified regarding their chemical structure (for example, indole, urea, or tropane derivatives) and psychoactive effect (psychotropic and non-psychotropic) (Tabrizi et al., 2017; Hryhorowicz et al., 2019).

Based on the effect of receptor binding, ligands can be divided into orthosteric and allosteric. An orthosteric ligand binds to the same site of the receptor as the natural agonist, and an allosteric ligand binds to a site different from the orthosteric site. Based on the mode of action, orthosteric ligands are further divided into agonists, antagonists, and inverse agonists. Agonists activate receptors to produce a measurable effect. Full agonists produce a maximal effect in given conditions, while partial agonists produce a detectable but submaximal effect. Inverse agonists produce an effect opposite to that of agonists. Antagonists have no effect on their own, but they block the effects of agonists and inverse agonists (Negus, 2006).

Many receptors exhibit basal activity because of their intrinsic structural properties and the complex interplay of molecular components within the cellular environment. Basal activity refers to the constitutive low-level signaling or activity exhibited by receptors in the absence of their cognate ligands. This intrinsic activity can arise from various factors, such as conformational dynamics of the receptor, interaction with downstream signaling molecules, and the intricacies of receptor-ligand binding kinetics. In this instance, agonists increase the

receptor's activity above its basal level, inverse agonists decrease this activity below the basal level, and antagonists do not affect the basal activity (Berg et al., 2018).

Allosteric ligands bind to the receptor and induce its distinct conformation. Allosteric ligands do not activate or inhibit the receptor; instead, they modulate the effect of orthosteric ligands. Some allosteric ligands perturb the receptor's signaling even in the absence of orthosteric ligands, an effect termed allo-agonism (Kenakin, 2001; May et al., 2007). Allosteric ligands are divided into positive allosteric modulators, negative allosteric modulators, and neutral allosteric ligands. Positive allosteric modulators enhance the effects of orthosteric ligands, negative allosteric modulators weaken their effects, and neutral allosteric ligands only bind to allosteric sites but have no effect on the receptor (Hryhorowicz et al., 2019).

The pharmacological activity of ligands can be described by potency and efficacy. Potency is the concentration or amount of a ligand required to produce a defined effect. Therefore, the higher the potency, the lower the ligand concentration is required to produce the same effect. For agonists, potency is defined as the molar concentration of an agonist that produces 50% of the maximum possible response for that agonist (EC50) (Pharmacology et al., 2000). The potency of receptor agonists reflects their binding affinity to the receptor in the receptor-effector system (Waldman, 2002).

Efficacy most commonly refers to the maximum effect that can be expected from the agonist (Neubig et al., 2003). Efficacy is determined by the interaction between the ligand and its receptor-effector system. Therefore, efficacy depends on experimental conditions, such as tissue, receptor expression levels, and the type of measurement. Moreover, the ability of ligands to interact with their effector system in the whole body is influenced by pharmacokinetic parameters, such as absorption, distribution, metabolism, and excretion. Therefore, the efficacy of ligands does not define their clinical efficacy, which reflects the therapeutic benefits (Waldman, 2002).

Novel cannabinoid ligands that mimic THC properties

THC and CBD are the major phytocannabinoids in the *Cannabis sativa* plant, and these compounds have been recognized for their various psychotropic and therapeutic effects. However, the botanical composition of the cannabis plant extends far beyond THC and CBD. More than 400 different compounds have been identified in the cannabis plant, including other cannabinoids, terpenes, alkaloids, and flavonoids (ElSohly et al., 2005; Radwan et al., 2021).

Minor cannabinoid compounds have gained increasing attention from biochemists because these lesser-known compounds may have chemical and therapeutic profiles different from those of THC and CBD. For example, many minor cannabinoids share the overall structure with THC, but they differ in the number and orientation of methyl groups, degree of hydrogenation, and length of the side chain, among other factors. Due to these differences, certain minor cannabinoids may have different stability, bioavailability, potency, or efficacy. Thus, novel cannabinoid ligands may become more stable drugs that require lower doses and that have minimized side effects.

Among minor cannabinoids, hexahydrocannabinol (HHC) has garnered notable attention. HHC is found in minute quantities in the cannabis plant, but it can be conveniently synthesized by acid treatment of CBD (Gaoni et al., 1966). Because of the ease in the regulation of the CBD production, the synthesis and use of HHC is facilitated. Moreover, HHC itself remains largely unregulated by governing authorities in most countries. Because HHC is not scheduled by the 1971 Convention on Psychotropic Substances, which controls tetrahydrocannabinol isomers only, HHC has emerged as a legal alternative to more commonly known THC; however, HHC might transition into a controlled substance category due to the insufficiency of comprehensive data regarding its activity, potency, toxicity, and overall safety (Casati et al., 2022; Tanaka et al., 2023; Ujvary, 2023; Ujvary et al., 2023).

The synthesis of HHC yields its two distinct epimers: (9S)-HHC and (9R)-HHC. These epimers differ in the orientation of the single methyl group at atom 9 (Figure 6). In (9S)-HHC, the methyl group is axial, and in (9R)-HHC, the methyl group is equatorial. This seemingly minor stereochemical difference substantially affects receptor binding, resulting in a higher affinity of (9R)-HHC epimer for CB1R than that of (9S)-HHC epimer. Initial attempts to compare HHC and its epimers were hindered by the presence of impurities within the compounds themselves, leading to compromised outcomes (Adams et al., 1940; Mechoulam et al., 1980). A recent study that used highly-purified HHC epimers showed that the effect of (9R)-HHC on mouse behavior is close to that of THC, while (9S)-HHC has little or no cannabimimetic effect (Russo et al., 2023). The proper pharmacological profiling of HHC requires more studies employing animal models as well as cell-based assays to evaluate the effects of HHC epimers on CB1R and the endocannabinoid system and compare their effects to those of the commonly used cannabinoids.

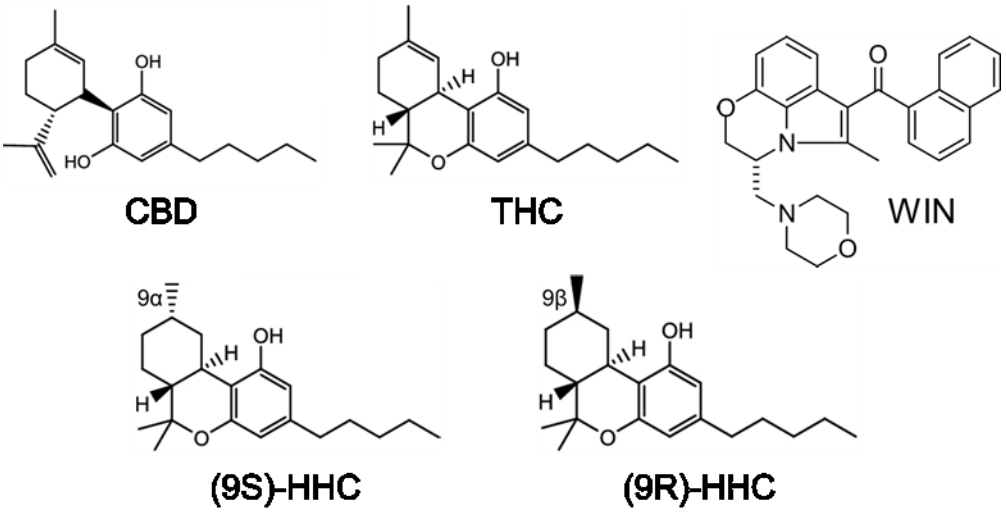

Figure 6. Structures of phytocannabinoids cannabidiol (CBD) and Δ^9-tetrahydrocannabinol (THC), a synthetic cannabinoid WIN 55,212-2 (WIN), and epimers of semi-synthetic cannabinoid hexahydrocannabinol (HHC), (9S)-HHC and (9R)-HHC. HHC epimers differ in the spatial position of the C-11 methyl group. In (9S)-HHC, the methyl group is axial (9α-HHC), and in (9R)-HHC, the methyl group is equatorial (9β-HHC).

2. AIMS OF THE STUDY

Hypothesis 1. SGIP1 is a CB1R-associated protein, and *Sgip1* deletion in mice reduces acute nociception and increases the potency of the analgesic effect of THC in the acute pain model. CB1R is involved in the processing of both acute and chronic pain. In chronic pain, pain processing circuits often become altered due to long-lasting activation, and the CB1R-SGIP1 relationship may be modified. Therefore, the effect of *Sgip1* deletion on chronic pain in mice should be evaluated.

Aim 1. To determine the effect of *Sgip1* deletion on the sensitivity to mechanical stimulation in the mouse model of chronic inflammatory pain, induced by carrageenan injection, and the efficiency of THC-induced analgesic effect in this mouse model.

Hypothesis 2. SGIP1 has been reported to be expressed as four splice isoforms in different studies; these isoforms are SGIP1 806, SGIP1 854 (termed SGIP1α), SGIP1 826, and SGIP1 660 (termed SGIP1β). The NCBI Gene database predicts that 20 *Sgip1* splice variants can be transcribed in mice. These splice variants may differ in function or properties. It is not known which splice variant is more abundant in the brain and if they have different properties.

Aim 2. To clone splice variants of *Sgip1* from the mouse brain, evaluate their relative abundance, compare their properties, and unify their nomenclature.

Hypothesis 3. The currently available drugs targeting CB1R are limited. The development of new drugs is hampered by the psychotropic effects of modulation of CB1R activity and other off-target effects. Minor constituents of the cannabis plant are being tested to explore their therapeutic potential. Among these constituents, HHC has gained much interest from researchers and public due to its THC-like effects and facile synthesis. Little information regarding HHC's effect on CB1R signaling is available; therefore, such HHC-induced signaling should be investigated and compared to commonly used cannabinoids.

Aim 3. To characterize the effect of the HHC epimers on the signaling pathways elicited by CB1R and compare their effects to those of THC and WIN.

3. METHODS

3.1. Materials and methods specific for aim 1

3.1.1. Animals

Adult wild-type C57BL/6NCrl and *Sgip1* knock-out mice (characterized in (Dvorakova et al., 2021)) were group-housed in plastic cages with soft bedding in a pathogen-free facility at 22 ± 2°C, 45% humidity, 12 h light/12 h dark cycle, and food and water *ad libitum*. The mice were acclimated in the facility for at least one week prior to experiments. The mice were tested during the light phase of the circadian cycle and at the same time of the day. Before testing, the mice were acclimated for one hour in the experimental room with low noise and light levels.

3.1.2. Drug injections

Stock solutions of WIN 55,212-2 mesylate (WIN) (Tocris) and rimonabant hydrochloride (Sigma) were prepared in dimethyl sulfoxide (DMSO) and of Δ^9-tetrahydrocannabinol (THC) (provided by Dr. Martin Kuchar, UCT Prague) was prepared in ethanol. Solutions for injections were prepared by dissolving one volume of either the drug or the vehicle solution in one volume of Kolliphor EL (Sigma) and 18 volumes of normal saline. All the drugs were injected intraperitoneally at doses 10 mg/g, and the injection volume was 10 ul/g of mouse weight. The drugs were injected on day 1, and the behavioral testing was performed 1 h after the injections.

3.1.3. Inflammation induction and mechanical hyperalgesia assessment

Inflammatory pain in mice was induced by injecting 30 ul of 1% lambda carrageenan (Sigma) in normal saline into the left hind paw of the mice on day 0. The mice were anesthetized by 5% isoflurane (Baxter) in the air.

The mice were habituated for 20 min before the testing in the testing chamber (10*7*10 cm, length*width*height), which was placed onto a wire floor grid (wire size 1 mm, the distance between wires 5 mm). Then, we applied a rigid plastic tip of an electronic von Frey instrument (Bioseb) to the plantar surface of the hind paw until we observed a withdrawal response and recorded the pressure in grams. Each mouse was tested five times at one-minute intervals. The testing chamber and the wire floor grid were cleaned with water and 70% isopropanol in water after each tested animal. The von Frey tests were performed on day -1 (baseline), day 0 (2 h after the carrageenan injection), day 1 (1 h after the drug injection), and day 2. Additionally, the

mice were habituated in the testing chambers one day before the first (baseline) measurement was performed.

3.1.4. Behavioral data analysis

Withdrawal thresholds from five trials of the same mouse were averaged, and the resulting data are presented as means ± standard error of the mean (SEM). Because the datasets did not meet the criteria for a multifactorial analysis of variance (ANOVA) (the distribution different from normal in Shapiro-Wilk test, unequal variances in Bartlett test, and contained outliers determined by boxplot methods), we applied the aligned rank transformation (ART) (Wobbrock et al., 2011) and then conducted a repeated measures analysis of variance on linear models built from the transformed data. Significant interactions were further subjected to the Wilcoxon post hoc test with BH p adjustment method. The data analysis was performed using R 4.0.5 in R studio 1.4.1106 for Windows, involving libraries ARTool, rstatix, stats. The graphs were created in GraphPad Prism 9.4.1 for Windows. Throughout the study, the following confidence thresholds were used: * $p < 0.05$, ** $p < 0.01$, *** $p < 0.001$.

3.2 Materials and methods specific for aim 2

3.2.1. Tissue collection

Brain tissue was obtained from decapitated C57Bl/NCrl mice. The animals were handled in a manner that avoids distress, and they were decapitated in a way that minimizes suffering; these procedures followed local laws, Guide for the Care and Use of Laboratory Animals, National Research Council (US) Committee for the Update of the Guide for the Care and Use of Laboratory Animals, and Directive 2010/63/EU.

3.2.2. Complementary DNA synthesis

To obtain RNA samples, we dissected the whole brain or prefrontal cortex (PFC), hippocampus (HC), and cerebellum (CB) and used the TRIzol Plus RNA purification kit (Invitrogen, US) according to the manufacturer's instructions. Then, we used 5 µg of the obtained RNA in a reverse transcription reaction with 300 units (U) of SuperScript III reverse transcriptase, 2.5 µg of an anchored oligo$(dT)_{20}$ primer, 0.5 mM of dATP, dGTP, dCTP, and dTTP each and 5 mM dithiothreitol (DTT) in 20 µL volume (all from Invitrogen, US). Primer hybridization was at 65 °C for 5 min, followed by incubation at 4 °C for at least 1 min. First-

strand complementary DNA (cDNA) synthesis was performed at 50 °C for 30 min, then at 55 °C for 30 min, followed by the enzyme inactivation at 70 °C for 15 min. We used 1/40 of the reverse transcription reaction volume for cDNA amplification reaction.

3.2.3. Cloning, clone selection, and subcloning into eukaryotic expression vectors

We amplified the *Sgip1* cDNA using Phusion High-Fidelity DNA polymerase (Thermo Scientific, Lithuania) with the primers annealing to the first and last exons of the *Sgip1* gene (Primers A and J in Table 1). The polymerase chain reaction (PCR) contained 0.2 U of the polymerase, 0.2 mM of dATP, dGTP, dCTP, and dTTP each, and 0.2 mM of each primer in 10 µL volume. The primer sequences are provided in Table 1. For amplification, initial denaturation was at 98 °C, 30 s, followed by 30 cycles of denaturation at 98 °C, 30 s; annealing at 57.5 °C, 30 s and extension at 72 °C, 60 s each; the reaction ended with a final extension at 72 °C, 7 min.

Table 1. The oligonucleotide primers used in the study.

Primer	Sequence (5'-3')	Internal ID
A	GGATCCGTGCCACCATGATGGAAG	1271
B	CCATTTGGTGCCCCATTGC	1282
C	CAATGGGGCACCAAATGG	1283
D	ACTTGGGTTCATCGGTTGG	1284
E	CAGGCCAACCGATGAACC	830
F	AGGAGTGTATGGGTGGGCT	831
G	TTCAATATCGTCAACTAACTCACTG	832
H	GAAAGCTGCTGCGACCG	1286
I	CACAGAAACTGTCAACGC	1287
J	TTAGTTATCTGCCAAGTACTTTC	1272

Table 2. PCR conditions for the primer pairs used in the study.

Primer pair	Initial denaturation	30 cycles of:			Final extension
		Denaturation	Annealing	Extension	
A+B	98°C, 2 min	98°C, 30 s	60°C, 30 s	72°C, 30 s	72°C, 5 min
C+D			59°C, 30 s	72°C, 40 s	
E+F			61°C, 30 s	72°C, 60 s	
G+H			60°C, 30 s	72°C, 40 s	
I+J			56°C, 30 s	72°C, 60 s	
A+J			58°C, 30 s	72°C, 3 min	

Next, we purified the PCR products from 1.5% agarose gel using the QIAquick gel extraction kit (QIAGEN). To prepare the PCR products for TA cloning, we added single A-overhangs to the products using 10 U of GoTaq G2 DNA polymerase, 2 mM dATP (both from Promega) in 10 µL volume and incubated the reaction at 72 °C for 7 min. Then, we ligated the A-tailed products with pGEM-T Easy vector using T4 DNA ligase (3 U) (both from Promega) in 10 µL volume. Last, we transformed chemically competent *E.coli* DH5α cells (New England Biolabs) with the ligation reaction and spread the cells on Luria-Bertani (LB)-agar plates with 0.5 mM IPTG (Sigma) and 80 µg/mL X-Gal (Duchefa Biochemie) for blue-white colony screen.

For screening, we purified plasmid DNA from single white colonies propagated in LB medium containing 100 µg/mL ampicillin using the QIAprep Miniprep kit (QIAGEN) and digested the plasmid DNA with restriction enzymes EcoRI or EcoRI and XagI (Fermentas). Finally, the selected plasmids were sequenced by the dideoxy chain termination method (Eurofins Genomics).

To express Sgip1 splice isoforms in human embryonic kidney 293 (HEK293) cells, we transferred the coding sequence of the *Sgip1* splice variants from pGEM-T Easy vectors into pRK5 and pRK5-EYFP vectors. First, we released the insert from the pGEM-T Easy vector by digestion with BamHI and SalI (Fermentas) and purified it from 1.0% agarose gel using the QIAquick gel extraction kit (QIAGEN). Next, we ligated the inserts with the linearized pRK5 or pRK5-EYFP vectors using 0.5 U of T4 DNA ligase (Invitrogen) in 10 µL volume. The pRK5

vector expresses untagged Sgip1 splice isoforms, and the pRK5-EYFP vector expresses the splice variants N-terminally tagged with EYFP with a Trp-Ile-Arg linker.

3.2.4. Polymerase chain reaction

To confirm the presence of *Sgip1* splice variant mRNAs in the brain, we amplified 1/40 of the reverse transcription reaction from mouse brain cDNA using primers annealing to different exons within the *Sgip1* sequence. The reaction contained GoTaq G2 Green Master Mix 1x (Promega) and 0.2 mM of each primer in 10 µL volume. To amplify the complete coding sequence of *Sgip1* from different brain regions, we used 1/40 of the cDNA synthesis reactions involving the RNA from PFC, HC, and CB with GoTaq G2 Green Master Mix using primes A and J. The primer sequences are provided in Table 1, and the amplification parameters for different primer pairs are provided in Table 2. The PCR products were resolved in 1.5% agarose gel stained with 0.2 µg/mL ethidium bromide (Top-Bio) and visualized under UV light (Bio-Rad Universal Hood II).

3.2.5. Oligonucleotide primer design and database search

We used SnapGene 5.3 and PerlPrimer v1.1.21 (Marshall, 2004) for primer design and analysis. Primer sequences were designed to minimize hybridization with regions of single nucleotide polymorphisms in the *Sgip1* gene from the Ensembl database (Howe et al., 2021). Oligonucleotide primers were custom-synthesized by Sigma. To search the possible *Sgip1* transcripts, we used NCBI, Uniprot, and Ensembl databases. For multiple sequence alignment, we used CLUSTAL O (1.2.4) (Madeira et al., 2022).

3.2.6. Microscopy and image processing

Human Embryonic Kidney 293 (HEK293) cells were cultured in DMEM – high glucose (Sigma) supplemented with 10% fetal bovine serum (Gibco) at 37 °C and 5% CO_2 in air and humidity of 95%. HEK293 cells grown on 18-mm glass coverslips were transfected with plasmid DNA encoding *Sgip1* splice variants using the calcium phosphate method. The plasmid DNA (1.2 µg) was mixed with 6.2 µL of 2 M $CaCl_2$ in a total volume of 50 µL, followed by the addition of the equal volume of 2x HBS (42 mM HEPES, 1.4 mM Na_2HPO_4, 274 mM NaCl, 10 mM KCl, 15 mM D-glucose, pH 7.05) and vigorous mixing. After 5 min of incubation, the transfection solution was added to the cells. The cells 24 h post-transfection were fixed in 4%

paraformaldehyde in PBS (137 mM NaCl, 2.7 mM KCl, 8 mM Na_2HPO_4, 1.8 mM KH_2PO_4) for 15 min, then washed four times with PBS, rinsed with distilled water, dried and mounted in Fluoroshield mounting medium with DAPI (Sigma). Microscopy was performed on the Leica TCS SP8 confocal microscope using HC PL APO 63x/1.40 OIL objective and 2x digital zoom, resulting in a pixel size of 71 nm. The EYFP was excited with a 488 nm solid-state laser, and the EYFP emission was detected in a range of 498–542 nm using the HyD detector at 50% gain. The images in a Z-plane were taken with a step of 0.299 μm. The microscopic images were processed in Fiji distribution of ImageJ 1.53c (Schindelin et al., 2012). Z-stacks were projected using maximum intensity projection. Image adjustments, including brightness and contrast change, were applied to the whole area of the image.

3.2.7. Antibodies

The polyclonal guinea pig anti-Sgip1 antibody was described previously (Hajkova et al., 2016). In this study, we used the affinity-purified fraction of this antibody by the SulfoLink Coupling Resin (Thermo Scientific). The peptide used for the purification was identical to the one used for the immunization (N-terminal 27 aa followed by cysteine: MMEGLKKRTRKAFGIRKKEKDTDSTGSC). The mouse monoclonal anti-Sgip1 antibody, clone 7G9/B6/G3, was generated in-house by hybridoma technology against the same peptide that was used for the production of the guinea pig anti-Sgip1 antibody. This monoclonal antibody was represented by IgG1 fraction and was characterized by immunoblotting against brain lysates from the wild-type and *Sgip1* knock-out mice (Figure 12B).

The mouse anti-β-tubulin antibody, clone KMX-1, was described previously (Birkett et al., 1985). The rabbit anti-ubiquitin antibody was from Sigma, USA (ref U0508). The horseradish peroxidase (HRP)-conjugated goat anti-guinea pig antibody was from Santa Cruz Biotechnology, USA (ref. c-2438). The goat anti-mouse HRP-conjugated antibody (ref. W402B) and the goat anti-rabbit HRP-conjugated antibody (ref W401B) were from Promega, USA.

3.2.8. Protein sample preparation, protein dephosphorylation, and immunoblot analysis

The samples from the prefrontal cortex, hippocampus, and cerebellum were homogenized in radioimmunoprecipitation assay (RIPA) buffer (50 mM Tris-HCl, 150 mM NaCl, 1% Triton

X-100, 0.5% sodium deoxycholate, 0.1% sodium dodecyl sulfate (SDS), pH 8.0) supplemented with protease inhibitor cocktail (Roche) and incubated with equal volumes of treatment buffer (125 mM Tris-HCl, 4% SDS, 20% glycerol, 0.02% bromophenol blue, 400 mM DTT, pH 6.8) for 5 min at 80 °C.

For protein dephosphorylation, the prefrontal cortex tissue was homogenized in the supplemented RIPA buffer without sodium deoxycholate and SDS. Then, 850 ug of protein was incubated with 5 U of shrimp alkaline phosphatase (SAP) (Fermentas) in 100 µL volume for 1 h at 37 °C. The reaction was terminated by the addition of equal volumes of treatment buffer and incubation at 80 °C for 10 min. Sgip1 was immunoprecipitated as in the following section, after which the samples were mixed with the treatment buffer and incubated at 80 °C for 10 min.

The protein samples were separated in SDS-polyacrylamide gel (SDS-PAGE) and transferred onto a nitrocellulose membrane (Schleicher & Schuell) using the Trans-Blot Turbo Transfer System (Bio-Rad, Singapore). The membranes were blocked in 5% powdered milk in PBST (137 mM NaCl, 2.7 mM KCl, 8 mM Na_2HPO_4, 1.8 mM KH_2PO_4, 0.1% Tween 20) overnight at 4 °C. Then, the membranes were incubated with one of the primary antibodies as indicated. The guinea pig anti-Sgip1 antibody was diluted 1:500 to a final concentration of 0.0008 mg/mL in 2% milk in PBST and incubated for 3 h at 4 °C. The supernatant of the mouse anti-Sgip1 antibody-producing hybridoma was incubated with the membranes for 3 h at 4 °C. The anti-β-tubulin antibody was diluted 1:200 in 1% milk in PBST and incubated overnight at 4 °C. The anti-ubiquitin antibody was diluted 1:1000 in 2% milk in PBST and incubated for 3 h at 4 °C. After washing in PBST three times 15 min each, the membranes were incubated with the secondary antibody. The HRP-conjugated goat anti-guinea pig antibody diluted 1:5000 in 0.5% milk in PBST. The HRP-conjugated goat anti-mouse antibody and the HRP-conjugated goat anti-rabbit antibody were diluted 1:10 000 in 1% milk in PBST and incubated for 1 h at room temperature. The blots were visualized using SuperSignal West Pico or Femto chemiluminescent substrates (Thermo Fisher Scientific, USA) and detected on the Alliance Q9 Atom system (Uvitec, UK).

3.2.9. Mass spectrometry sample preparation and immunoprecipitation

Brain tissue was prepared for mass spectrometry (MS) analysis according to the following protocol. The samples were homogenized and lysed by boiling at 95 °C for 10 min in 100 mM

triethylamonium bicarbonate (TEAB) containing 2% sodium deoxycholate (SDC), 40 mM chloroacetamide, 10 mM tris(2-carboxyethyl)phosphine (TCEP) and further sonicated (Bandelin Sonoplus Mini 20, MS 1.5). Protein concentration was determined using bicinchoninic acid (BCA) protein assay kit (Thermo Fisher Scientific), and 30 µg of protein per sample was used for MS sample preparation. The samples were further processed using SP3 beads, according to Hughes et al. (Hughes et al., 2019). Briefly, 5 µL of SP3 beads was added to 30 µg of protein in TEAB lysis buffer and filled to 50 µL with 100 mM TEAB. Protein binding was induced by the addition of ethanol to 60% (vol./vol.) final concentration. The samples were then mixed and incubated for 5 min at room temperature. After binding, the tubes were placed into a magnetic rack, and the unbound supernatant was discarded. Beads were subsequently washed two times with 180 µL of 80% ethanol. After washing, the samples were digested with trypsin (trypsin/protein ratio 1/30) and reconstituted in 100 mM TEAB at 37 °C overnight. After the digestion, the samples were acidified with trifluoroacetic acid (TFA) to 1% final concentration, and peptides were desalted using in-house-made stage tips packed with C18 disks (Empore) according to (Rappsilber et al., 2007).

Sgip1 splice isoforms were immunoprecipitated from the brain tissue and prepared for mass spectrometry as follows. Per sample, we used 20 µL of Protein A/G agarose beads slurry (Thermo Scientific), which was washed two times with Buffer A (100 mM NaCl, 20 mM Tris-HCl, 0.1% Triton X-100, pH 7.4) and resuspended in 980 µL of Buffer A. Afterwards, 1 mL of beads slurry was incubated overnight with 2 µL of the anti-Sgip1 antibody (Hajkova et al., 2016) that was affinity purified as described above. The following day, mouse brain tissue was isolated and homogenized at 5 mg/mL of total protein in Buffer A containing protease inhibitor cocktail (Roche) and 1% CHAPS (3-[(3-cholamidopropyl) dimethylammonio]-1- propanesulfonate) and incubated on ice for 30 min followed by centrifugation at 100 000 g for 1 h. Meanwhile, the antibody-conjugated beads were washed three times with Buffer A and subsequently blocked by 1 h incubation in Buffer A containing 1 mg/mL bovine serum albumin (BSA). Next, the brain sample supernatant was diluted 1:10 with Buffer A, and 1 mL of the diluted sample was mixed with the Protein A/G beads and incubated in a sample mixer at 4 °C for 2 h. After the incubation, the beads were washed three times with Buffer A, followed by additional three washes with PBS. Next, the bead samples were resuspended in 100 mM triethylammonium bicarbonate (TEAB) containing 2% sodium deoxycholate (SDC). Cysteines were reduced with a 10 mM final concentration of Tris(2-carboxyethyl)phosphine (TCEP) and blocked with a 40 mM final

concentration of chloroacetamide (60 °C for 30 min). The samples were cleaved on the beads with 1 µg of trypsin at 37 °C overnight. After the digestion, the samples were centrifuged, and the supernatants were collected and acidified with TFA to 1% final concentration. SDC was removed by extraction of ethyl acetate (Masuda et al., 2008). Peptides were desalted using in-house-made stage tips packed with C18 disks (Empore), according to Rappsilber et al. (Rappsilber et al., 2007).

3.3. Materials and methods common for aims 2 and 3

3.3.1. Chemicals

Stock solutions of 50 mM WIN 55,212-2 mesylate (WIN) (Tocris), 100 mM (9S)-HHC, and 100 mM (9R)-HHC were prepared in dimethyl sulfoxide (DMSO) and of 100 mM Δ^9-tetrahydrocannabinol (THC) was prepared in ethanol. THC, (9S)-HHC, and (9R)-HHC was provided by Dr. Martin Kuchar, UCT Prague. The IUPAC names of hexahydrocannabinol epimers (9S)-HHC and (9R)-HHC are (9S)-6,6,9-trimethyl-3-pentyl-6*a*,7,8,9,10,10*a*-hexahydro-6H-benzo[c]chromen-1-ol and (9R)-6,6,9-trimethyl-3-pentyl-6*a*,7,8,9,10,10*a*-hexahydro-6H-benzo[c]chromen-1-ol, respectively. The stock solutions were further diluted in their vehicles by the factor of 10 to obtain their concentrations in the range 0.001 nM - 10 mM (10^{-12} M - 10^{-5} M). The stock solutions of met-enkephalin and carbamoylcholine chloride (carbachol) (Sigma) were prepared in water.

3.3.2. Cell culture and transfection

HEK293 cells were cultured in Dulbecco's Modified Eagle's Medium (DMEM) – high glucose (Sigma) supplemented with 10% fetal bovine serum (Gibco) at 37 °C, 5% CO_2 in the air, and 95% humidity. The cells were plated in the 96-well plates (Greiner BioOne, UK) at 50 000 cells per well and transfected with 150 ng of plasmid DNA per well using Lipofectamine 2000 (Invitrogen) according to the manufacturer's instructions. The transfected cells were tested 24 h after transfection.

3.3.3. Bioluminescence resonance energy transfer assay

Bioluminescence resonance energy transfer (BRET) assay was used to measure CB1R-induced G protein dissociation and beta-arrestin interaction with CB1R, as described previously (Hajkova et al., 2016; Gazdarica et al., 2021). To measure G protein dissociation, we transfected

the cells with $G\alpha_{i1}$-Rluc8 or $G\alpha_{oA}$-Rluc8, $G\beta_2$-Flag, $G\gamma_2$-EYFP, and SNAP-CB1R plasmids in a mass ratio of 1:1:1:2. To measure β-arrestin 2 interaction with CB1R, we transfected the cells with β -arrestin2-Rluc and CB1R-YFP plasmids in a mass ratio of 1:2. To study GRK3-CB1R interaction, the cells were transiently transfected with GRK3-Rluc8 and CB1R-YFP plasmids (1:2 ratio). Before the measurements, the transfected cells were washed with PBS (137 mM NaCl, 2.7 mM KCl, 8 mM Na_2HPO_4, 1.8 mM KH_2PO_4) and incubated in Tyrode's solution (137 mM NaCl, 0.9 mM KCl, 1 mM $MgCl_2$, 1 mM $CaCl_2$, 11.9 mM $NaHCO_3$, 3.6 mM NaH_2PO_4, 5.5 mM D-glucose, 25 mM HEPES, pH 7.4) at 37 °C for at least 30 min. Next, we added coelenterazine h (NanoLight) at a final concentration of 5 μM to the cells, followed by the addition of increasing concentrations of compounds (9S)-HHC, (9R)-HHC, THC, WIN, or their vehicles. The BRET donor and acceptor emission was measured 12 minutes after the addition of the compounds using Mithras LB940 plate reader (Berthold Biotechnologies, Germany). For enhanced bystander BRET measurements, we transfected the cells with rGFP-CAAX and RlucII-tagged cannabinoid receptor 1 (CB1R), μ opioid receptor (MOR), and muscarinic acetylcholine M3 receptor (M3R) in a mass ratio of 6:1. Next, we added coelenterazine Prolume Purple (NanoLight) to a final concentration of 1 μM, and the transfected cells were stimulated with 1 μM WIN 55,212-2 (WIN), 10 μM met-enkephalin, or 10 μM carbachol, respectively. The BRET donor and acceptor emission was measured for 1 hour after the addition of the compounds using the Spark microplate reader (Tecan).

3.3.4. BRET data analysis

The BRET ratio was obtained by dividing the acceptor emission (540 ± 20 nm) by the donor emission (480 ± 10 nm). After subtracting the BRET ratio of the vehicle addition from the BRET ratio of the compounds, we obtained deltaBRET (ΔBRET). Data analysis was performed using GraphPad Prism 9.3.1 for Windows (GraphPad Software, USA). The dose-response curves were fitted using the non-linear regression function. The model used for fitting the data was Y=Bottom + (Top-Bottom)/(1+10^((LogEC50-X))), assuming the Hill slope of 1.0. The radar charts were created in R 4.0.5 in R studio 1.4.1106 for Windows using the fmsb package.

4. RESULTS

4.1. The effect of Sgip1 on chronic pain processing

4.1.1. Induction of chronic pain model in mice

We previously found that *Sgip1* deletion reduces acute nociception and increases the potency of analgesics in acute pain (Dvorakova et al., 2021). We then asked if *Sgip1* deletion modifies chronic nociception. The nociception pathways may become altered due to overstimulation in chronic pain, which may alter the effect of Sgip1 on nociception. To test the effect of *Sgip1* deletion on chronic nociception, we induced chronic inflammatory pain in the hind paw of wild-type and *Sgip1* knock-out mice and evaluated the mechanical sensitivity in these mice. Inflammation was induced by carrageenan injection in the hind paw, which caused edema, hyperalgesia, and mechanical allodynia. Hyperalgesia is an increased sensitivity to a painful stimulus, and mechanical allodynia is an increased sensitivity to a mechanical stimulus (such as touch) that normally does not cause pain. We measured the sensitivity of the mice to mechanical stimulation by applying the rigid tip of the electronic von Frey apparatus.

To evaluate the changes in mechanical nociception in the mice after the carrageenan injection, we applied the following scheme. On day -1, we measured the baseline responses in all the mice. On day 0, we injected carrageenan or vehicle (saline) in one hind paw and measured the mechanical sensitivity 2 h after the injection. We then repeated the measurements until 3 days after the injection to monitor the course of inflammation.

Carrageenan injection caused a decrease in the withdrawal threshold of the paw, reflecting increased sensitivity to the mechanical stimulation 2 h after the injection. This decrease in paw withdrawal threshold persisted for two days after the injection, which is characteristic of carrageenan-induced inflammation. Vehicle injection did not affect the mechanical sensitivity. In male mice, the paw withdrawal threshold of *Sgip1* knock-out mice was significantly lower ($p = 0.0317$ on Day 1 after the carrageenan injection) than that of wild-type mice, and this difference persisted throughout the course of the inflammation (Figure 7A).

Because vehicle injection did not affect the paw withdrawal threshold of the male mice, we injected the female mice with carrageenan only. We found that in the female mice, the paw withdrawal threshold of *Sgip1* knock-out mice was not different from that of wild-type mice (Figure 7B).

There were no differences between *Sgip1* knock-out and wild-type mice before inducing the inflammation (on Day -1) or at the end of the experiment (on Day 3). In sum, we detected the nociceptive effect of *Sgip1* deletion in male but not in female mice.

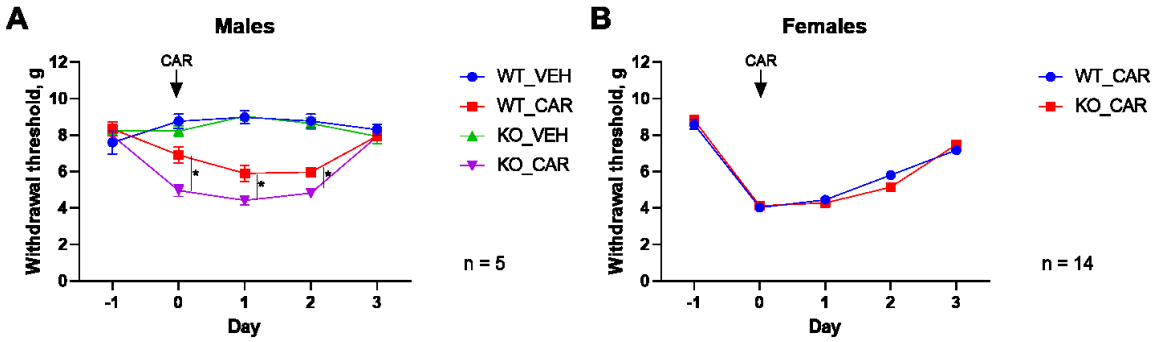

Figure 7. The effect of *Sgip1* deletion on mechanical sensitivity in male (A) and female (B) mice. The baseline mechanical sensitivity of the left hindpaw of wild-type (WT) and *Sgip1* knock-out (KO) mice was determined on day -1, and carrageenan (CAR) was injected into the left hindpaw on day 0. Mechanical thresholds of the left hindpaw were measured on days 0, 1, 2, and 3. Each point is the mean ± SEM of 5 (male) or 14 (female) mice. The statistical analysis of the data is presented in Table 3. * $p < 0.05$.

4.1.2. The effects of cannabinoids on chronic pain sensitivity in *Sgip1* knock-out and wild-type mice

Injections of cannabinoids WIN 55,212-2 (WIN) and Δ^9-tetrahydrocannabinol (THC) increased the paw withdrawal threshold in carrageenan-treated wild-type and *Sgip1* knock-out mice. However, the antinociceptive effect of the drugs varied depending on the genotype, sex, and drug.

WIN injection in males increased the threshold of *Sgip1* knock-out mice by 77% and that of wild-type mice by 91%. The threshold of WIN-treated *Sgip1* knock-out males was significantly lower ($p = 0.0232$) than that of wild-type males (Figure 8A). WIN injection in females increased the threshold of *Sgip1* knock-out mice by 75% and that of wild-type mice by 96%. However, the threshold of WIN-treated *Sgip1* knock-out females was similar to that of wild-type females (Figure 8B).

After THC injections, the mechanical thresholds of male mice followed a pattern similar to the WIN injections. THC in males led to a 63% increase in the threshold of *Sgip1* knock-out

mice and a 55% increase in wild-type mice. The threshold of THC-treated *Sgip1* knock-out males was significantly higher ($p = 0.00376$) than that of wild-type males (Figure 9A). THC treatment of females led to a 60% increase in the threshold of *Sgip1* knock-out mice and only a 28% increase in wild-type mice. As a result, the threshold of THC-treated *Sgip1* knock-out females was significantly higher ($p = 0.00935$) than that of wild-type females (Figure 9B). In sum, while the antinociceptive effect of WIN was lower in *Sgip1* knock-out mice, the effect of THC was higher in *Sgip1* knock-out mice.

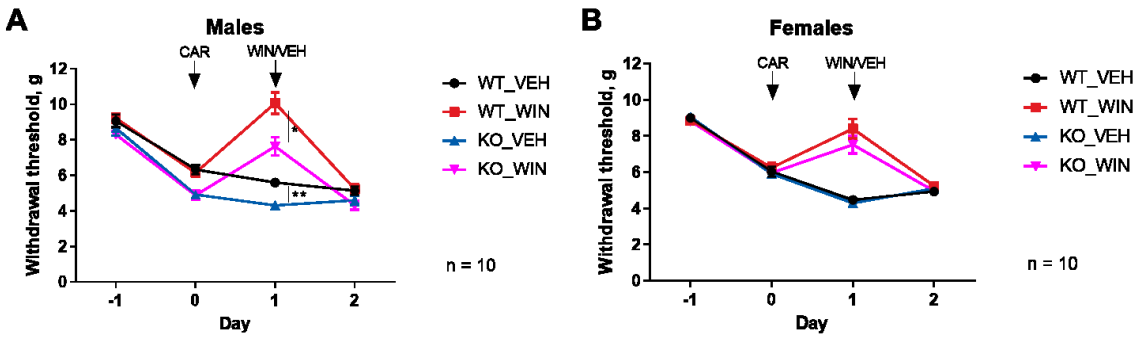

Figure 8. The effect of WIN 55,212-2 (WIN) and the deletion of *Sgip1* on mechanical sensitivity in male (A) and female (B) mice. The baseline mechanical sensitivity of the left hindpaw of wild-type (WT) and *Sgip1* knock-out (KO) mice was determined on day -1, carrageenan (CAR) was injected into the left hindpaw on day 0, and 10 mg/kg WIN or vehicle (VEH) was injected i.p. on day 1. Mechanical thresholds of the left hindpaw were measured on days 0, 1, 2, and 3. Each point is the mean ± SEM of 10 mice. The statistical analysis of the data is presented in Table 3. * $p < 0.05$, ** $p < 0.01$.

WIN is a cannabinoid that can activate both CB1R and CB2R. CB1R expression is restricted to neuronal tissues, and CB2R expression is often associated with peripheral tissues and inflammation. Therefore, both CB1R and CB1R may mediate nociception. We thus tested whether CB2R affects chronic pain sensitivity by application of CB1R-specific reverse agonist rimonabant. We found that rimonabant injection, but not the vehicle, completely abolished the antinociceptive effect of WIN in wild-type and *Sgip1* knock-out mice (Figure 10). These data indicate that the antinociceptive effect of cannabinoids on chronic nociception is mediated through activation of CB1R.

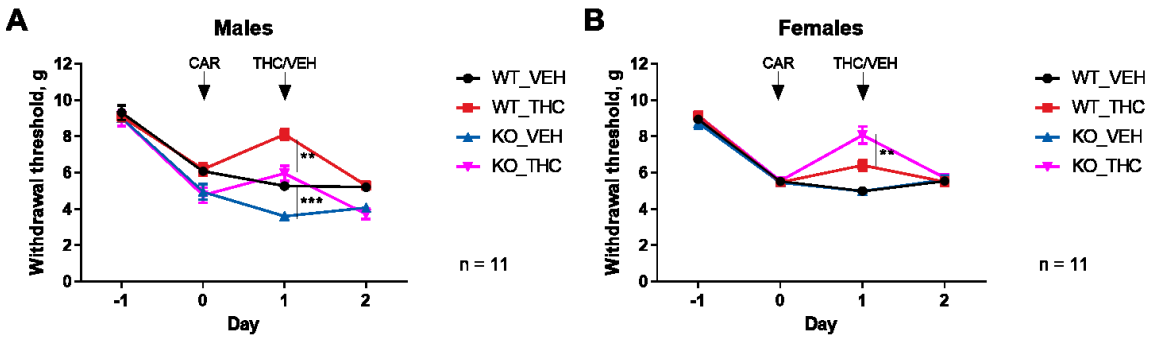

Figure 9. The effect of Δ^9-tetrahydrocannabinol (THC) and the deletion of *Sgip1* on mechanical sensitivity in male (A) and female (B) mice. The baseline mechanical sensitivity of the left hindpaw of wild-type (WT) and *Sgip1* knock-out (KO) mice was determined on day -1, carrageenan (CAR) was injected into the left hindpaw on day 0, and 10 mg/kg THC or vehicle (VEH) was injected i.p. on day 1. Mechanical thresholds of the left hindpaw were measured on days 0, 1, 2, and 3. Each point is the mean ± SEM of 11 mice. The statistical analysis of the data is presented in Table 3. * $p < 0.05$, ** $p < 0.01$, *** $p < 0.001$.

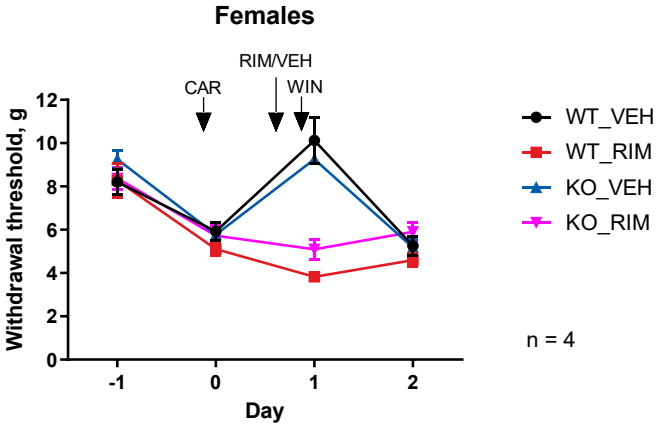

Figure 10. The effect of rimonabant (RIM) application on WIN-induced antinociceptive effect in *Sgip1* knock-out and wild-type female mice. Baseline mechanical sensitivity of the left hindpaw of wild-type (WT) and *Sgip1* knock-out (KO) mice was determined on day -1, carrageenan (CAR) was injected into the left hindpaw on day 0, rimonabant (10 mg/kg) or vehicle (VEH) was injected i.p. 1 h before WIN injection (10 mg/kg) on day 1. Mechanical thresholds of the left hindpaw were measured on days 0, 1, 2, and 3. Each point is the mean ± SEM of 4 mice.

Table 3. Results of statistical tests performed with the data presented in Figures 7-9. Output of Analysis of Variance of Aligned Rank Transformed data and *post hoc* tests.

Figure 7A

ANOVA of ART data

		Error	Df	Df.res	F value	Pr(>F)	
1	treatment	id	1	16	68.2657	3.6398e-07	***
2	genotype	id	1	16	3.7308	0.0713282	.
3	time	Withn	4	64	14.2906	2.1713e-08	***
4	treatment:genotype	id	1	16	3.3837	0.0844735	.
5	treatment:time	Withn	4	64	46.5620	< 2.22e-16	***
6	genotype:time	Withn	4	64	4.1854	0.0045024	**
7	treatment:genotype:time	Withn	4	64	1.9877	0.1069830	

Post hoc Wilcoxon Tests

	time	treatment	.y.	group1	group2	n1	n2	statistic	p	p.signif
1	day-1	car	threshold	ko	wt	5	5	12	1	ns
2	day-1	veh	threshold	ko	wt	5	5	18	0.31	ns
3	day0	car	threshold	ko	wt	5	5	1	0.0212	*
4	day0	veh	threshold	ko	wt	5	5	6	0.206	ns
5	day1	car	threshold	ko	wt	5	5	2	0.0317	*
6	day1	veh	threshold	ko	wt	5	5	12.5	1	ns
7	day2	car	threshold	ko	wt	5	5	1	0.0159	*
8	day2	veh	threshold	ko	wt	5	5	10.5	0.753	ns
9	day3	car	threshold	ko	wt	5	5	8.5	0.451	ns
10	day3	veh	threshold	ko	wt	5	5	9	0.528	ns

Figure 7B

ANOVA of ART data

		Error	Df	Df.res	F value	Pr(>F)	
1	treatment	id	1	16	68.2657	3.6398e-07	***
2	genotype	id	1	16	3.7308	0.0713282	.
3	time	Withn	4	64	14.2906	2.1713e-08	***
4	treatment:genotype	id	1	16	3.3837	0.0844735	.
5	treatment:time	Withn	4	64	46.5620	< 2.22e-16	***
6	genotype:time	Withn	4	64	4.1854	0.0045024	**
7	treatment:genotype:time	Withn	4	64	1.9877	0.1069830	

Post hoc Wilcoxon Tests

	time	treatment	.y.	group1	group2	n1	n2	statistic	p	p.signif
1	day-1	car	threshold	ko	wt	14	14	114.	0.489	ns
2	day0	car	threshold	ko	wt	14	14	108.	0.645	ns
3	day1	car	threshold	ko	wt	14	14	81.5	0.46	ns
4	day2	car	threshold	ko	wt	14	14	45	0.0156	*
5	day3	car	threshold	ko	wt	14	14	110	0.596	ns

Figure 8A

ANOVA of ART data

		Error	Df	Df.res	F value	Pr(>F)	
1	treatment	id	1	36	24.73302	1.6304e-05	***
2	genotype	id	1	36	38.65262	3.5666e-07	***
3	time	Withn	3	108	139.15365	< 2.22e-16	***
4	treatment:genotype	id	1	36	1.41088	0.242688	
5	treatment:time	Withn	3	108	44.15148	< 2.22e-16	***
6	genotype:time	Withn	3	108	2.62320	0.054289	.
7	treatment:genotype:time	Withn	3	108	0.41406	0.743239	

Post hoc Wilcoxon Tests

	time	treatment	.y.	group1	group2	n1	n2	statistic	p	p.signif
1	day-1	veh	threshold	ko	wt	10	10	39	0.427	ns
2	day-1	win	threshold	ko	wt	10	10	20	0.0254	*
3	day0	veh	threshold	ko	wt	10	10	9.5	0.00247	**
4	day0	win	threshold	ko	wt	10	10	11.5	0.00404	**
5	day1	veh	threshold	ko	wt	10	10	7.5	0.00147	**
6	day1	win	threshold	ko	wt	10	10	19.5	0.0232	*
7	day2	veh	threshold	ko	wt	10	10	28	0.103	ns
8	day2	win	threshold	ko	wt	10	10	20	0.0254	*

Figure 8B

ANOVA of ART data

		Error	Df	Df.res	F value	Pr(>F)	
1	treatment	id	1	35	72.64078	4.6591e-10	***
2	genotype	id	1	35	5.73060	0.022165	*
3	time	id	1	35	1.40302	0.244199	
4	time	Withn	3	107	92.54406	< 2.22e-16	***
5	treatment:genotype	id	1	35	2.80984	0.102600	
6	treatment:time	Withn	3	107	53.26620	< 2.22e-16	***
7	genotype:time	Withn	3	107	1.23226	0.301670	
8	treatment:genotype:time	Withn	3	107	0.50245	0.681395	

Post hoc Wilcoxon Tests

	time	treatment	.y.	group1	group2	n1	n2	statistic	p	p.signif
1	day-1	veh	threshold	ko	wt	10	10	48.5	0.939	ns
2	day-1	win	threshold	ko	wt	10	10	46	0.79	ns
3	day0	veh	threshold	ko	wt	10	10	36	0.306	ns
4	day0	win	threshold	ko	wt	10	10	39	0.427	ns
5	day1	veh	threshold	ko	wt	10	10	34.5	0.254	ns
6	day1	win	threshold	ko	wt	10	10	30	0.139	ns
7	day2	veh	threshold	ko	wt	9	10	48.5	0.805	ns
8	day2	win	threshold	ko	wt	10	10	38	0.384	ns

Figure 9A

ANOVA of ART data

		Error	Df	Df.res	F value	Pr(>F)	
1	treatment	id	1	40	8.49489	0.0058077	**
2	genotype	id	1	40	41.17426	1.2271e-07	***
3	time	Withn	3	120	127.76672	< 2.22e-16	***
4	treatment:genotype	id	1	40	0.95422	0.3345188	
5	treatment:time	Withn	3	120	26.47673	3.2586e-13	***
6	genotype:time	Withn	3	120	7.89709	7.4971e-05	***
7	treatment:genotype:time	Withn	3	120	0.19474	0.8998067	

Post hoc Wilcoxon Tests

	time	treatment	.y.	group1	group2	n1	n2	statistic	p	p.signif
1	day-1	thc	threshold	ko	wt	11	11	55	0.742	ns
2	day-1	veh	threshold	ko	wt	11	11	59	0.948	ns
3	day0	thc	threshold	ko	wt	11	11	23	0.0151	*
4	day0	veh	threshold	ko	wt	11	11	32.5	0.0702	ns
5	day1	thc	threshold	ko	wt	11	11	16	0.00376	**
6	day1	veh	threshold	ko	wt	11	11	1	0.000104	***
7	day2	thc	threshold	ko	wt	11	11	15	0.0031	**
8	day2	veh	threshold	ko	wt	11	11	15.5	0.00342	**

Figure 9B

ANOVA of ART data

		Error	Df	Df.res	F value	Pr(>F)	
1	treatment	id	1	40	28.7161	3.7521e-06	***
2	genotype	id	1	40	2.2449	0.141908	
3	time	Withn	3	120	81.3262	< 2.22e-16	***
4	treatment:genotype	id	1	40	4.9335	0.032067	*
5	treatment:time	Withn	3	120	20.6899	7.1433e-11	***
6	genotype:time	Withn	3	120	3.6419	0.014763	*
7	treatment:genotype:time	Withn	3	120	2.0983	0.104051	

Post hoc Wilcoxon Tests

	time	treatment	.y.	group1	group2	n1	n2	statistic	p	p.signif
1	day-1	thc	threshold	ko	wt	11	11	64	0.843	ns
2	day-1	veh	threshold	ko	wt	11	11	42	0.236	ns
3	day0	thc	threshold	ko	wt	11	11	54	0.693	ns
4	day0	veh	threshold	ko	wt	11	11	54	0.693	ns
5	day1	thc	threshold	ko	wt	11	11	100.	0.00935	**
6	day1	veh	threshold	ko	wt	11	11	60.5	1	ns
7	day2	thc	threshold	ko	wt	11	11	75	0.357	ns
8	day2	veh	threshold	ko	wt	11	11	57.5	0.869	ns

4.2. Identification and characterization of *Sgip1* splice variants in the brain

4.2.1. Expression patterns of Sgip1 in the brain

Several Sgip1 protein isoforms have been reported in different studies to date. These isoforms likely result from the alternative splicing of the *Sgip1* gene. The Sgip1 isoforms include proteins containing 806 aa, 854 aa (termed Sgip1α), 826 aa, and 660 aa (termed Sgip1β) (Li et al., 2011; Hajkova et al., 2016; Lee et al., 2019; Fletcher-Jones et al., 2023). We discriminate Sgip1 splice isoforms by their amino acid length, resulting in isoforms Sgip1 806, Sgip1 854, Sgip1 826, and Sgip1 660. These variants were studied separately from other variants, and only one study attempted to compare two of the variants (Lee et al., 2021). The relative abundances of the variants in the brain are unknown. In addition, a classification of *Sgip1* splice variants is needed due to the gradual discovery of other *Sgip1* splice variants.

In our previous experiments, the anti-Sgip1 antibody stained two immunoreactive bands in the immunoblot of different brain samples. We therefore analyzed samples prepared from the mouse prefrontal cortex (PFC), hippocampus (HC), and cerebellum (CB) by immunoblotting that employs the anti-Sgip1 antibody. The anti-Sgip1 antibody recognized two immunoreactive bands in the PFC and HC samples and one band in the CB sample (Figure 11A). The upper immunoreactive band was intensively stained and corresponded to a molecular weight of approximately 130 kDa. The bottom band was weakly stained and corresponded to 110 kDa. The staining intensity of the bottom band varied between the samples and was undetectable in

the CB sample. The equal protein loading was confirmed by the anti-tubulin antibody. The two bands in the immunoblot results represent specific Sgip1 binding because the anti-Sgip1 antibody does not stain samples from the brain of *Sgip1* knock-out mice (Dvorakova et al., 2021). Post-translational modifications, such as phosphorylation and ubiquitination, may distort the migration pattern of proteins. Dephosphorylation of the protein sample altered the migration pace of Sgip1 (Figure 12A), but ubiquitin did not precipitate with Sgip1 from the detergent-soluble fraction of the PFC tissue (Figure 12B). These results indicate that in the brain, Sgip1 protein is phosphorylated but is not ubiquitinated.

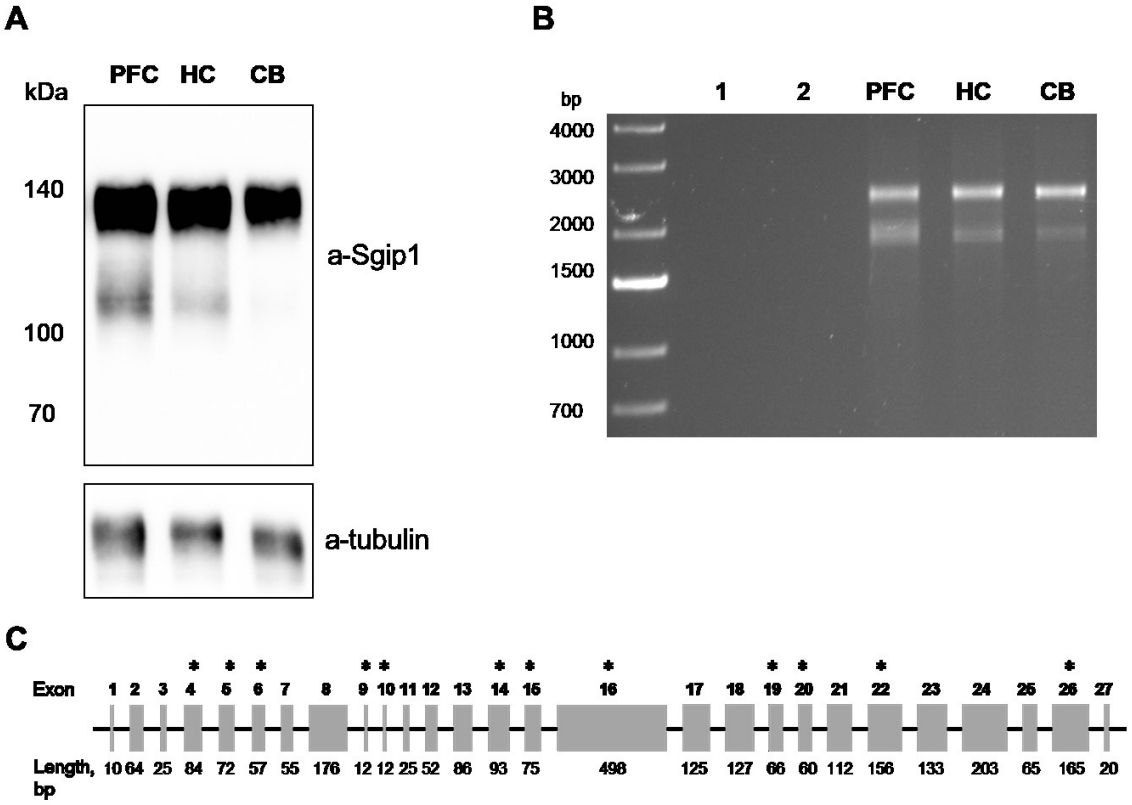

Figure 11. Expression patterns of *Sgip1* in the mouse brain. (A) The samples from the mouse prefrontal cortex (PFC), hippocampus (HC), and cerebellum (CB) were resolved in the SDS-PAGE and probed with the anti-Sgip1 antibody. (B) The full-length *Sgip1* sequence was amplified in the RT-PCR using RNA obtained from the PFC, HC, and CB and resolved in an agarose gel. Similar to the western blot pattern in Figure 11A, the PCR products were concentrated in two bands. 1 - no PCR template control, 2 - no RT control. (C) The mouse *Sgip1* gene contains 27 exons, several of which allow in-frame deletion, preserving the reading frame when these exons are omitted during splicing. These exons allow the expression of *Sgip1* splice variants, and these exons are marked with an asterisk (*).

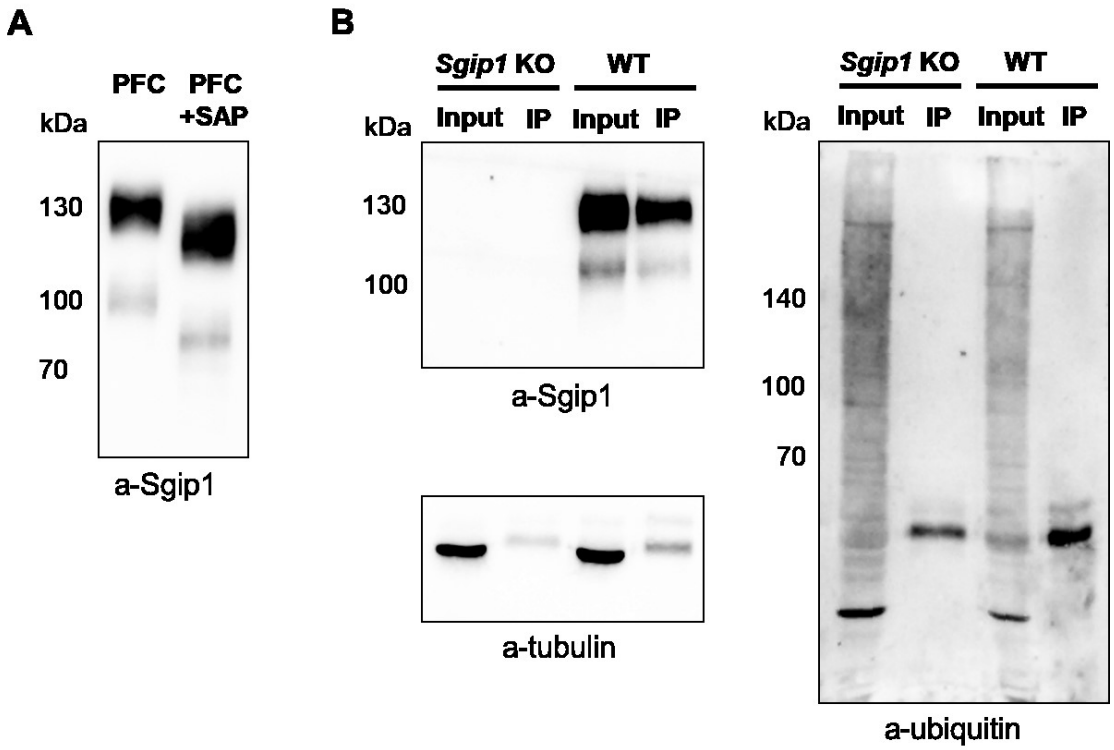

Figure 12. Post-translational modifications of Sgip1. (A) The sample from the prefrontal cortex (PFC) was treated with shrimp alkaline phosphatase (SAP), resolved in SDS-PAGE, and probed with the anti-Sgip1 antibody. The dephosphorylation substantially altered the migration pace of Sgip1. (B) Sgip1 was immunoprecipitated from the detergent-soluble fraction of the PFC tissue from *Sgip1* knock-out (KO) and wild-type (WT) mice, resolved in the SDS-PAGE, and probed with the in-house-developed monoclonal anti-Sgip1 antibody (left panel) or anti-ubiquitin antibody (right panel).

Next, we investigated the pattern of the transcripts of the *Sgip1* gene. For this purpose, we obtained RNA samples from the same brain regions (PFC, HC, and CB) and synthesized cDNA. We then amplified the full-length *Sgip1* sequence by employing primers annealing to the first and last exons of the *Sgip1* gene. The PCR was used to detect *Sgip1* transcripts in a qualitative manner. Amplification of *Sgip1* cDNA resulted in products concentrated in two bands in the agarose gel (Figure 11B). This amplification pattern is similar to the immunoblot pattern presented in Figure 11A. However, unlike in the immunoblot of the sample derived from the CB, the bottom band was still detectable after the amplification of cDNA from this region.

Based on the immunoblot and amplification patterns of *Sgip1*, it is possible that at least two *Sgip1* splice variants are present in the mouse brain: the longer, more abundant variant and the

shorter, less abundant one. These two splice variants may constitute the two bands that we detected in our samples. According to the NCBI Gene and Ensembl databases, the mouse *Sgip1* gene contains 27 exons, 12 of which do not create a frameshift mutation when omitted from the transcript (Figure 11C). The combinations of these 12 exons may potentially lead to the production of numerous isoforms of Sgip1. It is important to note that some splice variants may contain alternative exons or different numbers of exons, but they may still have similar or identical lengths. In this way, more than one splice variant may constitute one band in our results. Large exons have a more pronounced effect on migration patterns. Deletion of large exons, such as exon 16 of *Sgip1*, may cause a substantial difference in the mobility of the protein or DNA in the gel.

4.2.2. Cloning and identification of *Sgip1* splice variants

To clone the *Sgip1* transcripts from the brain, we first isolated RNA from the mouse brain and performed RT-PCR using an anchored oligo$(dT)_{20}$ primer for cDNA synthesis and primers annealing to the first and last exons of the *Sgip1* gene. This primer combination allows amplification of the full-length *Sgip1* coding transcripts (Figure 13A-B). Next, we purified the RT-PCR products from the two bands in the agarose gel and ligated the purified products with the pGEM-T Easy vector. As a result, we created a library of *Sgip1* transcripts (Figure 13C). After the transformation of the *E.coli* cells and screening by restriction analysis, we obtained 15 unique non-redundant clones that can be discriminated by enzymatic digestion by EcoRI and XagI enzymes (Figure 13D). These 15 unique clones were further sequenced. In total, we analyzed 63 clones, and the numbers of clones containing each splice variant are provided in Table 4. The longest *Sgip1* transcript contained 27 exons (876 aa in length), and the shortest transcript contained only 20 exons (527 aa). Most *Sgip1* transcripts contained variations in exon composition within the N-terminal (exons 4-5) and central (exons 16, 20) regions (Figure 14). Some *Sgip1* splice variants resulted from alternative splicing by skipping exons 9-10, 15-19, or 19, which was often unique for the particular splice variant, and only one splice variant retained exon 19 (Figure 14). Due to the large number of the detected *Sgip1* splice variants, we indicate each *Sgip1* transcript with its length. In addition to the described 15 clones, we also detected five mis-spliced transcripts that contain premature termination codons.

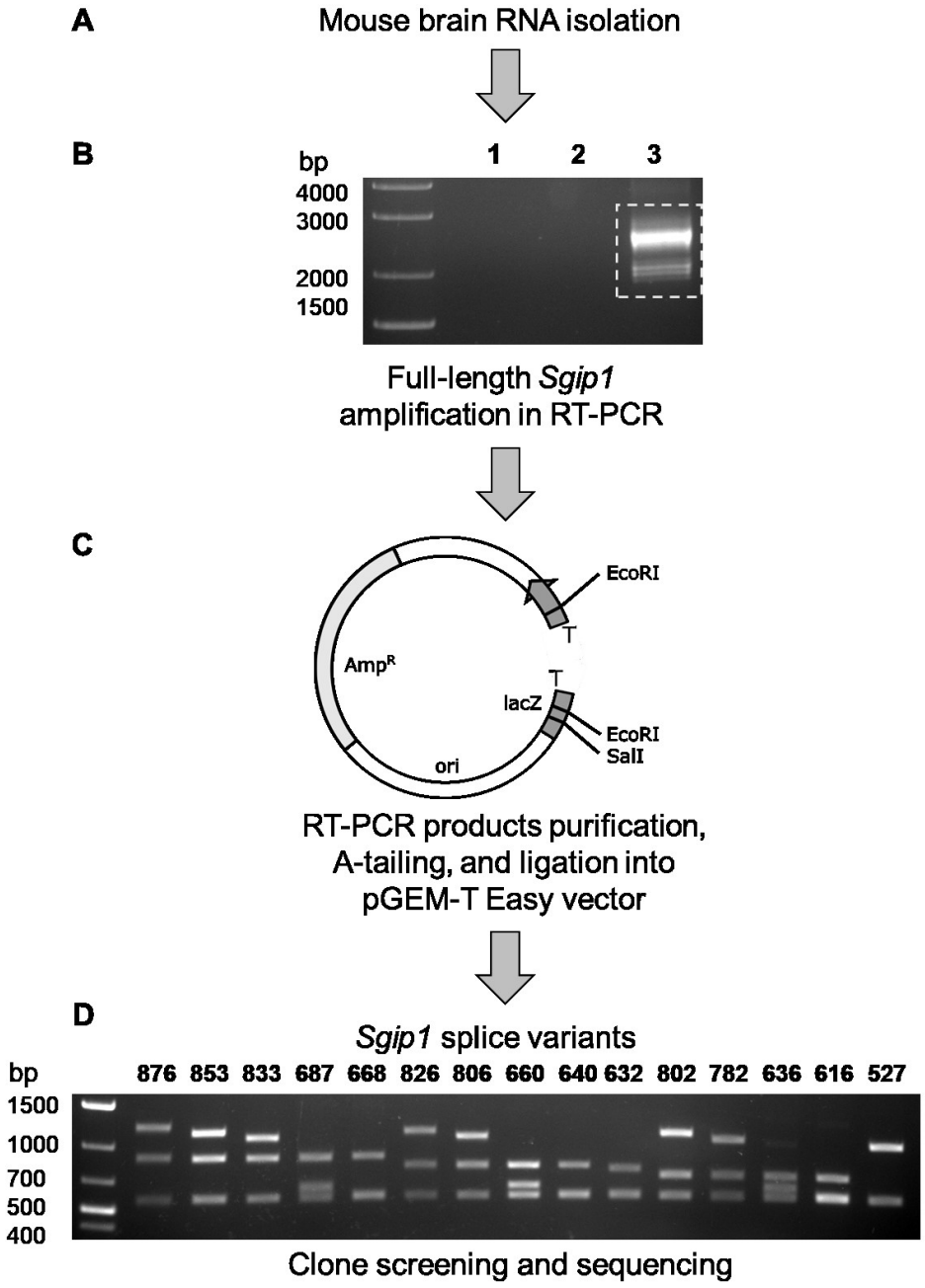

Figure 13. Cloning and identification of *Sgip1* spice variants. (A, B) The RNA from the mouse brain was used in RT-PCR employing an anchored oligo(dT)$_{20}$ primer and primers binding to the first and the last exon of the *Sgip1* gene. 1 - no PCR template control, 2 - no RT control, 3 - RT-PCR products. (C) The purified PCR products (dashed rectangle in Figure 13B) were ligated with the pGEM-T Easy vector. (D) The colonies were screened by enzymatic digestion with EcoRI and XagI, and unique non-redundant clones were sequenced. Enzymatic digestion revealed patterns of bands unique for each splice variant. *Sgip1* splice variants are marked with their amino acid length (527-876).

Table 4. Numbers of the *Sgip1* splice variants among all of the detected clones. The total number of analyzed clones is 63.

***Sgip1* splice variant**	**Number of clones**
***Sgip1* 876**	1
***Sgip1* 853**	2
***Sgip1* 833**	2
***Sgip1* 687**	1
***Sgip1* 668**	2
***Sgip1* 826**	7
***Sgip1* 806**	4
***Sgip1* 660**	7
***Sgip1* 640**	6
***Sgip1* 632**	3
***Sgip1* 802**	5
***Sgip1* 782**	4
***Sgip1* 636**	5
***Sgip1* 616**	8
***Sgip1* 527**	1
Transcripts containing premature translation-termination codons	5

We detected *Sgip1* splice variants that result from numerous exon combinations during alternative splicing by the exon skipping type. Most of the skipped exons are relatively short (12 to 84 bp), and because of this small difference in length, the splice variants have similar sizes. On the other hand, the deletion of exon 16 (498 bp in size) results in a considerable change in the size of the splice variants. Therefore, the presence or absence of exon 16 may affect the localization of the splice variant to the upper or the bottom bands in our results.

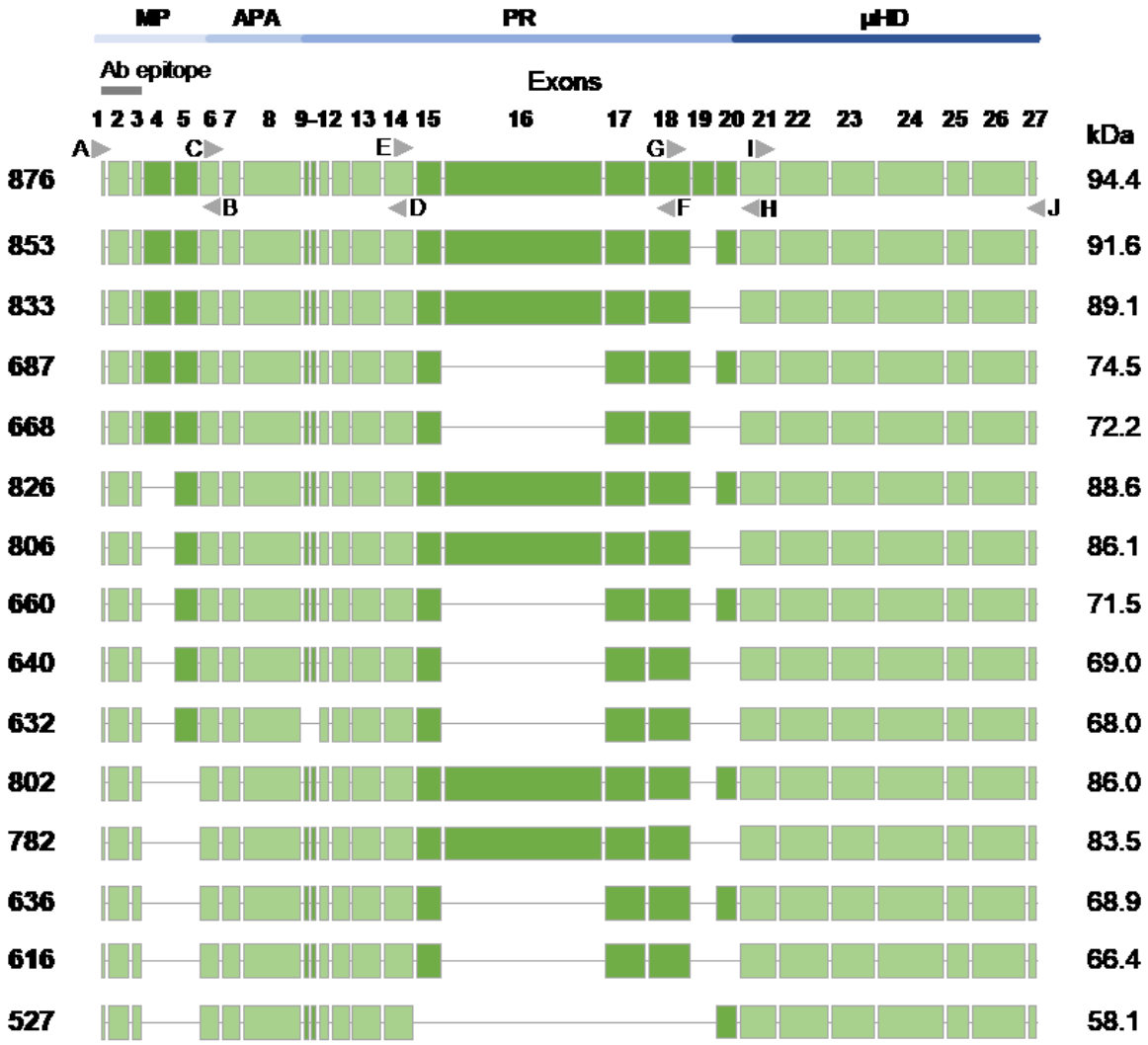

Figure 14. Schematic representation of the exon composition of the detected *Sgip1* splice variants. We detected 15 *Sgip1* splice variants, which are marked with their amino acid length (527-876). The variations in exon composition occur in the regions that correspond to two regions of the Sgip1 protein: the MP domain and the proline-rich region. The domain structure of Sgip1 is represented by: MP - membrane phospholipid-binding domain, APA - AP2 activator domain, PR - proline-rich region, µHD - µ homology domain. The antibody (Ab) epitope indicates the recognition site of the polyclonal anti-Sgip1 antibody that we used in the study. The primers used in the PCR within the study are marked with arrowheads and letters A-J. The estimated molecular weights of the proteins coded by the splice variants are provided in kDa.

To check if the cloned splice variants represent all of the *Sgip1* mRNA transcripts in the brain, we used the following approach to amplify regions of the *Sgip1* sequence that undergo

alternative splicing. We designed primers flanking regions of the *Sgip1* sequence within specific exons (primers A-J, as in Figure 14) and performed RT-PCR using combinations of these primers. Then, we compared the sizes of amplification products of the brain cDNA to the sizes of amplification products of the cloned splice variants (which served as controls). In result, the primer combinations produced patterns indicating the presence of the transcripts that we detected by cloning (Figure 15).

Using primer pair A+B, we amplified the cDNA within exons 1-6 of *Sgip1* and obtained amplicons of three sizes (Figure 15, A+B, lane 3), indicating that, within this region, one or two exons can be omitted. Specifically, exons 4 or 5 can be skipped because the tree amplicons are similar in size to the detected control splice variants (Figure 15, A+B, lanes 4-6). The predicted sizes of amplification products using different primer combinations in this study are provided in Table 5. Similarly, we found multiple bands in the PCR results analysis when we used primer pairs E+F, G+H, and E+H, and the sizes of these bands corresponded to those of the control splice variants. However, in the E+H pair, the upper and bottom bands, characteristic of splice variants *Sgip1* 876 and *Sgip1* 527, respectively, were not present after amplification of the brain sample (Figure 15, E+H, lane 3, compared to lane 4 and 9), which may indicate low abundancy of the splice variants containing exon 19 and lacking exons 15-19. However, the upper band, corresponding to the presence of exon 19, was detected when we used primer pair G+H (Figure 15, G+H, lane 3). Splice variant lacking exons 9 and 10 was not detectable in the brain sample as well using primer pair C+D (Figure 15, C+D, lane 3). Lastly, using primer pair I+J, we confirmed that no exon is omitted at the C-terminal part of Sgip1 that corresponds to exons 21-27 (Figure 15, I+J, lane 3).

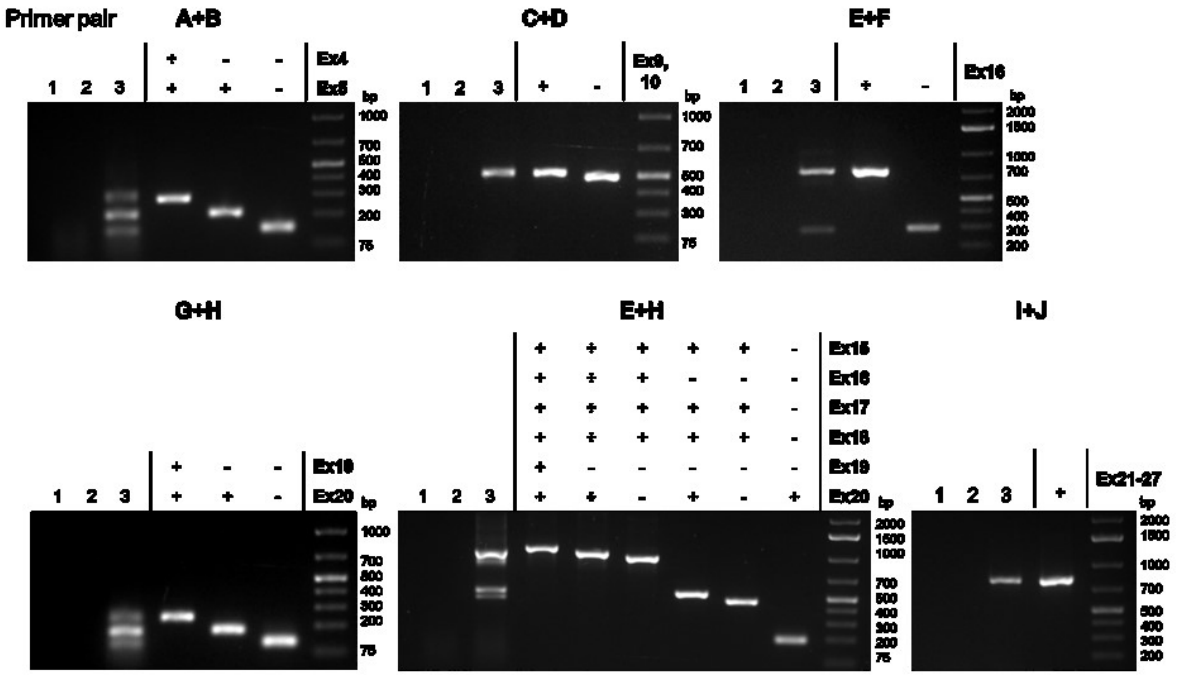

Figure 15. Amplification of various regions of *Sgip1*. We performed RT-PCR of the RNA sample using an anchored oligo(dT)20 primer and primers binding to different exons of *Sgip1* (A-J, as shown in Figure 14). Primers A-J flank variable and constant regions of the *Sgip1* sequence. The sizes of amplification products of the brain cDNA correspond to the sizes of amplification products of the cloned splice variants (which served as controls). 1 - no template control, 2 - no RT control, 3 - cDNA amplification products, lane 4 and the following - positive controls that contain or lack specific exons. The calculated sizes of amplification products using different primer combinations in this study are provided in Table 5.

Table 5. Calculated sizes of amplification products shown in Figure 15.

Primer pair	**Exon composition of the template and size of amplification products in bp**			
A+B	Ex4	+	-	-
	Ex5	+	+	-
		292	**211**	**138**
C+D	Ex9,10	+	-	
		520	**496**	
E+F	Ex16	+	-	
		792	**294**	

G+H	Ex19	+	-	-			
	Ex20	+	+	-			
		244	**178**	**118**			
E+H	Ex15	+	+	+	+	+	-
	Ex16	+	+	+	-	-	-
	Ex17	+	+	+	+	+	-
	Ex18	+	+	+	+	+	-
	Ex19	+	-	-	-	-	-
	Ex20	+	+	-	+	-	+
		1082	**1016**	**956**	**518**	**458**	**191**
I+J	Ex21-21	+					
		790					

To evaluate which Sgip1 isoform is present in the mouse brain at detectable levels, we analyzed the brain homogenate and Sgip1 immunoprecipitate from the brain by mass spectrometry (MS). After trypsin digestion of the brain homogenate sample, we detected 33 peptides. Most of the peptides did not cover regions of exon junctions, or the peptides covered the regions of the *Sgip1* sequence that are present in all splice variants. We centered the analysis on the splice variants *Sgip1* 853, *Sgip1* 826, *Sgip1* 806, and *Sgip1* 833 because they most likely constitute the upper bands in the immunoblot results (Figure 11A). Two detected peptides were unique for splice variants *Sgip1* 853 and *Sgip1* 826: AESTSSISSTNSLSAATTPTVENE-QPSLVWFDR and FYLTFEGSSR because they indicate a fusion of exons 18 and 20 for the former sequence and fusion of exons 20 and 21 for the latter sequence. We did not detect peptides that cover the N-terminus of Sgip1, which corresponds to exons 1-5, in the brain sample. Then, to enrich the sample, we immunoprecipitated Sgip1 from the SDS-soluble fraction of the brain using the polyclonal anti-Sgip1 antibody. The mass spectrometry analysis identified 33 peptides, including AESTSSISSTNSLSAATTPTVGSSR, specific for *Sgip1* 806 and *Sgip1* 833 splice variants because it indicates fusion of exons 18 and 21, and peptide DGMQPSPHEPPYHSK, specific for *Sgip1* 806 and *Sgip1* 826 splice variants because it indicates fusion of exons 3 and 5 (Figure 16). Other detected peptides were common for all splice variants.

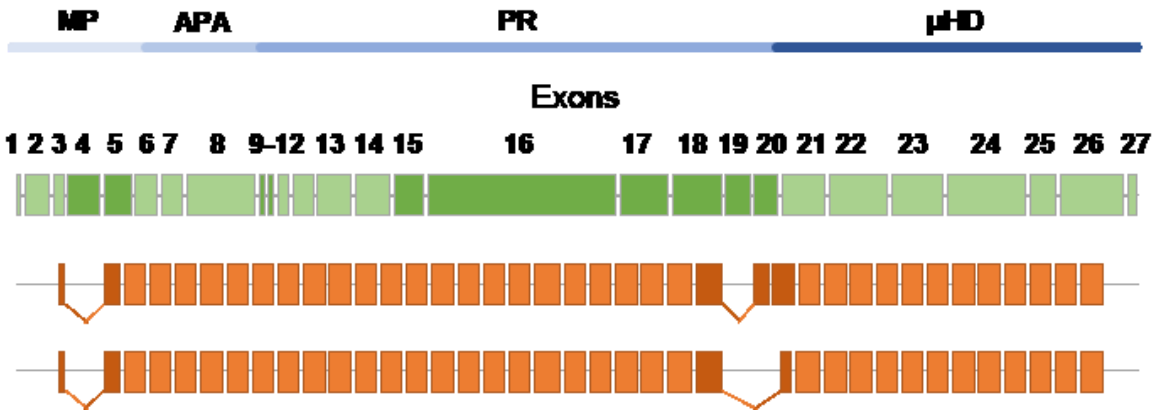

Figure 16. Sgip1-specific peptides detected by mass spectrometry analysis. The detected peptides (in orange) were aligned to the exons of the *Sgip1* gene (in green). The peptides indicating the presence of specific Sgip1 isoforms contain fusions of exons: 1) 3 and 5, indicating Sgip1 806 and Sgip1 826 variants; 2) 18 and 20, indicating Sgip1 853 and Sgip1 826 variants; 3) 18 and 21, indicating Sgip1 806 and Sgip1 833 variants; and 4) 20 and 21, indicating Sgip1 853 and Sgip1 826 variants. Peptides that do not cover exon junction regions or that cover the common regions of the Sgip1 sequence (in light orange) are drawn not to scale. The Sgip1-specific peptides likely reflect the presence of Sgip1 isoforms Sgip1 826 and Sgip1 806 in the brain. MP - membrane phospholipid-binding domain, APA - AP2 activator domain, PR - proline-rich region, μHD - μ homology domain.

4.2.3. Characterization of the *Sgip1* splice variants

We found that most *Sgip1* transcripts are alternatively spliced within the N-terminal (exons 4, 5) and central (exons 16, 20) regions of the Sgip1 protein. The variations in these regions may substantially affect the protein's properties. To test this possibility, we chose a subset of *Sgip1* splice variants that have various combinations of exons 4, 5, 16, and 20, namely *Sgip1* 853, *Sgip1* 826, *Sgip1* 806, *Sgip1* 802, *Sgip1* 660, and *Sgip1* 640 (Figure 17A), and tested the expression of these splice variants by fluorescent microscopy.

We transfected HEK293 cells with the EYFP-tagged *Sgip1* splice variants to assess their intracellular distribution by microscopy. We found that the splice variants were represented by a major pool of the protein located in the cytoplasm (Figure 17B), and a fraction of the proteins formed puncta at the plasma membrane (Figure 17B, insets). Except for the Sgip1 853 splice isoform, there were no apparent differences in the localization patterns between the Sgip1 isoforms, and this pattern was in line with the previous reports regarding the intracellular

distribution of Sgip1 (Uezu et al., 2007; Wilhelm et al., 2014). However, in approximately half of the cells transfected with the Sgip1 853 isoform, we found an accumulation of the protein in the cytoplasm in the form of vesicles or inclusion bodies (Figure 17B').

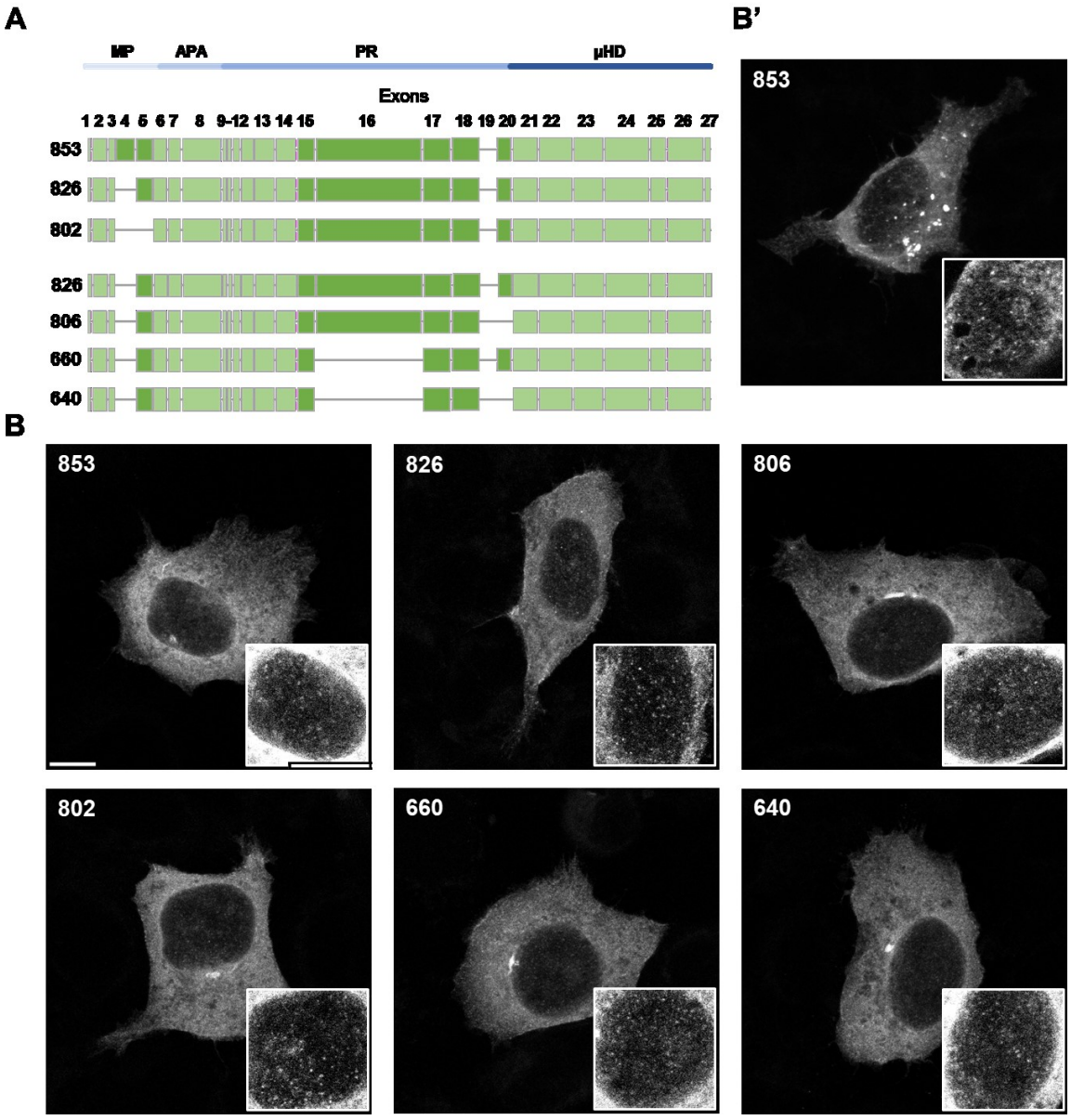

Figure 17. Characterization of *Sgip1* splice variants in HEK293 cells. (A) The subset of the *Sgip1* splice variants chosen for testing, extracted from Figure 14. By comparing these splice variants, we can determine the effect of deletion of single exons. Splice variants *Sgip1* 853, *Sgip1* 826, and *Sgip1* 802 differ in the MP domain composition. Splice variants *Sgip1* 826, *Sgip1* 806, *Sgip1* 660, and *Sgip1* 640 differ in the composition of the proline-rich region. Note that the *Sgip1* 826 variant is depicted twice for comparison. (B) The *Sgip1* splice variants were cloned

into the pRK5-EYFP vector, transfected in HEK293 cells, and analyzed under the confocal microscope. Some of the cells transfected with the Sgip1 853 variant showed accumulation of the protein in the cytoplasm (B'). The images are maximal intensity projections of the Z-stacks taken every 0.3 μm. Insets show membrane planes of the cells with enhanced brightness and contrast. All of the tested isoforms showed an association with the plasma membrane, observed as punctate distribution, which is the best visible in the membrane planes of the cells. Scale bars represent 10 μm. PFC - the prefrontal cortex, MP - membrane phospholipid-binding domain, APA - AP2 activator domain, PR - proline-rich region, μHD - μ homology domain.

4.2.4. Specificity of the effect of SGIP1 on the CB1R internalization

To monitor the internalization of CB1R and MOR, we adapted the enhanced bystander BRET-based system (Namkung et al., 2016). This system is composed of the receptor, fused with the BRET donor (RlucII), and the BRET acceptor (rGFP), fused with the plasma membrane-targeting sequence (CAAX). When the receptor is located in the plasma membrane, the proximity of the BRET donor and acceptor results in a high BRET ratio (Figure 18A). During internalization, the receptor is removed from the plasma membrane, so the BRET donor and acceptor separate, causing a decrease in the BRET ratio.

First, we tested the internalization of the CB1R-RlucII construct that we developed for this internalization assay. Application of WIN resulted in the progressive internalization of CB1R, which started to be evident 15 min after stimulation. Expression of SGIP1 inhibited the internalization of CB1R, resulting in the internalization rate about twice as low as that of CB1R alone (Figure 18B).

To test the specificity of the effect of SGIP1 on internalization, we used μ opioid receptor (MOR) and muscarinic acetylcholine M3 receptor (M3R). Application of MOR agonist met-enkephalin and M3R agonist carbachol resulted in the rapid and massive internalization of the receptors. SGIP1 expression did not affect the internalization rates of MOR and M3R (Figure 18C-D). Overall, our results demonstrate that SGIP1 is a specific inhibitor of CB1R endocytosis.

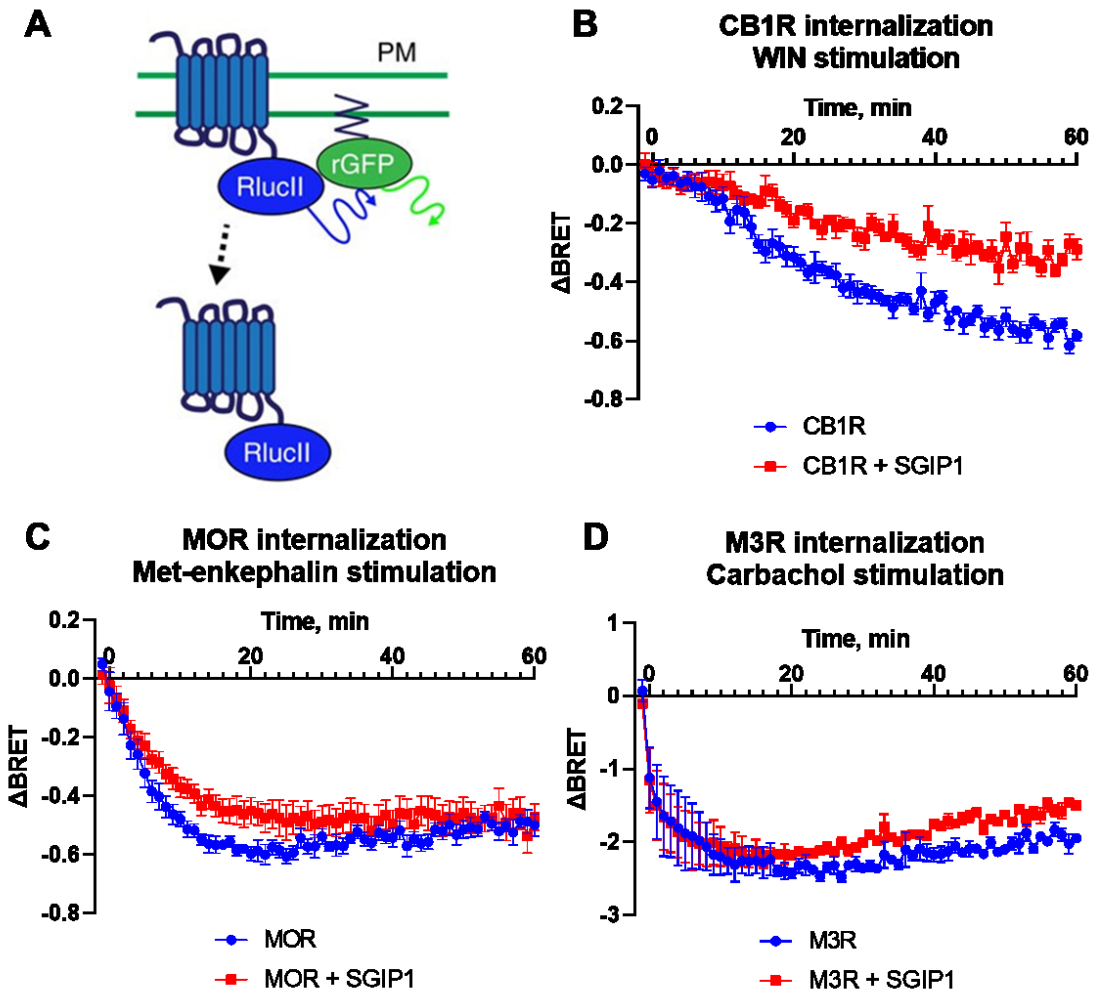

Figure 18. The effect of SGIP1 on internalization of cannabinoid receptor 1 (CB1R), μ opioid receptor (MOR), and muscarinic acetylcholine M3 receptor (M3R). The cells were transfected with rGFP-CAAX and RlucII-tagged CB1R, MOR, or M3R. Then, we cells were stimulated with the respectable agonists: 1 μM WIN 55,212-2 (WIN), 10 μM met-enkephalin, or 10 μM carbachol. (A) Schematic representation of the enhanced bystander BRET-based system used in the study (Namkung et al., 2016). During internalization of the receptor, the BRET donor (RlucII) and acceptor (rGFP) separate, resulting in a decrease in the BRET ratio. (B) SGIP1 inhibits CB1R internalization. (C) SGIP1 does not affect MOR internalization. (D) SGIP1 does not affect M3R internalization. The data are presented as means ± SEM from five independent experiments.

4.3. Pharmacodynamic studies of the hexahydrocannabinol effect on CB1R

4.3.1. Effects on G protein activation

CB1R elicits its primary effect on cell signaling by activating G proteins. Various ligands modulate the activity of CB1R and, therefore, its effect on signaling. We employed the BRET-based G protein activation assay to measure the dissociation of α and βγ subunits of the G protein upon its activation by CB1R. We evaluated the G protein activation elicited by the hexahydrocannabinol (HHC) epimers (9S)-HHC and (9R)-HHC and compared their effects to those elicited by THC and WIN.

Application of all of the tested ligands led to the activation of G_{i1} and G_{oA} proteins, but their pharmacological activity differed (Figure 19). (9S)-HHC had lower potency (logEC50 = -6.597) and efficacy than (9R)-HHC (logEC50 = -7.650) in the G_{i1} activation assay (Figure 19A and Table 6). The lower potency of (9S)-HHC indicates its lower affinity to CB1R. The potency and efficacy of (9R)-HHC were similar to those of THC (logEC50 = -7.876). The potency of (9S)-HHC was similar to that of WIN (logEC50 = -6.818), but the efficacy of (9S)-HHC was much lower than that of WIN (Figure 19A).

In the G_{oA} activation assay, the potency (logEC50 = -6.633) and efficacy of (9S)-HHC were lower than those of (9R)-HHC (logEC50 = -7.623) (Figure 19B and Table 7). The potency and efficacy of (9R)-HHC were similar to those of THC (logEC50 = -8.069) and WIN (logEC50 = -7.223). Overall, the results indicate that the effect of (9R)-HHC epimer on the G protein activation is similar to that of THC, and (9S)-HHC has much lower pharmacological activity.

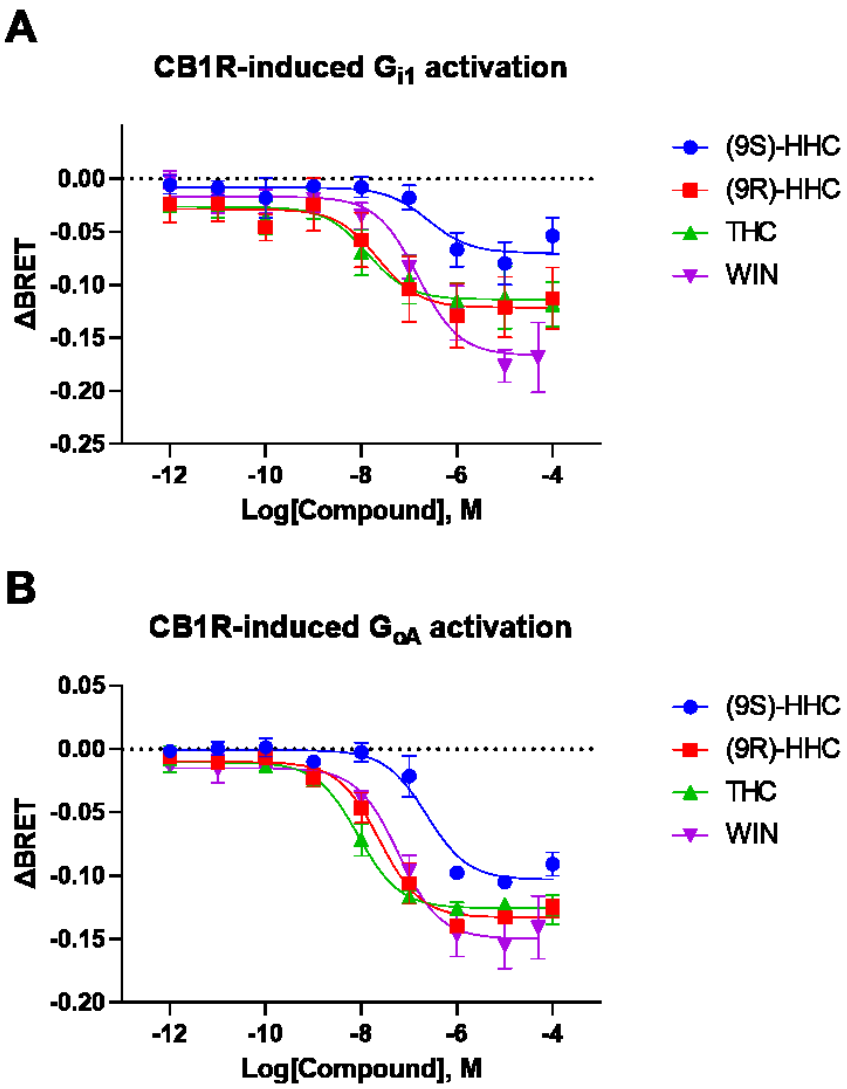

Figure 19. G protein activation induced by CB1R agonists. HEK293 cells were transfected with $G_{\alpha i1}$-Rluc8 or $G_{\alpha oA}$-Rluc8, $G_{\beta 2}$-Flag, $G_{\gamma 2}$-EYFP, and SNAP-CB1R. The cells were then stimulated with increasing concentrations of (9S)-HHC, (9R)-HHC, THC, WIN, or their vehicles. The BRET donor and acceptor emissions were measured 12 minutes after the stimulations. A) Dose-response relationship of G_{i1} activation after CB1R stimulation. B) Dose-response relationship of G_{oA} activation after CB1R stimulation. The data are presented as means ± SEM from three independent experiments. The statistical analysis of the data is presented in Tables 6 and 7.

Table 6. Statistical analysis of the dose-response data of CB1R-induced G_{i1} activation, presented in Figure 19A. LogEC50 and EC50 represent the potency of the ligands, and Top represents the efficacy of the ligands.

Compound	(9S)-HHC	(9R)-HHC	THC	WIN
Best-fit values				
Bottom	-0.008036	-0.02847	-0.02623	-0.01680
Top	-0.06988	-0.1214	-0.1137	-0.1664
LogEC50	-6.597	-7.650	-7.876	-6.818
EC50	2.532e-007	2.238e-008	1.330e-008	1.522e-007
Span	-0.06184	-0.09290	-0.08749	-0.1496
95% CI (profile likelihood)				
Bottom	-0.01980 to 0.003972	-0.05146 to -0.004468	-0.04467 to -0.007311	-0.03316 to -0.0002765
Top	-0.08842 to -0.05251	-0.1484 to -0.09620	-0.1339 to -0.09491	-0.1921 to -0.1434
LogEC50	-7.327 to -5.928	-8.599 to -6.712	-8.648 to -6.966	-7.336 to -6.229
EC50	4.705e-008 to 1.179e-006	2.515e-009 to 1.943e-007	2.248e-009 to 1.081e-007	4.612e-008 to 5.905e-007
Goodness of Fit				
Degrees of Freedom	24	24	24	24
R squared	0.6062	0.5710	0.6702	0.8489
Sum of Squares	0.01192	0.03509	0.02047	0.01982
Sy.x	0.02229	0.03824	0.02921	0.02874

Table 7. Statistical analysis of the dose-response data of CB1R-induced G_{oA} activation, presented in Figure 19B. LogEC50 and EC50 represent the potency of the ligands, and Top represents the efficacy of the ligands.

Compound	(9S)-HHC	(9R)-HHC	THC	WIN
Best-fit values				
Bottom	-0.0007050	-0.009940	-0.01025	-0.01486
Top	-0.1031	-0.1330	-0.1255	-0.1498
LogEC50	-6.633	-7.623	-8.069	-7.223
EC50	2.329e-007	2.381e-008	8.529e-009	5.986e-008
Span	-0.1024	-0.1230	-0.1153	-0.1349
95% CI (profile likelihood)				
Bottom	-0.008361 to 0.007019	-0.01821 to -0.001553	-0.01768 to -0.002737	-0.02691 to -0.002565
Top	-0.1148 to -0.09178	-0.1423 to -0.1238	-0.1329 to -0.1182	-0.1654 to -0.1345
LogEC50	-6.911 to -6.357	-7.884 to -7.357	-8.298 to -7.846	-7.611 to -6.872

EC50	1.228e-007 to 4.393e-007	1.307e-008 to 4.397e-008	5.036e-009 to 1.425e-008	2.447e-008 to 1.341e-007
Goodness of Fit				
Degrees of Freedom	24	24	24	24
R squared	0.9117	0.9496	0.9581	0.9015
Sum of Squares	0.004908	0.004340	0.003158	0.01042
Sy.x	0.01430	0.01345	0.01147	0.02084

4.3.2. Effects on GRK3 and β-arrestin signaling

The signaling of CB1R is regulated in a process known as desensitization, which involves GRK3-mediated phosphorylation of the receptor and its binding by β arrestins. We employed the BRET-based interaction assays to measure the association of GRK3 and CB1R during phosphorylation of the receptor and the interaction of β-arrestin 2 and the phosphorylated CB1R. We tested the GRK3-CB1R and β-arrestin 2-CB1R interactions elicited by the hexahydrocannabinol epimers (9S)-HHC and (9R)-HHC and compared their effects to the effects elicited by THC and WIN.

The ability of the tested ligands to elicit the responses varied. (9S)-HHC, (9R)-HHC, and THC had a low ability to stimulate the interactions, as opposed to WIN, which had the highest potency and efficacy (Figure 20). (9S)-HHC had lower potency (logEC50 = -4.983) and efficacy than (9R)-HHC (logEC50 = -6.172) in the GRK3-CB1R interaction assay (Figure 20A and Table 8). The potency of (9R)-HHC was similar to those of THC (logEC50 = -6.250) and WIN (logEC50 = -6.712), but (9R)-HHC had lower efficacy than WIN and higher potency than THC.

In the β-arrestin 2-CB1R interaction assay, (9S)-HHC and THC did not induce the interaction efficiently at the tested concentrations. The potency (logEC50 = -5.284) and efficacy of (9R)-HHC were lower than those of WIN (logEC50 = -6.344) (Figure 20B and Table 9). Overall, the results indicate that (9R)-HHC epimer stimulates GRK3-CB1R and β-arrestin 2-CB1R interactions more effectively than THC, and the (9S)-HHC epimer, similar to THC, has a low ability to stimulate the interactions that result in desensitization of CB1R.

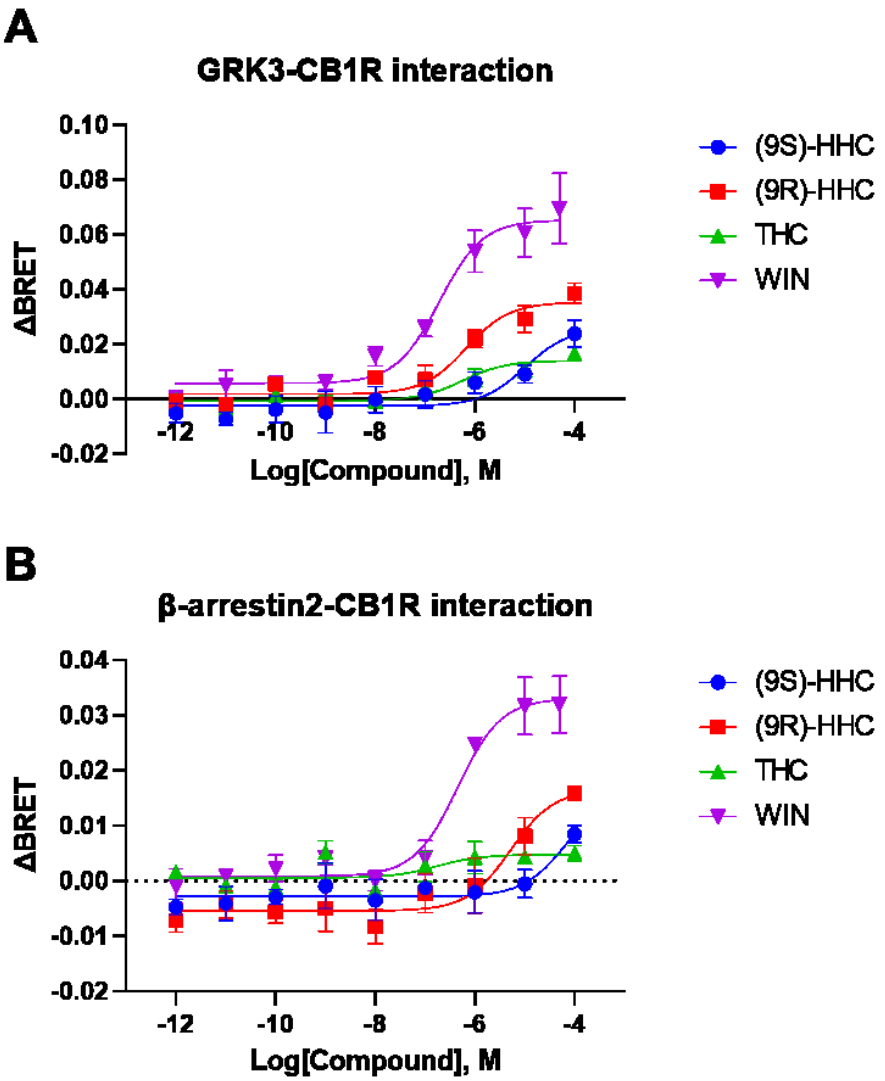

Figure 20. GRK3-CB1R and β-arrestin 2-CB1R interactions induced by CB1R agonists. HEK293 cells were transfected with CB1R-EYFP and β-arrestin 2-Rluc or GRK3-Rluc8. The cells were then stimulated with increasing concentrations of (9S)-HHC, (9R)-HHC, THC, WIN, or their vehicles. The BRET donor and acceptor emissions were measured 12 minutes after the stimulations. A) Dose-response relationship of GRK3 recruitment to CB1R after CB1R stimulation. B) Dose-response relationship of β-arrestin 2 recruitment to CB1R after CB1R stimulation. The data are presented as means ± SEM from three independent experiments. The statistical analysis of the data is presented in Tables 8 and 9.

Table 8. Statistical analysis of the dose-response data of GRK3-CB1R interaction, presented in Figure 20A. LogEC50 and EC50 represent the potency of the ligands, and Top represents the efficacy of the ligands.

Compound	(9S)-HHC	(9R)-HHC	THC	WIN
Best-fit values				
Bottom	-0.002394	0.001923	-0.0004729	0.005882
Top	0.02599	0.03543	0.01409	0.06538
LogEC50	-4.983	-6.172	-6.250	-6.712
EC50	1.041e-005	6.731e-007	5.624e-007	1.940e-007
Span	0.02838	0.03351	0.01456	0.05950
95% CI (profile likelihood)				
Bottom	-0.006911 to 0.001333	-0.001247 to 0.005034	-0.003035 to 0.001880	1.282e-005 to 0.01166
Top	0.01168 to 0.5234	0.02976 to 0.04153	0.009846 to 0.01960	0.05691 to 0.07450
LogEC50	-7.057 to -2.711	-6.690 to -5.700	-7.324 to -5.146	-7.163 to -6.245
EC50	8.780e-008 to 0.001943	2.044e-007 to 1.997e-006	4.737e-008 to 7.138e-006	6.872e-008 to 5.690e-007
Goodness of Fit				
Degrees of Freedom	24	24	24	24
R squared	0.5735	0.8513	0.6729	0.8692
Sum of Squares	0.001474	0.0008500	0.0004568	0.002604
Sy.x	0.007837	0.005951	0.004363	0.01042

Table 9. Statistical analysis of the dose-response data of β-arrestin 2-CB1R interaction, presented in Figure 20B. LogEC50 and EC50 represent the potency of the ligands, and Top represents the efficacy of the ligands.

Compound	(9S)-HHC	(9R)-HHC	THC	WIN
Best-fit values				
Bottom	-0.002803	-0.005400	0.0005880	0.0008429
Top	0.01618	0.01657	0.004772	0.03307
LogEC50	-4.165	-5.284	-6.765	-6.344
EC50	6.846e-005	5.200e-006	1.717e-007	4.526e-007
Span	0.01899	0.02197	0.004184	0.03223
95% CI (profile likelihood)				
Bottom	-0.004790 to -0.0008480	-0.007917 to -0.002964	-0.001292 to 0.002402	-0.001783 to 0.003441
Top	0.004019 to ND	0.009883 to 0.02542	0.002288 to 0.009830	0.02875 to 0.03762
LogEC50	-5.513 to ND	-6.082 to -4.612	-10.35 to -3.970	-6.687 to -6.013

EC50	3.070e-006 to ND	8.281e-007 to 2.444e-005	4.417e-011 to 0.0001070	2.056e-007 to 9.701e-007
Goodness of Fit				
Degrees of Freedom	24	24	24	24
R squared	0.4298	0.7050	0.2390	0.8877
Sum of Squares	0.0004427	0.0006098	0.0002752	0.0005947
Sy.x	0.004295	0.005041	0.003386	0.004978

5. DISCUSSION

5.1. The effect of Sgip1 on chronic pain processing

We found that deletion of *Sgip1* in mice affects the reaction to stimuli within the chronic inflammatory pain model, and this effect is sex-specific. *Sgip1* knock-out male mice had increased responses, but *Sgip1* knock-out female mice did not show a change in nociception compared to wild-type mice. Injections of WIN or THC to males had antinociceptive effects, but *Sgip1* knock-out males still had a lower withdrawal threshold than wild-type males. After WIN injection in females, the mechanical sensitivity of *Sgip1* knock-out females was not different from that of wild-type females; however, after THC injection, *Sgip1* knock-out females were less sensitive to pain in the von Frey test than wild-type females.

Our current and previous results suggest that Sgip1 is involved in the regulation of acute and chronic inflammatory pain. The effect of Sgip1 on pain perception could be explained by its interaction with CB1R, which is an essential component in the regulation of pain perception. The interaction of Sgip1 and CB1R affects the signaling of CB1R and, notably, inhibits the internalization of the receptor. Because of the inhibition of internalization, neuronal trafficking of CB1R may be altered, and CB1R may be retained at particular compartments, such as the axonal or synaptic plasma membrane. Indeed, several reports suggest that the mobility or trafficking of CB1R is restricted to particular neuronal compartments (McDonald et al., 2007; Mikasova et al., 2008; Simon et al., 2013). Sgip1 may stabilize such CB1R at axonal or synaptic compartments and, by means of that, optimize CB1R signaling and availability. Consequently, Sgip1 deletion would liberate CB1R, impair its polarized trafficking, and compromise its effects on neuronal circuits and, therefore, on behavior. In our previous study, we observed signs of altered CB1R activity in *Sgip1* knock-out mice, such as decreased anxiety-like behaviors and acute nociception, facilitated fear extinction to tone, and higher sensitivity to analgesics (Dvorakova et al., 2021).

Long-term WIN incubations (for 16-17 h) result in a complete loss of CB1R surface staining in neuronal cultures (Coutts et al., 2001; McDonald et al., 2007). This observation might suggest the transient interaction of Sgip1 with CB1R, which ceases after prolonged stimulation of the receptor. CB1R may be persistently stimulated as a result of sensitization of the nervous system during chronic pain; therefore, the effect of Sgip1 on the receptor may be lost or altered. The

increased sensitivity to chronic pain in the absence of Sgip1, which we observed in the current study, may result from this transient effect of Sgip1 on CB1R.

Other effects potentially explaining the differences in the tests assessing acute and chronic nociception are pre-activation of the endocannabinoid system and altered endocannabinoid levels in the brain. Handling of animals during an experiment may result in the mobilization of endogenous cannabinoids and produce antinociception (Hohmann et al., 2005). Unlike the tail-flick test, which involves animal handling and is often used to assess acute pain, the von Frey test minimizes animal handling to prevent unintentional effects of endocannabinoid system activation. Endocannabinoid levels are regulated by feedback mechanisms, which are partly dependent on CB1R activity (Pacher et al., 2013). CB1R signaling and activity are likely to be altered in *Sgip1* knock-out mice, which may result in altered endocannabinoid levels. Endocannabinoid levels in mice lacking Sgip1 is an important issue that needs to be addressed in future experiments.

As opposed to the nociceptive effect of *Sgip1* deletion in the male mice, *Sgip1* deletion did not alter nociception in the female mice. Animal performance in tests assessing the endocannabinoid system may be affected by multiple sex-specific factors, such as differences in metabolism, cannabinoid receptor expression, sensitivity to cannabinoids, and the influence of hormones, which might stimulate the endocannabinoid system (Blanton et al., 2021). Approaches minimizing the effect of sex differences, such as determining the phase of the estrous cycle in females or ovariectomy, should be considered in future experiments.

Systemic intraperitoneal application of cannabinoids, besides causing factual antinociception through activation of the endocannabinoid system, might also produce central sedation and inhibition of locomotor activity, which influence the outcomes of behavioral tests assessing nociception (Craft et al., 2013). Local application of cannabinoids into the inflamed paw or application of peripherally-restricted cannabinoids may help to overcome the potential effects of the systemic action of cannabinoid drugs.

Given the non-desirable central effects of cannabinoids, such as sedation and psychotropic action, the ongoing cannabinoid research aims to unravel allosteric sites in CB1R and to develop the allosteric regulators as well as peripherally-restricted orthosteric ligands. Deciphering the complete cascade of CB1R signaling, including the role of CB1R-interacting proteins, will help to understand the effects of cannabinoid application and select better candidates for ortho- or allosteric binding sites of CB1R. Apart from *Sgip1* knock-out mice, several animal models that

target CB1R-related function have been described, such as GASP1 knock-out mice (Martini et al., 2010), BiP knock-out mice (Costas-Insua et al., 2021), β-arrestin knock-out mice (Breivogel et al., 2008; Nguyen et al., 2012), CB1R S426A/S430A mice (Morgan et al., 2014; Nealon et al., 2019), and S426A/S430A x beta-arrestin 2 double knock-out mice (Piscura et al., 2023). *Sgip1* knock-out mice will supplement the tools available for studying CB1R and the endocannabinoid system and potentially improve developments in therapeutics.

5.2. Identification and characterization of *Sgip1* splice variants in the brain

Expression patterns of Sgip1 in the brain

The patterns of *Sgip1* expression screened by immunoblotting and RT-PCR experiments predicted the presence of splice variants of *Sgip1* in the brain. We disregarded the possibility that the expression patterns of *Sgip1* result from unspecific binding of the antibody and phosphorylation or ubiquitination of Sgip1. The large number of exons that allow in-frame deletion in the *Sgip1* gene is likely responsible for this versatility of alternative splicing of *Sgip1*.

In the immunoblot, we detected two fractions of Sgip1 protein, corresponding to bands of approximately 130 and 110 kDa. The intensively-stained 130-kDa band, which represents most of the protein in the brain, has a larger molecular weight than the predicted weight of the longest Sgip1 isoform (Sgip1 876, 94.4 kDa). This discrepancy between the apparent and theoretical molecular weight of Sgip1 has been documented by other groups (Lee et al., 2019; Fletcher-Jones et al., 2023). The difference in mobility of Sgip1 in SDS-PAGE may result from post-translational modifications of Sgip1, such as phosphorylation or ubiquitination. Sgip1 contains multiple potential phosphorylation sites that are located predominantly at the proline-rich region, and Sgip1 was shown to be highly phosphorylated (Craft et al., 2008; Huttlin et al., 2010). To test the effect of dephosphorylation on Sgip1 mobility in SDS-PAGE, we treated the protein sample from the PFC with SAP. Dephosphorylation of the PFC sample substantially increased the migration pace of Sgip1, and the Sgip1-immunoreactive bands corresponded to approximately 120 and 80 kDa. Each phosphorylation of serine, threonine, or tyrosine adds 80 Da to the protein molecular weight (Yu et al., 2021). Sgip1 806 contains 86 serines, 58 threonines, and 15 tyrosines. Therefore, the maximal shift of Sgip1 mobility in SDS-PAGE is 12.72 kDa. The dephosphorylation results suggest that most of Sgip1 is phosphorylated in the brain. While most of the residues might be constantly phosphorylated to maintain the charge of Sgip1, some phosphorylation sites, such as Ser-149, Ser-169, and Thr-409, were shown to be

dephosphorylated *in vivo* after nerve terminal depolarization (Munton et al., 2007; Craft et al., 2008). These phosphorylation sites may be directly involved in Sgip1's functions in the presynaptic compartment.

Ubiquitination of Sgip1 may explain the residual shift in the mobility of the protein in SDS-PAGE. Ubiquitination of the μHD domain was reported for the Sgip1 homolog, FCHO2 protein (Uezu et al., 2011). We did not detect ubiquitin when Sgip1 was immunoprecipitated from the detergent-soluble fraction of the PFC tissue. Therefore, ubiquitination does not affect the migration pace of Sgip1. Other post-translational modifications, such as glycosylation, myristoylation, methylation, acetylation, and SUMOylation, might affect the Sgip1's mobility.

Cloning and identification of *Sgip1* splice variants

We detected 15 *Sgip1* splice variants resulting from the *Sgip1* gene alternative splicing in the mouse brain, four of which have been described previously (Table 10). The remaining 11 detected *Sgip1* splice variants were predicted *in silico*. Due to the large number of the detected *Sgip1* splice variants, we indicate each *Sgip1* transcript with its length. We propose that *Sgip1* splice variants are indicated with their amino acid length, and this should be clearly stated in the scientific works to avoid misidentification of the *Sgip1* variants.

Sgip1 domain architecture contains the membrane phospholipid-binding (MP) domain, AP2 activator (APA) domain, proline-rich region, and μ homology domain (μHD) (Reider et al., 2009; Hollopeter et al., 2014). *Sgip1* variants arise from alternative splicing within the N-terminal (exons 4, 5) and central (exons 9, 10, 15-20) regions (Figure 14). The alternative splicing pattern of *Sgip1* follows the domain structure of the Sgip1 protein. Spliced exons 4 and 5 lie within the MP domain, and spliced exons 9, 10, 15-20 lie within the proline-rich region. Exons 1-3 are present in all of the detected *Sgip1* splice variants, which indicates that any splice variant can be detected using our anti-Sgip1 antibody.

Table 10. Detected *Sgip1* splice variants compared to the variants published or listed in the NCBI Gene, UniProt, and Ensembl databases. The splice variants are indicated by their length. Only variants containing C-terminus are included in the table. Protein variants that differ in one amino acid due to the NAGNAG acceptor motif are considered identical.

Detected *Sgip1* splice variant	**NCBI**	**Uniprot**	**Ensembl**	**Original name**	**Reference**
***Sgip1* 876**					
***Sgip1* 853**	854	854		SGIP1α	(Uezu et al., 2007)
***Sgip1* 833**	834				
***Sgip1* 687**	688				
***Sgip1* 668**	668				
***Sgip1* 826**	826	826	826	SGIP1	(Li et al., 2011)
***Sgip1* 806**	806	806	806	SGIP1	(Henne et al., 2010)
***Sgip1* 660**	659	659	659	SGIP1β	(Fletcher-Jones et al., 2023)
***Sgip1* 640**	639	639	639		
***Sgip1* 632**	632, 631				
***Sgip1* 802**	802				
***Sgip1* 782**	782				
***Sgip1* 636**	636				
***Sgip1* 616**					
***Sgip1* 527**					
	608		608		
	856				
	848				
	654				
	652				
	630				
	628				

Exons within the APA and μHD domains do not undergo alternative splicing (Figure 14). The APA domain was shown to interact with and activate the AP-2 complex (Hollopeter et al., 2014). The μHD interacts with endocytic adaptors and other proteins, such as EPS15 (Uezu et al., 2007) and CB1R (Hajkova et al., 2016). The absence of alternative splicing at the APA and μHD domain-coding exons underlines their functional importance because these domains preserve high homology between species and supports the notion that protein-protein interaction surfaces tend to be protected from exon removals (Colantoni et al., 2013).

The *Sgip1* 853 splice variant is one amino acid shorter than the previously reported Sgip1α, containing 854 aa. This difference may be explained by the presence of the NAGNAG tandem acceptor motif at the 5' end of exon 5. The NAGNAG motif creates two potential 3' splicing acceptor sites (Hiller et al., 2004). This process is likely responsible for the loss of one glutamine-coding codon in exon 5 of *Sgip1*.

Based on our immunoblot and RT-PCR results, we may speculate that *Sgip1* splice variants containing exon 16 prevail in the brain because they constitute the upper intensively-stained bands in the results. The mass spectrometry analysis supports the presence of Sgip1 isoforms that contain fusions of exons 3 to 5, 18 to 20, and 18 to 21. The *Sgip1* variants that lack exons 9, 10 (*Sgip1* 632), lack exon 15 (*Sgip1* 527), or contain exon 19 (*Sgip1* 876) presumably constitute a minor fraction of *Sgip1* transcripts because they were detected in single clones. These confinements describe Sgip1 isoforms Sgip1 806 or Sgip1 826. We obtained a higher number of clones that have the *Sgip1* 826 variant. Therefore, it is likely that both *Sgip1* variants *Sgip1* 806 and *Sgip1* 826 predominate or that *Sgip1* 826 variant is the major *Sgip1* splice variant expressed in the mouse brain.

The presence of multiple splicing regulators ensures fidelity of splicing because splice variants of a protein often have different properties or tissue localization. The brain is a tissue in which splicing is active at superior levels compared to other tissues (Yeo et al., 2004). Variations in splicing have been observed between brain regions (Schreiner et al., 2014) and sexes (Trabzuni et al., 2013). From numerous reports, a few examples of the role of splicing in the regulation of synaptic transmission can be found herein (Ahn et al., 1995; Kennedy, 1997; Berthele et al., 1998; Kumpost et al., 2008). Splicing in the brain has also been linked to the regulation of neurogenesis (Vuong et al., 2016), and variability in splicing has been associated with neurological disease states (Tollervey et al., 2011). From these examples, it is evident that splicing is associated with the signaling diversity of the brain.

The expression of *Sgip1* splice variants can be affected by multiple factors, such as tissue, brain region, or neuronal compartment localization, the developmental stage, and variations in translation efficiency between cells or tissues. *Sgip1* splice variants may differ in the neuronal localization and trafficking, the strength and specificity of lipid binding, the protein interaction profile, or the effect on the internalization of other molecules. Alternatively, the presence of multiple *Sgip1* splice variants may result from the high abundance of Sgip1, which constitutes 0.431% of total synaptic proteins (Wilhelm et al., 2014). In this way, the high rate of *Sgip1* expression would lead to the production of minimal amounts of its splice variants.

Characterization of the *Sgip1* splice variants

We tested various Sgip1 splice isoforms to evaluate the effect of deletions of certain protein regions that are coded by the variable exons. The variable exons 4 and 5 are located within the MP domain (Figure 14). The MP domain binds negatively-charged membrane phospholipids and deforms membranes (Trevaskis et al., 2005) by an undescribed mechanism. This mechanism may involve positively charged lysine, arginine, or histidine residues, which mediate interactions with membrane lipids in membrane-binding domains (Lemmon, 2008). In this study, we detected five *Sgip1* splice variants that contain exon 4, five that lack exon 4 but contain exon 5, and five that lack both exons 4 and 5. Splice variants with the different exon compositions of the MP domain formed puncta at the plasma membrane, indicating their membrane association. Our results suggest that the MP domain formed by exons 1-3 and a part of exon 6, containing eight lysine and four arginine residues, may be sufficient to mediate Sgip1 binding to the plasma membrane. Therefore, exon variations in the MP domain do not limit Sgip1 interactions with plasma membrane lipids; however, these variations may affect the strength and specificity of the lipid binding or have a direct effect on protein interactions or dimerization.

The Sgip1 853 isoform showed an accumulation in the cytoplasm in the form of vesicles or inclusion bodies in about half of the transfected cells. The Sgip1 853 isoform differs from Sgip1 826 isoform only in the presence of exon 4; therefore, exon 4 may cause the unusual pattern of Sgip1 853 expression. Exon 4 encodes a stretch of three lysine residues that may cause an increase in the propensity of the protein to aggregate and form the intracellular bodies. Besides lysines, exon 4 encodes a cysteine residue that is followed by two aromatic residues. These amino acid motifs are conserved across species. The cysteine may either be post-translationally

modified or may form a sulfur bridge with a cysteine from the same peptide or another peptide, promoting homodimerization. Because exon 4 codes a sequence located within the MP domain, the MP domain may define the intracellular distribution of Sgip1.

We detected *Sgip1* splice variants with various exon combinations within the proline-rich region. Variations in exons 16 and 20 within the proline-rich region did not affect the protein's stability and localization. The proline-rich region of Sgip1 contains multiple potential phosphorylation sites (Craft et al., 2008; Edbauer et al., 2009), SH3- and WW-domain binding domains (Zarrinpar et al., 2003). Among the phosphorylation sites, the Ser-149, Ser-169, and Thr-409 were demonstrated *in vivo* to be dephosphorylated upon depolarization of nerve terminals (Munton et al., 2007; Craft et al., 2008). Hyperphosphorylation of Sgip1 was found in the Huntington's disease mice (Mees et al., 2022). Sgip1 was shown to be a substrate of MAP kinases (Edbauer et al., 2009), and its phosphorylation may therefore be physiologically significant. The mechanisms by which these sites mediate or regulate Sgip1's function or interaction with other endocytic proteins are unknown.

Specificity of the effect of SGIP1 on the CB1R internalization

We demonstrated that SGIP1 is a specific inhibitor of CB1R internalization, because SGIP1 did not affect the internalization of MOR and M3R. The internalization rate of the CB1R-RlucII construct was similar to that of the previously published results (Hajkova et al., 2016). Our results are also in line with our recent finding demonstrating that SGIP1 splice variants do not affect MOR internalization (Durydivka et al., 2023a).

Our findings demonstrate that SGIP1 is an endocytic regulator of CB1R. However, SGIP1 was shown to affect the internalization of receptors that do not belong to GPCR, such as transferrin and epidermal growth factor receptors (Uezu et al., 2007). The physiological consequences of the SGIP1 effect on these receptors are unknown, and the *Sgip1* knock-out mice have a phenotype that indicates impairments of CB1R and the endocannabinoid system.

The enhanced bystander BRET system is a versatile tool that can be adapted for various applications. While we monitored the receptor internalization from the plasma membrane, this system can be used for monitoring receptor trafficking in early endosomes, lysosomes, mitochondria, Golgi apparatus, or other intracellular compartments. For these purposes, the BRET acceptor rGFP is targeted to the corresponding intracellular compartment. The CB1R-

RlucII construct can be used for these applications, which allows precise evaluation of the intracellular distribution of CB1R.

5.3. Pharmacodynamic studies of the hexahydrocannabinol effect on CB1R

The pharmacological activity of receptor ligands can be characterized by the potency and efficacy, among other measures. We evaluated signaling profiles of the ligands that act on CB1R by measuring the G protein activation, GRK3-CB1R interaction, and β-arrestin 2-CB1R interaction. The tested ligands were (9S)-HHC, (9R)-HHC, THC, and WIN. We found that the HHC epimers differed in their signaling outcomes.

In the G protein activation assay, the potency and efficacy of (9R)-HHC were similar to THC, as opposed to (9S)-HHC, which had low potency and efficacy in this assay (Figure 21). These data demonstrate that (9S)-HHC has a lower affinity to CB1R than (9R)-HHC, and the affinity of (9R)-HHC is similar to that of THC. Similarly, the biological activity of (9S)-HHC is lower than that of (9R)-HHC, and the activity of (9R)-HHC is close to that of THC (Russo et al., 2023).

In the GRK3 and β-arrestin 2 interaction assays, THC had very little efficacy (Figure 21), which makes the calculated potency value meaningless; therefore, we excluded THC from the comparison. The potency of (9S)-HHC was lower than that of (9R)-HHC; however, (9S)-HHC and (9R)-HHC had similar efficacies. These data demonstrate that (9S)-HHC has a lower affinity to CB1R than (9R)-HHC, but (9S)-HHC and (9R)-HHC have similar biological activity. However, because the signaling output of (9S)-HHC did not reach saturation, the calculated efficacy values for (9S)-HHC might not be entirely accurate (Tables 8 and 9).

Based on all the assays, (9S)-HHC has a lower affinity to CB1R than (9R)-HHC, and (9S)-HHC has a lower effect on G protein signaling than (9R)-HHC. However, in GRK3 and β-arrestin 2 signaling, the effects of (9S)-HHC and (9R)-HHC are similar.

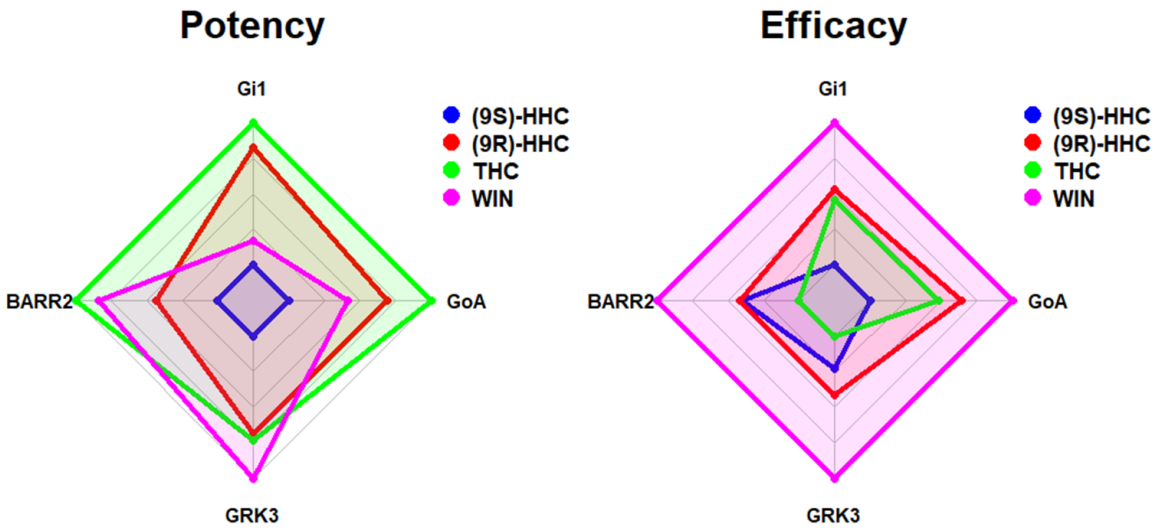

Figure 21. Potencies and efficacies of the tested ligands. The EC50 values reflecting the potency and maximal response values reflecting the efficacy were plotted on the x and y axes. The axes indicate signaling pathways: Gi1, GoA, GRK3, β-arrestin 2 (BARR2), and the normalized EC50 or maximal response values of the indicated ligands are plotted on these axes.

Our results correspond to the previous findings demonstrating the higher affinity of (9R)-HHC to CB1R than that of (9S)-HHC (Reggio et al., 1989). (9R)-HHC was shown to be more potent in cannabinoid-related tests in mice than (9S)-HHC. (9R)-HHC significantly affected two behaviors of the cannabinoid tetrad test: hypolocomotion, reflecting reduced spontaneous movements, and analgesia, reflecting pain relief (Russo et al., 2023). However, the ability of (9R)-HHC to affect mouse behavior was lower than that of THC. These findings suggest that (9R)-HHC, but not (9S)-HHC, may have a CB1R-mediated psychotropic effect.

While we tested the pharmacological activities of the highly pure preparations of the HHC epimers, the HHC available in the market usually contains a mix of two epimers. Because these two epimers differ in potency and efficacy, the proportion of (9R)-HHC and (9S)-HHC defines the overall biological activity of such preparations. The proportions of HHC epimers greatly depend on the way of synthesizing, but they can also have batch-to-batch variation. For example, hydrogenation of THC using platinum catalyst produces (9S)-HHC and (9R)-HHC in approximately 1:2 ratio. In contrast, when Δ^8-THC is used in the same conditions, the production of (9S)-HHC is favored, and the ratio of (9S)-HHC to (9R)-HHC is 3:1 or 3:2 (Gaoni et al., 1966; Archer et al., 1970; Turner et al., 1973). Thus, the ratio of the HHC epimers may

indicate the way of its synthesis. Moreover, the ratio affects the biological activity, so the epimer ratio should be determined for every preparation.

The emergence of new semi-synthetic cannabinoids represents an exciting frontier in cannabinoid research and drug development. These cannabinoids may have improved stability and therapeutic effects, making them promising candidates for a range of applications. They may substitute the currently available drugs targeting CB1R due to their facile production and potentially improved chemical stability. Alternatively, they can facilitate the development of new synthetic cannabinoids and the optimization of their chemical composition and structure. The currently available pharmaceuticals that target CB1R, such as dronabinol, nabilone, and nabiximols, have shown efficacy in various therapeutic conditions, including pain management, appetite stimulation, and nausea control, but often come with a suite of side effects that can be problematic for patients. Semi-synthetic cannabinoids could offer a more targeted and controlled approach to CB1R modulation, potentially reducing the incidence and severity of side effects.

The clinical applications of cannabinoids are limited by their psychoactive action. This limitation has impelled ongoing research efforts to develop cannabinoids that offer therapeutic benefits without unwanted psychoactive effects. The currently available drugs acting on CB1R can have a range of side effects, from cognitive impairment to mood alterations and even addiction, making the clinical use of these drugs challenging and less desirable for certain patients. By selectively targeting CB1R-mediated therapeutic pathways while reducing activation in regions associated with euphoria and intoxication, researchers aim to create medications that offer the benefits of cannabinoids without their drawbacks. Thus, the new cannabinoids may offer a more controlled approach to the modulation of CB1R and the endocannabinoid system with minimized side effects.

Currently, there are no studies on the pharmacological and behavioral effects of HHC in humans, and only the consumers indicate that its effects are similar to those of THC. Due to this fact, the European Monitoring Centre for Drugs and Drug Addiction (EMCDDA) closely monitors HHC as a new psychoactive substance through the European Union Early Warning System (EWS) (Ujvary et al., 2023).

The data on the safety of HHC is scarce. In one study, no toxic effects of HHC were observed up to HHC concentration of 50 uM, and HHC produced potential cytotoxic effects only when it exceeded the concentration of 10 mM (Collins et al., 2022). These findings indicate that safe

possible human consumption of THC is feasible without complications. However, contamination of HHC preparations with extraction residues or synthetic byproducts could pose unforeseen risks. Therefore, the HHC and other cannabinoid products on the market should be under close control of the authorities to ensure their quality and safety. In addition, more *in vitro* and *in vivo* studies are necessary to properly understand the effects of HHC on cell signaling and organism functions.

6. CONCLUSIONS

In this work, we studied the mechanisms influencing the signaling of cannabinoid receptor 1 (CB1R) on the molecular level and on the level of the organism. To study the role of SGIP1 in pain sensitivity, the alternative splicing of SGIP1, and the effect of minor cannabinoid hexahydrocannabinol (HHC) on CB1R, we employed various molecular biology and animal behavior approaches. These approaches included the behavioral testing of mechanical sensitivity, immunoblotting and PCR analysis, molecular cloning, light microscopy, and bioluminescence resonance energy transfer (BRET) assays.

First, we provide evidence that SGIP1 is an important player in inflammatory pain perception. Deletion of *Sgip1* resulted in the increase in chronic pain sensitivity in male but not in female mice during carrageenan-induced inflammation. After WIN or THC injections, *Sgip1* knock-out males preserved the increased nociception. The female mice had comparable pain thresholds after WIN application, but *Sgip1* knock-out female mice had higher pain thresholds after THC application than wild-type mice (Hypothesis 1, Aim 1).

Next, we cloned 15 *Sgip1* splice variants from the mouse brain. These splice variants result from alternative splicing of exons encoding the MP domain (exons 4 and 5) and proline-rich region (exons 9, 10, 15-20) of Sgip1 protein. Alterations within the MP domain or proline-rich region do not affect the stability of most Sgip1 splice isoforms and their subcellular localization (Hypothesis 2, Aim 2).

Further, we demonstrated that SGIP1 is a specific endocytic inhibitor of CB1R. SGIP1 inhibits CB1R internalization but do not affect internalization of other receptors, such as μ-opioid receptor and muscarinic acetylcholine M3 receptor.

Last, we evaluated the effects of HHC epimers (9S)-HHC and (9R)-HHC on CB1R signaling. We found that the potency and efficacy of (9R)-HHC to activate G proteins is higher than that of (9S)-HHC. However, the efficacy to cause GRK3 and β-arrestin 2 interactions with CB1R is similar for both (9R)-HHC and (9S)-HHC. Moreover, the pharmacological profile of (9R)-HHC is closer to that of THC (Hypothesis 3, Aim 3).

Taken together, we demonstrate that SGIP1 is a specific CB1R-interacting protein, involved in CB1R-mediated chronic pain sensitivity. SGIP1 modulates pain processing pathways, resulting in decreased chronic pain sensitivity. The presence of multiple splice variants of SGIP1 suggests that expression of certain SGIP1 splice variants might be tailored to specific functions.

The pharmacological activity of (9R)-HHC epimer, but not (9S)-HHC epimer, approximates that of THC. Due to the limited number of studies on HHC, its pharmacological potential should be assessed in future studies on its safety and biological action.

7. SUMMARY

7.1. The effect of Sgip1 on chronic pain processing

We tested the chronic nociception in *Sgip1* knock-out and wild-type mice. We found that *Sgip1* deletion results in an increase in chronic nociception in male but not in female mice. The increased chronic nociception persisted in *Sgip1* knock-out male mice even after cannabinoid drug injections. Therefore, the effect of Sgip1 on CB1R results in decreased chronic pain sensitivity.

7.2. Identification and characterization of *Sgip1* splice variants in the brain

We addressed the discrepancies regarding the use of different *Sgip1* splice variants present in the literature. We cloned 15 *Sgip1* splice variants from the mouse brain and found that exons that undergo alternative splicing encode portions of the MP domain (exons 4 and 5) and proline-rich region (exons 9, 10, 15-20) of the Sgip1 protein. While most of *Sgip1* splice variants had similar properties, the intracellular localization of *Sgip1* variants containing exon 4 was distorted, and this variant accumulated in the intracellular vesicles or bodies.

We also tested the effect of SGIP1 on internalization of CB1R, μ-opioid receptor, and muscarinic acetylcholine M3 receptor. We found that SGIP1 is a specific endocytic inhibitor of CB1R, as SGIP1 does not affect internalization of μ-opioid receptor and muscarinic acetylcholine M3 receptor.

7.3. Pharmacodynamic studies of the hexahydrocannabinol effect on CB1R

We measured the CB1R-related G protein, GRK3, and β-arrestin 2 signaling of hexahydrocannabinol (HHC) epimers. We found that (9R)-HHC epimer has the pharmacological activity higher than that of (9S)-HHC in the G protein activation. However, (9R)-HHC and (9S)-HHC have comparable effects on GRK3- and β-arrestin 2-related signaling. Overall, the potency and efficacy of (9R)-HHC is similar to that of THC.

8. LITERATURE REFERENCES

Adams, R., Loewe, S., Pease, D. C., Cain, C. K., Wearn, R. B., Baker, R. B., Wolff, H., 1940. Structure of cannabidiol. VIII. Position of the double bonds in cannabidiol. Marihuana activity of tetrahydro-cannabinols. Journal of the American Chemical Society 62, 2566-67. https://doi.org/10.1021/ja01866a510

Ahn, A. H., Kunkel, L. M., 1995. Syntrophin Binds to an Alternatively Spliced Exon of Dystrophin. Journal of Cell Biology 128, 363-71. https://doi.org/10.1083/jcb.128.3.363

Ahn, K. H., Nishiyama, A., Mierke, D. F., Kendall, D. A., 2010. Hydrophobic Residues in Helix 8 of Cannabinoid Receptor 1 Are Critical for Structural and Functional Properties. Biochemistry 49, 502-11. https://doi.org/10.1021/bi901619r

Al-Zoubi, R., Morales, P., Reggio, P. H., 2019. Structural Insights into CB1 Receptor Biased Signaling. International Journal of Molecular Sciences 20. https://doi.org/10.3390/ijms20081837

Antonny, B., Burd, C., De Camilli, P., Chen, E., Daumke, O., Faelber, K., Ford, M., Frolov, V. A., Frost, A., Hinshaw, J. E., Kirchhausen, T., Kozlov, M. M., Lenz, M., Low, H. H., McMahon, H., Merrifield, C., Pollard, T. D., Robinson, P. J., Roux, A., Schmid, S., 2016. Membrane fission by dynamin: what we know and what we need to know. Embo Journal 35, 2270-84. https://doi.org/10.15252/embj.201694613

Archer, R. A., Demarco, P. V., Tyminski, I. J., Allinger, N. L., Boyd, D. B., 1970. STRUCTURAL STUDIES OF CANNABINOIDS - A THEORETICAL AND PROTON MAGNETIC RESONANCE ANALYSIS. Journal of the American Chemical Society 92, 5200-&. https://doi.org/10.1021/ja00720a033

Ashery, Uri, Bielopolski, Noa, Lavi, Ayal, Barak, Boaz, Michaeli, Lirin, Ben-Simon, Yoav, Sheinin, Anton, Bar-On, Dana, Shapira, Zehavit, Gottfried, Irit, 2014. The Molecular Mechanisms Underlying Synaptic Transmission: A View of the Presynaptic Terminal. in Virginia Pickel and Menahem Segal (eds.), *The Synapse* (Academic Press: Boston).

Beacham, G. M., Partlow, E. A., Hollopeter, G., 2019. Conformational regulation of AP1 and AP2 clathrin adaptor complexes. Traffic 20, 741-51. https://doi.org/10.1111/tra.12677

Benard, G., Massa, F., Puente, N., Lourenco, J., Bellocchio, L., Soria-Gomez, E., Matias, I., Delamarre, A., Metna-Laurent, M., Cannich, A., Hebert-Chatelain, E., Mulle, C., Ortega-Gutierrez, S., Martin-Fontecha, M., Klugmann, M., Guggenhuber, S., Lutz, B., Gertsch, J., Chaouloff, F., Lopez-Rodriguez, M. L., Grandes, P., Rossignol, R., Marsicano, G., 2012. Mitochondrial CB1 receptors regulate neuronal energy metabolism. Nature Neuroscience 15, 558-64. https://doi.org/10.1038/nn.3053

Berg, K. A., Clarke, W. P., 2018. Making Sense of Pharmacology: Inverse Agonism and Functional Selectivity. International Journal of Neuropsychopharmacology 21, 962-77. https://doi.org/10.1093/ijnp/pyy071

Berthele, A., Laurie, D. J., Platzer, S., Zieglgansberger, W., Tolle, T. R., Sommer, B., 1998. Differential expression of rat and human type 1 metabotropic glutamate receptor splice variant messenger RNAs. Neuroscience 85, 733-49. https://doi.org/10.1016/S0306-4522(97)00670-2

Birkett, C. R., Foster, K. E., Johnson, L., Gull, K., 1985. Use of Monoclonal-Antibodies to Analyze the Expression of a Multi-Tubulin Family. Febs Letters 187, 211-18. https://doi.org/10.1016/0014-5793(85)81244-8

Blanton, H. L., Barnes, R. C., McHann, M. C., Bilbrey, J. A., Wilkerson, J. L., Guindon, J., 2021. Sex differences and the endocannabinoid system in pain. Pharmacology Biochemistry and Behavior 202. https://doi.org/10.1016/j.pbb.2021.173107

Blume, L. C., Eldeeb, K., Bass, C. E., Selley, D. E., Howlett, A. C., 2015. Cannabinoid receptor interacting protein (CRIP1a) attenuates CB1R signaling in neuronal cells. Cellular Signalling 27, 716-26. https://doi.org/10.1016/j.cellsig.2014.11.006

Blume, L. C., Leone-Kabler, S., Luessen, D. J., Marrs, G. S., Lyons, E., Bass, C. E., Chen, R., Selley, D. E., Howlett, A. C., 2016. Cannabinoid receptor interacting protein suppresses agonist-driven CB1 receptor internalization and regulates receptor replenishment in an agonist-biased manner. Journal of Neurochemistry 139, 396-407. https://doi.org/10.1111/jnc.13767

Bohn, L. M., 2007. Constitutive trafficking - More than just running in circles? Molecular Pharmacology 71, 957-58. https://doi.org/10.1124/mol.107.034223

Bosier, B., Muccioli, G. G., Hermans, E., Lambert, D. M., 2010. Functionally selective cannabinoid receptor signalling: Therapeutic implications and opportunities. Biochemical Pharmacology 80, 1-12. https://doi.org/10.1016/j.bcp.2010.02.013

Brailoiu, G. C., Oprea, T. I., Zhao, P. W., Abood, M. E., Brailoiu, E., 2011. Intracellular Cannabinoid Type 1 (CB1) Receptors Are Activated by Anandamide. Journal of Biological Chemistry 286, 29166-74. https://doi.org/10.1074/jbc.M110.217463

Breivogel, C. S., Lambert, J. M., Gerfin, S., Huffman, J. W., Razdan, R. K., 2008. Sensitivity to Delta 9-tetrahydrocannabinol is selectively enhanced in beta-arrestin2-/- mice. Behavioural Pharmacology 19, 298-307. https://doi.org/10.1097/FBP.0b013e328308f1e6

Bridges, D., Rice, A. S. C., Egertova, M., Elphick, M. R., Winter, J., Michael, G. J., 2003. Localisation of cannabinoid receptor 1 in rat dorsal root ganglion using in situ hybridisation and immunohistochemistry. Neuroscience 119, 803-12. https://doi.org/10.1016/s0306-4522(03)00200-8

Brown, A. J., 2007. Novel cannabinoid receptors. British Journal of Pharmacology 152, 567-75. https://doi.org/10.1038/sj.bjp.0707481

Busquets-Garcia, A., Bains, J., Marsicano, G., 2018. CB1 Receptor Signaling in the Brain: Extracting Specificity from Ubiquity. Neuropsychopharmacology 43, 4-20. https://doi.org/10.1038/npp.2017.206

Busquets-Garcia, A., Gomis-Gonzalez, M., Srivastava, R. K., Cutando, L., Ortega-Alvaro, A., Ruehle, S., Remmers, F., Bindila, L., Bellocchio, L., Marsicano, G., Lutz, B., Maldonado, R., Ozaita, A., 2016. Peripheral and central CB1 cannabinoid receptors control stress-induced impairment of memory consolidation. Proceedings of the National Academy of Sciences of the United States of America 113, 9904-09. https://doi.org/10.1073/pnas.1525066113

Calderon, R. O., Attema, B., Devries, G. H., 1995. Lipid-Composition of Neuronal Cell-Bodies and Neurites from Cultured Dorsal-Root Ganglia. Journal of Neurochemistry 64, 424-29. https://doi.org/10.1046/j.1471-4159.1995.64010424.x

Casati, S., Rota, P., Bergamaschi, R. F., Palmisano, E., La Rocca, P., Ravelli, A., Angeli, I., Minoli, M., Roda, G., Orioli, M., 2022. Hexahydrocannabinol on the Light Cannabis Market: The Latest "New" Entry. Cannabis and cannabinoid research. https://doi.org/10.1089/can.2022.0253

Castillo, P. E., Younts, T. J., Chavez, A. E., Hashimotodani, Y., 2012. Endocannabinoid Signaling and Synaptic Function. Neuron 76, 70-81. https://doi.org/10.1016/j.neuron.2012.09.020

Chaperon, F., Thiebot, M. H., 1999. Behavioral effects of cannabinoid agents in animals. Critical Reviews in Neurobiology 13, 243-81. https://doi.org/10.1615/CritRevNeurobiol.v13.i3.20

Chavez, A. E., Chiu, C. Q., Castillo, P. E., 2010. TRPV1 activation by endogenous anandamide triggers postsynaptic long-term depression in dentate gyrus. Nature Neuroscience 13, 1511-U99. https://doi.org/10.1038/nn.2684

Chevaleyre, V., Heifets, B. D., Kaeser, P. S., Sudhof, T. C., Purpura, D. P., Castillo, P. E., 2007. Endocannabinoid-mediated long-term plasticity requires cAMP/PKA signaling and RIM1 alpha. Neuron 54, 801-12. https://doi.org/10.1016/j.neuron.2007.05.020

Chwedorowicz, R., Raszewski, G., Kapka-Skrzypczak, L., Sawicki, K., Studzinski, T., 2016. Event-related potentials (ERP) and SGIP1 gene polymorphisms in alcoholics: relation to family history of alcoholism and drug usage. Annals of Agricultural and Environmental Medicine 23, 618-24. https://doi.org/10.5604/12321966.1226856

Colantoni, A., Bianchi, V., Gherardini, P. F., Tomba, G. S., Ausiello, G., Helmer-Citterich, M., Ferre, F., 2013. Alternative splicing tends to avoid partial removals of protein-protein interaction sites. Bmc Genomics 14. https://doi.org/10.1186/1471-2164-14-379

Collins, A. C., Tesfatsion, T. T., Ramirez, G. A., Ray, K. P., Cruces, W., 2022. Nonclinical In Vitro Safety Assesment Summary of Hemp Derived (R/S)-Hexahydrocannabinol ((R/S)-HHC). [Preprint] Research Square. https://doi.org/doi.org/10.21203/rs.3.rs-2299264/v1

Corder, G., Castro, D. C., Bruchas, M. R., Scherrer, G., 2018. Endogenous and Exogenous Opioids in Pain. Annual Review of Neuroscience, Vol 41 41, 453-73. https://doi.org/10.1146/annurev-neuro-080317-061522

Costas-Insua, C., Moreno, E., Maroto, I. B., Ruiz-Calvo, A., Bajo-Graneras, R., Martin-Gutierrez, D., Diez-Alarcia, R., Vilaro, M. T., Cortes, R., Garcia-Font, N., Martin, R., Espina, M., Botta, J., Gines, S., McCormick, P. J., Sanchez-Prieto, J., Galve-Roperh, I., Mengod, G., Uriguen, L., Marsicano, G., Bellocchio, L., Canela, E. I., Casado, V., Rodriguez-Crespo, I., Guzman, M., 2021. Identification of BiP as a CB1 Receptor-Interacting Protein That Fine-Tunes Cannabinoid Signaling in the Mouse Brain. Journal of Neuroscience 41, 7924-41. https://doi.org/10.1523/Jneurosci.0821-21.2021

Coutts, A. A., Anavi-Goffer, S., Ross, R. A., MacEwan, D. J., Mackie, K., Pertwee, R. G., Irving, A. J., 2001. Agonist-induced internalization and trafficking of cannabinoid CB1 receptors in hippocampal neurons. Journal of Neuroscience 21, 2425-33. https://doi.org/10.1523/JNEUROSCI.21-07-02425.2001

Craft, G. E., Graham, M. E., Bache, N., Larsen, M. R., Robinson, P. J., 2008. The in vivo phosphorylation sites in multiple isoforms of amphiphysin I from rat brain nerve terminals. Molecular & Cellular Proteomics 7, 1146-61. https://doi.org/10.1074/mcp.M700351-MCP200

Craft, R. M., Kandasamy, R., Davis, S. M., 2013. Sex differences in anti-allodynic, anti-hyperalgesic and anti-edema effects of Delta(9)-tetrahydrocannabinol in the rat. Pain 154, 1709-17. https://doi.org/10.1016/j.pain.2013.05.017

Cummings, N., Shields, K. A., Curran, J. E., Bozaoglu, K., Trevaskis, J., Gluschenko, K., Cai, G., Comuzzie, A. G., Dyer, T. D., Walder, K. R., Zimmet, P., Collier, G. R., Blangero, J., Jowett, J. B. M., 2012. Genetic variation in SH3-domain GRB2-like (endophilin)-interacting protein 1 has a major impact on fat mass. International Journal of Obesity 36, 201-06. https://doi.org/10.1038/ijo.2011.67

Curioni, C., Andre, C., Veras, R., 2006. Weight reduction for primary prevention of stroke in adults with overweight or obesity. Cochrane Database of Systematic Reviews. https://doi.org/10.1002/14651858.CD006062.pub2

De Petrocellis, L., Starowicz, K., Moriello, A. S., Vivese, M., Orlando, P., Di Marzo, V., 2007. Regulation of transient receptor potential channels of melastatin type 8 (TRPM8): Effect of cAMP, cannabinoid CB, receptors and endovanilloids. Experimental Cell Research 313, 1911-20. https://doi.org/10.1016/j.yexcr.2007.01.008

Delgado-Peraza, F., Ahn, K. H., Nogueras-Ortiz, C., Mungrue, I. N., Mackie, K., Kendall, D. A., Yudowski, G. A., 2016. Mechanisms of Biased beta-Arrestin-Mediated Signaling Downstream from the Cannabinoid 1 Receptor. Molecular Pharmacology 89, 618-29. https://doi.org/10.1124/mol.115.103176

Dergai, O., Novokhatska, O., Dergai, M., Skrypkina, I., Tsyba, L., Moreau, J., Rynditch, A., 2010. Intersectin 1 forms complexes with SGIP1 and Reps1 in clathrin-coated pits. Biochemical and Biophysical Research Communications 402, 408-13. https://doi.org/10.1016/j.bbrc.2010.10.045

Derkinderen, P., Valjent, E., Toutant, M., Corvol, J. C., Enslen, H., Ledent, C., Trzaskos, J., Caboche, J., Girault, J. A., 2003. Regulation of extracellular signal-regulated kinase by cannabinoids in hippocampus. Journal of Neuroscience 23, 2371-82.

Di Marzo, V., 2011. Endocannabinoid signaling in the brain: biosynthetic mechanisms in the limelight. Nature Neuroscience 14, 9-15. https://doi.org/10.1038/nn.2720

Di Marzo, V., De Petrocellis, L., 2012. Why do cannabinoid receptors have more than one endogenous ligand? Philosophical Transactions of the Royal Society B-Biological Sciences 367, 3216-28. https://doi.org/10.1098/rstb.2011.0382

Di Marzo, V., Despres, J. P., 2009. CB1 antagonists for obesity-what lessons have we learned from rimonabant? Nature Reviews Endocrinology 5, 633-38. https://doi.org/10.1038/nrendo.2009.197

Dimarzo, V., Fontana, A., Cadas, H., Schinelli, S., Cimino, G., Schwartz, J. C., Piomelli, D., 1994. FORMATION AND INACTIVATION OF ENDOGENOUS CANNABINOID ANANDAMIDE IN CENTRAL NEURONS. Nature 372, 686-91. https://doi.org/10.1038/372686a0

Domenici, M. R., Azad, S. C., Marsicano, G., Schierloh, A., Wotjak, C. T., Dodt, H. U., Zieglgansberger, W., Lutz, B., Rammes, G., 2006. Cannabinoid receptor type 1 located on presynaptic terminals of principal neurons in the forebrain controls glutamatergic synaptic transmission. Journal of Neuroscience 26, 5794-99. https://doi.org/10.1523/jneurosci.0372-06.2006

Durydivka, O., Gazdarica, M., Vecerkova, K., Radenkovic, S., Blahos, J., 2023a. Multiple Sgip1 Splice Variants Inhibit Cannabinoid Receptor 1 Internalization. Gene, 147851. https://doi.org/10.1016/j.gene.2023.147851

Durydivka, O., Mackie, K., Blahos, J., 2023b. SGIP1 in axons prevents internalization of desensitized CB1R and modifies its function. Frontiers in Neuroscience 17. https://doi.org/10.3389/fnins.2023.1213094

Dvorakova, M., Kubik-Zahorodna, A., Straiker, A., Sedlacek, R., Hajkova, A., Mackie, K., Blahos, J., 2021. SGIP1 is involved in regulation of emotionality, mood, and nociception and modulates in vivo signalling of cannabinoid CB1 receptors. British Journal of Pharmacology 178, 1588-604. https://doi.org/10.1111/bph.15383

Edbauer, D., Cheng, D. M., Batterton, M. N., Wang, C. F., Duong, D. M., Yaffe, M. B., Peng, J. M., Sheng, M., 2009. Identification and Characterization of Neuronal Mitogen-

activated Protein Kinase Substrates Using a Specific Phosphomotif Antibody. Molecular & Cellular Proteomics 8, 681-95. https://doi.org/10.1074/mcp.M800233-MCP200

ElSohly, M. A., Slade, D., 2005. Chemical constituents of marijuana: The complex mixture of natural cannabinoids. Life Sciences 78, 539-48. https://doi.org/10.1016/j.lfs.2005.09.011

Faelber, K., Posor, Y., Gao, S., Held, M., Roske, Y., Schulze, D., Haucke, V., Noe, F., Daumke, O., 2011. Crystal structure of nucleotide-free dynamin. Nature 477, 556-U318. https://doi.org/10.1038/nature10369

Finn, D. P., Haroutounian, S., Hohmann, A. G., Krane, E., Soliman, N., Rice, A. S. C., 2021. Cannabinoids, the endocannabinoid system, and pain: a review of preclinical studies. Pain 162, S5-S25. https://doi.org/10.1097/j.pain.0000000000002268

Fitzner, D., Bader, J. M., Penkert, H., Bergner, C. G., Su, M. H., Weil, M. T., Surma, M. A., Mann, M., Klose, C., Simons, M., 2020. Cell-Type- and Brain-Region-Resolved Mouse Brain Lipidome. Cell Reports 32. https://doi.org/10.1016/j.celrep.2020.108132

Fletcher-Jones, A., Hildick, K. L., Evans, A. J., Nakamura, Y., Henley, J. M., Wilkinson, K. A., 2020. Protein Interactors and Trafficking Pathways That Regulate the Cannabinoid Type 1 Receptor (CB1R). Frontiers in Molecular Neuroscience 13. https://doi.org/10.3389/fnmol.2020.00108

Fletcher-Jones, A., Hildick, K. L., Evans, A. J., Nakamura, Y., Wilkinson, K. A., Henley, J. M., 2019. The C-terminal helix 9 motif in rat cannabinoid receptor type 1 regulates axonal trafficking and surface expression. Elife 8. https://doi.org/10.7554/eLife.44252

Fletcher-Jones, Alexandra, Spackman, Ellen, Craig, Tim J., Nakamura, Yasuko, Wilkinson, Kevin A., Henley, Jeremy M., 2023. SGIP1 binding to the α-helical H9 domain of cannabinoid receptor 1 promotes axonal surface expression. bioRxiv, 2023.07.18.549510. https://doi.org/10.1101/2023.07.18.549510

Flores-Otero, J., Ahn, K. H., Delgado-Peraza, F., Mackie, K., Kendall, D. A., Yudowski, G. A., 2014. Ligand-specific endocytic dwell times control functional selectivity of the cannabinoid receptor 1. Nature Communications 5. https://doi.org/10.1038/ncomms5589

Foltin, R. W., Brady, J. V., Fischman, M. W., 1986. Behavioral-Analysis of Marijuana Effects on Food-Intake in Humans. Pharmacology Biochemistry and Behavior 25, 577-82. https://doi.org/10.1016/0091-3057(86)90144-9

Fotin, A., Cheng, Y. F., Sliz, P., Grigorieff, N., Harrison, S. C., Kirchhausen, T., Walz, T., 2004. Molecular model for a complete clathrin lattice from electron cryomicroscopy. Nature 432, 573-79. https://doi.org/10.1038/nature03079

Francis, D. L., Schneider, C., 1971. Jumping after Naloxone Precipitated Withdrawal of Chronic Morphine in Rat. British Journal of Pharmacology 41, P424-+.

Frost, A., Perera, R., Roux, A., Spasov, K., Destaing, O., Egelman, E. H., De Camilli, P., Unger, V. M., 2008. Structural basis of membrane invagination by F-BAR domains. Cell 132, 807-17. https://doi.org/10.1016/j.cell.2007.12.041

Gaoni, Y., Mechoulam, R., 1966. Hashish .7. Isomerization of Cannabidiol to Tetrahydrocannabinols. Tetrahedron 22, 1481-+. https://doi.org/10.1016/S0040-4020(01)99446-3

Gatchel, R. J., McGeary, D. D., McGeary, C. A., Lippe, B., 2014. Interdisciplinary Chronic Pain Management Past, Present, and Future. American Psychologist 69, 119-30. https://doi.org/10.1037/a0035514

Gazdarica, M., Noda, J., Durydivka, O., Novosadova, V., Mackie, K., Pin, J. P., Prezeau, L., Blahos, J., 2021. SGIP1 modulates kinetics and interactions of the cannabinoid receptor

1 and G protein-coupled receptor kinase 3 signalosome. Journal of Neurochemistry. https://doi.org/10.1111/jnc.15569

Goonawardena, A. V., Robinson, L., Hampson, R. E., Riedel, G., 2010. Cannabinoid and cholinergic systems interact during performance of a short-term memory task in the rat. Learning & Memory 17, 502-11. https://doi.org/10.1101/lm.1893710

Guardia, C. M., De Pace, R., Mattera, R., Bonifacino, J. S., 2018. Neuronal functions of adaptor complexes involved in protein sorting. Current Opinion in Neurobiology 51, 103-10. https://doi.org/10.1016/j.conb.2018.02.021

Guggenhuber, S., Alpar, A., Chen, R. Q., Schmitz, N., Wickert, M., Mattheus, T., Harasta, A. E., Purrio, M., Kaiser, N., Elphick, M. R., Monory, K., Kilb, W., Luhmann, H. J., Harkany, T., Lutz, B., Klugmann, M., 2016. Cannabinoid receptor-interacting protein Crip1a modulates CB1 receptor signaling in mouse hippocampus. Brain Structure & Function 221, 2061-74. https://doi.org/10.1007/s00429-015-1027-6

Guzikowski, N. J., Kavalali, E. T., 2021. Nano-Organization at the Synapse: Segregation of Distinct Forms of Neurotransmission. Frontiers in Synaptic Neuroscience 13. https://doi.org/10.3389/fnsyn.2021.796498

Hajkova, A., Techlovska, S., Dvorakova, M., Chambers, J. N., Kumpost, J., Hubalkova, P., Prezeau, L., Blahos, J., 2016. SGIP1 alters internalization and modulates signaling of activated cannabinoid receptor 1 in a biased manner. Neuropharmacology 107, 201-14. https://doi.org/10.1016/j.neuropharm.2016.03.008

Haring, M., Enk, V., Rey, A. A., Loch, S., de Azua, I. R., Weber, T., Bartsch, D., Monory, K., Lutz, B., 2015. Cannabinoid type-1 receptor signaling in central serotonergic neurons regulates anxiety-like behavior and sociability. Frontiers in Behavioral Neuroscience 9. https://doi.org/10.3389/tnbeh.2015.00235

Hebert-Chatelain, E., Desprez, T., Serrat, R., Bellocchio, L., Soria-Gomez, E., Busquets-Garcia, A., Zottola, A. C. P., Delamarre, A., Cannich, A., Vincent, P., Varilh, M., Robin, L. M., Terral, G., Garcia-Fernandez, M. D., Colavita, M., Mazier, W., Drago, F., Puente, N., Reguero, L., Elezgarai, I., Dupuy, J. W., Cota, D., Lopez-Rodriguez, M. L., Barreda-Gomez, G., Massa, F., Grandes, P., Benard, G., Marsicano, G., 2016. A cannabinoid link between mitochondria and memory. Nature 539, 555-+. https://doi.org/10.1038/nature20127

Heifets, B. D., Castillo, P. E., 2009. Endocannabinoid Signaling and Long-Term Synaptic Plasticity. Annual Review of Physiology 71, 283-306. https://doi.org/10.1146/annurev.physiol.010908.163149

Heinricher, M. M., Tavares, I., Leith, J. L., Lumb, B. M., 2009. Descending control of nociception: Specificity, recruitment and plasticity. Brain Research Reviews 60, 214-25. https://doi.org/10.1016/j.brainresrev.2008.12.009

Henne, W. M., Boucrot, E., Meinecke, M., Evergren, E., Vallis, Y., Mittal, R., McMahon, H. T., 2010. FCHo Proteins Are Nucleators of Clathrin-Mediated Endocytosis. Science 328, 1281-84. https://doi.org/10.1126/science.1188462

Henne, W. M., Kent, H. M., Ford, M. G. J., Hegde, B. G., Daumke, O., Butler, P. J. G., Mittal, R., Langen, R., Evans, P. R., McMahon, H. T., 2007. Structure and analysis of FCHo2F-BAR domain: A dimerizing and membrane recruitment module that effects membrane curvature. Structure 15, 839-52. https://doi.org/10.1016/j.str.2007.05.002

Herkenham, M., Lynn, A. B., Johnson, M. R., Melvin, L. S., Decosta, B. R., Rice, K. C., 1991. Characterization and Localization of Cannabinoid Receptors in Rat-Brain - a Quantitative Invitro Autoradiographic Study. Journal of Neuroscience 11, 563-83. https://doi.org/10.1523/jneurosci.11-02-00563.1991

Herkenham, M., Lynn, A. B., Little, M. D., Johnson, M. R., Melvin, L. S., Decosta, B. R., Rice, K. C., 1990. Cannabinoid Receptor Localization in Brain. Proceedings of the National Academy of Sciences of the United States of America 87, 1932-36. https://doi.org/10.1073/pnas.87.5.1932

Hiller, M., Huse, K., Szafranski, K., Jahn, N., Hampe, J., Schreiber, S., Backofen, R., Platzer, M., 2004. Widespread occurrence of alternative splicing at NAGNAG acceptors contributes to proteome plasticity. Nature Genetics 36, 1255-57. https://doi.org/10.1038/ng1469

Hirst, J., Schlacht, A., Norcott, J. P., Traynor, D., Bloomfield, G., Antrobus, R., Kay, R. R., Dacks, J. B., Robinson, M. S., 2014. Characterization of TSET, an ancient and widespread membrane trafficking complex. Elife 3. https://doi.org/10.7554/eLife.02866

Hodgkinson, C. A., Enoch, M. A., Srivastava, V., Cummins-Oman, J. S., Ferrier, C., Iarikova, P., Sankararaman, S., Yamini, G., Yuan, Q. P., Zhou, Z. F., Albaugh, B., White, K. V., Shen, P. H., Goldman, D., 2010. Genome-wide association identifies candidate genes that influence the human electroencephalogram. Proceedings of the National Academy of Sciences of the United States of America 107, 8695-700. https://doi.org/10.1073/pnas.0908134107

Hoffman, A. F., Lupica, C. R., 2000. Mechanisms of cannabinoid inhibition of GABA(A) synaptic transmission in the hippocampus. Journal of Neuroscience 20, 2470-79.

Hohmann, A. G., Suplita, R. L., Bolton, N. M., Neely, M. H., Fegley, D., Mangieri, R., Krey, J. F., Walker, J. M., Holmes, P. V., Crystal, J. D., Duranti, A., Tontini, A., Mor, M., Tarzia, G., Piomelli, D., 2005. An endocannabinoid mechanism for stress-induced analgesia. Nature 435, 1108-12. https://doi.org/10.1038/nature03658

Hollopeter, G., Lange, J. J., Zhang, Y., Vu, T. N., Gu, M. Y., Ailion, M., Lambie, E. J., Slaughter, B. D., Unruh, J. R., Florens, L., Jorgensen, E. M., 2014. The Membrane-Associated Proteins FCHo and SGIP Are Allosteric Activators of the AP2 Clathrin Adaptor Complex. Elife 3, 65. https://doi.org/10.7554/eLife.03648

Howe, K. L., Achuthan, P., Allen, J., Allen, J., Alvarez-Jarreta, J., Amode, M. R., Armean, I. M., Azov, A. G., Bennett, R., Bhai, J., Billis, K., Boddu, S., Charkhchi, M., Cummins, C., Fioretto, L. R., Davidson, C., Dodiya, K., El Houdaigui, B., Fatima, R., Gall, A., Giron, C. G., Grego, T., Guijarro-Clarke, C., Haggerty, L., Hemrom, A., Hourlier, T., Izuogu, O. G., Juettemann, T., Kaikala, V., Kay, M., Lavidas, I., Le, T., Lemos, D., Martinez, J. G., Marugan, J. C., Maurel, T., McMahon, A. C., Mohanan, S., Moore, B., Muffato, M., Oheh, D. N., Paraschas, D., Parker, A., Parton, A., Prosovetskaia, I., Sakthivel, M. P., Salam, A. I. A., Schmitt, B. M., Schuilenburg, H., Sheppard, N., Steed, E., Szpak, M., Szuba, M., Taylor, K., Thormann, A., Threadgold, G., Walts, B., Winterbottom, A., Chakiachvili, M., Chaubal, A., De Silva, N., Flint, B., Frankish, A., Hunt, S. E., IIsley, G. R., Langridge, N., Loveland, J. E., Martin, F. J., Mudge, J. M., Morales, J., Perry, E., Ruffier, M., Tate, J., Thybert, D., Trevanion, S. J., Cunningham, F., Yates, A. D., Zerbino, D. R., Flicek, P., 2021. Ensembl 2021. Nucleic Acids Research 49, D884-D91. https://doi.org/10.1093/nar/gkaa942

Howlett, A. C., 2002. The cannabinoid receptors. Prostaglandins & Other Lipid Mediators 68-9, 619-31. https://doi.org/10.1016/S0090-6980(02)00060-6

Howlett, A. C., 2005. Cannabinoid receptor signaling. Targeting Trafficking in Drug Development, 53-79. https://doi.org/10.1007/3-540-26573-2_2

Howlett, A. C., Bidautrussell, M., Devane, W. A., Melvin, L. S., Johnson, M. R., Herkenham, M., 1990. The Cannabinoid Receptor - Biochemical, Anatomical and Behavioral

Characterization. Trends in Neurosciences 13, 420-23. https://doi.org/10.1016/0166-2236(90)90124-S

Howlett, A. C., Reggio, P. H., Childers, S. R., Hampson, R. E., Ulloa, N. M., Deutsch, D. G., 2011. Endocannabinoid tone versus constitutive activity of cannabinoid receptors. British Journal of Pharmacology 163, 1329-43. https://doi.org/10.1111/j.1476-5381.2011.01364.x

Hryhorowicz, S., Kaczmarek-Rys, M., Andrzejewska, A., Staszak, K., Hryhorowicz, M., Korcz, A., Slomski, R., 2019. Allosteric Modulation of Cannabinoid Receptor 1-Current Challenges and Future Opportunities. International Journal of Molecular Sciences 20. https://doi.org/10.3390/ijms20235874

Hsieh, C., Brown, S., Derleth, C., Mackie, K., 1999. Internalization and recycling of the CB1 cannabinoid receptor. Journal of Neurochemistry 73, 493-501. https://doi.org/10.1046/j.1471-4159.1999.0730493.x

Hughes, C. S., Moggridge, S., Muller, T., Sorensen, P. H., Morin, G. B., Krijgsveld, J., 2019. Single-pot, solid-phase-enhanced sample preparation for proteomics experiments. Nature Protocols 14, 68-+. https://doi.org/10.1038/s41596-018-0082-x

Huttlin, E. L., Jedrychowski, M. P., Elias, J. E., Goswami, T., Rad, R., Beausoleil, S. A., Villen, J., Haas, W., Sowa, M. E., Gygi, S. P., 2010. A Tissue-Specific Atlas of Mouse Protein Phosphorylation and Expression. Cell 143, 1174-89. https://doi.org/10.1016/j.cell.2010.12.001

Ibsen, M. S., Connor, M., Glass, M., 2017. Cannabinoid CB1 and CB2 Receptor Signaling and Bias. Cannabis and cannabinoid research 2, 48-60. https://doi.org/10.1089/can.2016.0037

Ibsen, M. S., Finlay, D. B., Patel, M., Javitch, J. A., Glass, M., Grimsey, N. L., 2019. Cannabinoid CB1 and CB2 Receptor-Mediated Arrestin Translocation: Species, Subtype, and Agonist-Dependence. Frontiers in Pharmacology 10. https://doi.org/10.3389/fphar.2019.00350

Irving, A. J., Coutts, A. A., Harvey, J., Rae, M. G., Mackie, K., Bewick, G. S., Pertwee, R. G., 2000. Functional expression of cell surface cannabinoid CB1 receptors on presynaptic inhibitory terminals in cultured rat hippocampal neurons. Neuroscience 98, 253-62. https://doi.org/10.1016/S0306-4522(00)00120-2

Jenniches, I., Ternes, S., Albayram, O., Otte, D. M., Bach, K., Bindila, L., Michel, K., Lutz, B., Bilkei-Gorzo, A., Zimmer, A., 2016. Anxiety, Stress, and Fear Response in Mice With Reduced Endocannabinoid Levels. Biological Psychiatry 79, 858-68. https://doi.org/10.1016/j.biopsych.2015.03.033

Jin, W. Z., Brown, S., Roche, J. P., Hsieh, C., Celver, J. P., Kovoor, A., Chavkin, C., Mackie, K., 1999. Distinct domains of the CB1 cannabinoid receptor mediate desensitization and internalization. Journal of Neuroscience 19, 3773-80. https://doi.org/10.1523/JNEUROSCI.19-10-03773.1999

Johns, D. G., Behm, D. J., Walker, D. J., Ao, Z., Shapland, E. M., Daniels, D. A., Riddick, M., Dowell, S., Staton, P. C., Green, P., Shabon, U., Bao, W., Aiyar, N., Yue, T. L., Brown, A. J., Morrison, A. D., Douglas, S. A., 2007. The novel endocannabinoid receptor GPR55 is activated by atypical cannabinoids but does not mediate their vasodilator effects. British Journal of Pharmacology 152, 825-31. https://doi.org/10.1038/sj.bjp.0707419

Kano, M., Ohno-Shosaku, T., Hashimotodani, Y., Uchigashima, M., Watanabe, M., 2009. Endocannabinoid-Mediated Control of Synaptic Transmission. Physiological Reviews 89, 309-80. https://doi.org/10.1152/physrev.00019.2008

Kathuria, S., Gaetani, S., Fegley, D., Valino, F., Duranti, A., Tontini, A., Mor, M., Tarzia, G., La Rana, G., Calignano, A., Giustino, A., Tattoli, M., Palmery, M., Cuomo, V., Piomelli, D., 2003. Modulation of anxiety through blockade of anandamide hydrolysis. Nature Medicine 9, 76-81. https://doi.org/10.1038/nm803

Katona, I., Freund, T. F., 2008. Endocannabinoid signaling as a synaptic circuit breaker in neurological disease. Nature Medicine 14, 923-30. https://doi.org/10.1038/nm.f.1869

Katona, I., Sperlagh, B., Sik, A., Kafalvi, A., Vizi, E. S., Mackie, K., Freund, T. F., 1999. Presynaptically located CB1 cannabinoid receptors regulate GABA release from axon terminals of specific hippocampal interneurons. Journal of Neuroscience 19, 4544-58.

Kawamura, Y., Fukaya, M., Maejima, T., Yoshida, T., Miura, E., Watanabe, M., Ohno-Shosaku, T., Kano, M., 2006. The CB1 cannabinoid receptor is the major cannabinoid receptor at excitatory presynaptic sites in the hippocampus and cerebellum. Journal of Neuroscience 26, 2991-3001. https://doi.org/10.1523/jneurosci.4872-05.2006

Kelly, B. T., Graham, S. C., Liska, N., Dannhauser, P. N., Honing, S., Ungewickell, E. J., Owen, D. J., 2014. AP2 controls clathrin polymerization with a membrane-activated switch. Science 345, 459-63. https://doi.org/10.1126/science.1254836

Kenakin, T., 1995. Agonist-Receptor Efficacy .2. Agonist Trafficking of Receptor Signals. Trends in Pharmacological Sciences 16, 232-38. https://doi.org/10.1016/S0165-6147(00)89032-X

Kenakin, T., 2001. Inverse, protean, and ligand-selective agonism: matters of receptor conformation. Faseb Journal 15, 598-611. https://doi.org/10.1096/fj.00-0438rev

Kennedy, M. B., 1997. The postsynaptic density at glutamatergic synapses. Trends in Neurosciences 20, 264-68. https://doi.org/10.1016/S0166-2236(96)01033-8

Kovtun, O., Dickson, V. K., Kelly, B. T., Owen, D. J., Briggs, J. A. G., 2020. Architecture of the AP2/clathrin coat on the membranes of clathrin-coated vesicles. Science Advances 6, 9. https://doi.org/10.1126/sciadv.aba8381

Kreitzer, A. C., Regehr, W. G., 2001a. Cerebellar depolarization-induced suppression of inhibition is mediated by endogenous cannabinoids. Journal of Neuroscience 21, art. no.-RC174. https://doi.org/10.1523/JNEUROSCI.21-20-j0005.2001

Kreitzer, A. C., Regehr, W. G., 2001b. Retrograde inhibition of presynaptic calcium influx by endogenous cannabinoids at excitatory synapses onto Purkinje cells. Neuron 29, 717-27. https://doi.org/10.1016/S0896-6273(01)00246-X

Kumpost, J., Syrova, Z., Frankova, D., Kulihova, L., Bologna, J., Prezeau, L., Pin, J. P., Blahos, J., 2008. Surface expression of metabotropic glutamate receptor variants mGluR1a and mGluR1b in transfected HEK293 cells. Neuropharmacology 55, 605-05. https://doi.org/10.1016/j.neuropharm.2008.06.073

Lau, T., Schloss, P., 2008. The cannabinoid CB1 receptor is expressed on serotonergic and dopaminergic neurons. European Journal of Pharmacology 578, 137-41. https://doi.org/10.1016/j.ejphar.2007.09.022

Lee, S. E., Cho, E., Jeong, S., Song, Y., Kang, S., Chang, S., 2021. SGIP1alpha, but Not SGIP1, is an Ortholog of FCHo Proteins and Functions as an Endocytic Regulator. Frontiers in Cell and Developmental Biology 9, 801420. https://doi.org/10.3389/fcell.2021.801420

Lee, Sang-Eun, Jeong, Soomin, Lee, Unghwi, Chang, Sunghoe, 2019. SGIP1α functions as a selective endocytic adaptor for the internalization of synaptotagmin 1 at synapses. Molecular Brain 12, 41. https://doi.org/10.1186/s13041-019-0464-1

Lein, E. S., Hawrylycz, M. J., Ao, N., Ayres, M., Bensinger, A., Bernard, A., Boe, A. F., Boguski, M. S., Brockway, K. S., Byrnes, E. J., Chen, L., Chen, L., Chen, T. M., Chin, M. C., Chong, J., Crook, B. E., Czaplinska, A., Dang, C. N., Datta, S., Dee, N. R.,

Desaki, A. L., Desta, T., Diep, E., Dolbeare, T. A., Donelan, M. J., Dong, H. W., Dougherty, J. G., Duncan, B. J., Ebbert, A. J., Eichele, G., Estin, L. K., Faber, C., Facer, B. A., Fields, R., Fischer, S. R., Fliss, T. P., Frensley, C., Gates, S. N., Glattfelder, K. J., Halverson, K. R., Hart, M. R., Hohmann, J. G., Howell, M. P., Jeung, D. P., Johnson, R. A., Karr, P. T., Kawal, R., Kidney, J. M., Knapik, R. H., Kuan, C. L., Lake, J. H., Laramee, A. R., Larsen, K. D., Lau, C., Lemon, T. A., Liang, A. J., Liu, Y., Luong, L. T., Michaels, J., Morgan, J. J., Morgan, R. J., Mortrud, M. T., Mosqueda, N. F., Ng, L. L., Ng, R., Orta, G. J., Overly, C. C., Pak, T. H., Parry, S. E., Pathak, S. D., Pearson, O. C., Puchalski, R. B., Riley, Z. L., Rockett, H. R., Rowland, S. A., Royall, J. J., Ruiz, M. J., Sarno, N. R., Schaffnit, K., Shapovalova, N. V., Sivisay, T., Slaughterbeck, C. R., Smith, S. C., Smith, K. A., Smith, B. I., Sodt, A. J., Stewart, N. N., Stumpf, K. R., Sunkin, S. M., Sutram, M., Tam, A., Teemer, C. D., Thaller, C., Thompson, C. L., Varnam, L. R., Visel, A., Whitlock, R. M., Wohnoutka, P. E., Wolkey, C. K., Wong, V. Y., Wood, M., Yaylaoglu, M. B., Young, R. C., Youngstrom, B. L., Yuan, X. F., Zhang, B., Zwingman, T. A., Jones, A. R., 2007. Genome-wide atlas of gene expression in the adult mouse brain. Nature 445, 168-76. https://doi.org/10.1038/nature05453

Lemmon, M. A., 2008. Membrane recognition by phospholipid-binding domains. Nature Reviews Molecular Cell Biology 9, 99-111. https://doi.org/10.1038/nrm2328

Leo, L. M., Abood, M. E., 2021. CB1 Cannabinoid Receptor Signaling and Biased Signaling. Molecules 26. https://doi.org/10.3390/molecules26175413

Leterrier, C., 2018. The Axon Initial Segment: An Updated Viewpoint. Journal of Neuroscience 38, 2135-45. https://doi.org/10.1523/Jneurosci.1922-17.2018

Leterrier, C., Laine, J., Darmon, M., Boudin, H., Rossier, J., Lenkei, Z., 2006. Constitutive activation drives compartment-selective endocytosis and axonal targeting of type 1 cannabinoid receptors. Journal of Neuroscience 26, 3141-53. https://doi.org/10.1523/Jneurosci.5437-05.2006

Li, H. D., Liu, W. X., Michalak, M., 2011. Enhanced Clathrin-Dependent Endocytosis in the Absence of Calnexin. Plos One 6, 11. https://doi.org/10.1371/journal.pone.0021678

Liu, J., Gao, B., Mirshahi, F., Sanyal, A. J., Khanolkar, A. D., Makriyannis, A., Kunos, G., 2000. Functional CB1 cannabinoid receptors in human vascular endothelial cells. Biochemical Journal 346, 835-40. https://doi.org/10.1042/0264-6021:3460835

Liu, Q., Fang, L. M., Wu, C. J., 2022. Alternative Splicing and Isoforms: From Mechanisms to Diseases. Genes 13. https://doi.org/10.3390/genes13030401

Lu, H. C., Mackie, K., 2016. An Introduction to the Endogenous Cannabinoid System. Biological Psychiatry 79, 516-25. https://doi.org/10.1016/j.biopsych.2015.07.028

Lutz, B., Marsicano, G., Maldonado, R., Hillard, C. J., 2015. The endocannabinoid system in guarding against fear, anxiety and stress. Nature Reviews Neuroscience 16, 705-18. https://doi.org/10.1038/nrn4036

Mackie, K., 2005. Distribution of cannabinoid receptors in the central and peripheral nervous system. Handbook of Experimental Pharmacology, 299-325. https://doi.org/10.1007/3-540-26573-2_10

Madeira, F., Pearce, M., Tivey, A. R. N., Basutkar, P., Lee, J., Edbali, O., Madhusoodanan, N., Kolesnikov, A., Lopez, R., 2022. Search and sequence analysis tools services from EMBL-EBI in 2022. Nucleic Acids Research 50, W276-W79. https://doi.org/10.1093/nar/gkac240

Marshall, O. J., 2004. PerlPrimer: cross-platform, graphical primer design for standard, bisulphite and real-time PCR. Bioinformatics 20, 2471-72. https://doi.org/10.1093/bioinformatics/bth254

Martini, L., Thompson, D., Kharazia, V., Whistler, J. L., 2010. Differential Regulation of Behavioral Tolerance to WIN55,212-2 by GASP1. Neuropsychopharmacology 35, 1363-73. https://doi.org/10.1038/npp.2010.6

Martini, L., Waldhoer, M., Pusch, M., Kharazia, V., Fong, J., Lee, J. H., Freissmuth, C., Whistler, J. L., 2007. Ligand-induced down-regulation of the cannabinoid 1 receptor is mediated by the G-protein-coupled receptor-associated sorting protein GASP1. Faseb Journal 21, 802-11. https://doi.org/10.1096/fj.06-7132com

Mascia, F., Klotz, L., Lerch, J., Ahmed, M. H., Zhang, Y., Enz, R., 2017. CRIP1a inhibits endocytosis of G-protein coupled receptors activated by endocannabinoids and glutamate by a common molecular mechanism. Journal of Neurochemistry 141, 577-91. https://doi.org/10.1111/jnc.14021

Masuda, T., Tomita, M., Ishihama, Y., 2008. Phase transfer surfactant-aided trypsin digestion for membrane proteome analysis. Journal of Proteome Research 7, 731-40. https://doi.org/10.1021/pr700658q

May, L. T., Leach, K., Sexton, P. M., Christopoulos, A., 2007. Allosteric modulation of G protein-coupled receptors. Annual Review of Pharmacology and Toxicology 47, 1-51. https://doi.org/10.1146/annurev.pharmtox.47.120505.105159

McDonald, N. A., Henstridge, C. M., Connolly, C. N., Irving, A. J., 2007. An essential role for constitutive endocytosis, but not activity, in the axonal targeting of the CB1 cannabinoid receptor. Molecular Pharmacology 71, 976-84. https://doi.org/10.1124/mol.106.029348

McHugh, D., Hu, S. S. J., Rimmerman, N., Juknat, A., Vogel, Z., Walker, J. M., Bradshaw, H. B., 2010. -arachidonoyl glycine, an abundant endogenous lipid, potently drives directed cellular migration through GPR18, the putative abnormal cannabidiol receptor. Bmc Neuroscience 11. https://doi.org/10.1186/1471-2202-11-44

McIntosh, H. H., Song, C., Howlett, A. C., 1998. CB1 cannabinoid receptor: cellular regulation and distribution in N18TG2 neuroblastoma cells. Molecular Brain Research 53, 163-73. https://doi.org/10.1016/S0169-328x(97)00294-5

McMahon, H. T., Boucrot, E., 2011. Molecular mechanism and physiological functions of clathrin-mediated endocytosis. Nature Reviews Molecular Cell Biology 12, 517-33. https://doi.org/10.1038/nrm3151

Mecha, M., Feliu, A., Carrillo-Salinas, F. J., Rueda-Zubiaurre, A., Ortega-Gutierrez, S., de Sola, R. G., Guaza, C., 2015. Endocannabinoids drive the acquisition of an alternative phenotype in microglia. Brain Behavior and Immunity 49, 233-45. https://doi.org/10.1016/j.bbi.2015.06.002

Mechoulam, R., Lander, N., Varkony, T. H., Kimmel, I., Becker, O., Benzvi, Z., Edery, H., Porath, G., 1980. Stereochemical Requirements for Cannabinoid Activity. Journal of Medicinal Chemistry 23, 1068-72. https://doi.org/10.1021/jm00184a002

Mechoulam, R., Parker, L. A., 2013. The Endocannabinoid System and the Brain. Annual Review of Psychology, Vol 64 64, 21-47. https://doi.org/10.1146/annurev-psych-113011-143739

Mees, I., Li, S. S., Tran, H., Ang, C. S., Williamson, N. A., Hannan, A. J., Renoir, T., 2022. Phosphoproteomic dysregulation in Huntington's disease mice is rescued by environmental enrichment. Brain Communications 4. https://doi.org/10.1093/braincomms/fcac305

Micale, V., Di Marzo, V., Sulcova, A., Wotjak, C. T., Drago, F., 2013. Endocannabinoid system and mood disorders: Priming a target for new therapies. Pharmacology & Therapeutics 138, 18-37. https://doi.org/10.1016/j.pharmthera.2012.12.002

Mikasova, L., Groc, L., Choquet, D., Manzoni, O. J., 2008. Altered surface trafficking of presynaptic cannabinoid type 1 receptor in and out synaptic terminals parallels receptor desensitization. Proceedings of the National Academy of Sciences of the United States of America 105, 18596-601. https://doi.org/10.1073/pnas.0805959105

Miller, L. K., Devi, L. A., 2011. The Highs and Lows of Cannabinoid Receptor Expression in Disease: Mechanisms and Their Therapeutic Implications. Pharmacological Reviews 63, 461-70. https://doi.org/10.1124/pr.110.003491

Milligan, A. L., Szabo-Pardi, T. A., Burton, M. D., 2020. Cannabinoid Receptor Type 1 and Its Role as an Analgesic: An Opioid Alternative? Journal of Dual Diagnosis 16, 106-19. https://doi.org/10.1080/15504263.2019.1668100

Mishra, R., Sengul, G. F., Candiello, E., Schu, P., 2021. Synaptic AP2 CCV life cycle regulation by the Eps15, ITSN1, Sgip1/AP2, synaptojanin1 interactome. Scientific Reports 11. https://doi.org/10.1038/s41598-021-87591-3

Moreira, F. A., Kaiser, N., Monory, K., Lutz, B., 2008. Reduced anxiety-like behaviour induced by genetic and pharmacological inhibition of the endocannabinoid-degrading enzyme fatty acid amide hydrolase (FAAH) is mediated by CB1 receptors. Neuropharmacology 54, 141-50. https://doi.org/10.1016/j.neuropharm.2007.07.005

Morena, M., Patel, S., Bains, J. S., Hill, M. N., 2016. Neurobiological Interactions Between Stress and the Endocannabinoid System. Neuropsychopharmacology 41, 80-102. https://doi.org/10.1038/npp.2015.166

Morgan, D. J., Davis, B. J., Kearn, C. S., Marcus, D., Cook, A. J., Wager-Miller, J., Straiker, A., Myoga, M. H., Karduck, J., Leishman, E., Sim-Selley, L. J., Czyzyk, T. A., Bradshaw, H. B., Selley, D. E., Mackie, K., 2014. Mutation of Putative GRK Phosphorylation Sites in the Cannabinoid Receptor 1 (CB1R) Confers Resistance to Cannabinoid Tolerance and Hypersensitivity to Cannabinoids in Mice. Journal of Neuroscience 34, 5152-63. https://doi.org/10.1523/jneurosci.3445-12.2014

Munton, R. P., Tweedie-Cullen, R., Livingstone-Zatchej, M., Weinandy, F., Waidelich, M., Longo, D., Gehrig, P., Potthast, F., Rutishauser, D., Gerrits, B., Panse, C., Schlapbach, R., Mansuy, I. M., 2007. Qualitative and quantitative analyses of protein phosphorylation in naive and stimulated mouse synaptosomal preparations. Molecular & Cellular Proteomics 6, 283-93. https://doi.org/10.1074/mcp.M600046-MCP200

Murataeva, N., Straiker, A., Mackie, K., 2014. Parsing the players: 2-arachidonoylglycerol synthesis and degradation in the CNS. British Journal of Pharmacology 171, 1379-91. https://doi.org/10.1111/bph.12411

Namkung, Y., Le Gouill, C., Lukashova, V., Kobayashi, H., Hogue, M., Khoury, E., Song, M., Bouvier, M., Laporte, S. A., 2016. Monitoring G protein-coupled receptor and beta-arrestin trafficking in live cells using enhanced bystander BRET. Nature Communications 7. https://doi.org/10.1038/ncomms12178

Nealon, C. M., Henderson-Redmond, A. N., Hale, D. E., Morgan, D. J., 2019. Tolerance to WIN55,212-2 is delayed in desensitization-resistant S426A/S430A mice. Neuropharmacology 148, 151-59. https://doi.org/10.1016/j.neuropharm.2018.12.026

Negus, S. S., 2006. Some implications of receptor theory for in vivo assessment of agonists, antagonists and inverse agonists. Biochemical Pharmacology 71, 1663-70. https://doi.org/10.1016/j.bcp.2005.12.038

Neubert, M. J., Kincaid, W., Heinricher, M. M., 2004. Nociceptive facilitating neurons in the rostral ventromedial medulla. Pain 110, 158-65. https://doi.org/10.1016/j.pain.2004.03.017

Neubig, R. R., Spedding, M., Kenakin, T., Christopoulos, A., 2003. International Union of Pharmacology Committee on Receptor Nomenclature and Drug Classification. XXXVIII. Update on terms and symbols in quantitative pharmacology. Pharmacological Reviews 55, 597-606. https://doi.org/10.1124/pr.55.4.4

Nguyen, P. T., Schmid, C. L., Raehal, K. M., Selley, D. E., Bohn, L. M., Sim-Selley, L. J., 2012. beta-Arrestin2 Regulates Cannabinoid CB1 Receptor Signaling and Adaptation in a Central Nervous System Region-Dependent Manner. Biological Psychiatry 71, 714-24. https://doi.org/10.1016/j.biopsych.2011.11.027

Niciu, M. J., Kelmendi, B., Sanacora, G., 2012. Overview of glutamatergic neurotransmission in the nervous system. Pharmacology Biochemistry and Behavior 100, 656-64. https://doi.org/10.1016/j.pbb.2011.08.008

Niehaus, J. L., Liu, Y., Wallis, K. T., Egertova, M., Bhartur, S. G., Mukhopadhyay, S., Shi, S., He, H., Selley, D. E., Howlett, A. C., Elphick, M. R., Lewis, D. L., 2007. CB1 cannabinoid receptor activity is modulated by the cannabinoid receptor interacting protein CRIP 1a. Molecular Pharmacology 72, 1557-66. https://doi.org/10.1124/mol.107.039263

Pacher, P., Kunos, G., 2013. Modulating the endocannabinoid system in human health and disease successes and failures. Febs Journal 280, 1918-43. https://doi.org/10.1111/febs.12260

Pan, X. H., Ikeda, S. R., Lewis, D. L., 1996. Rat brain cannabinoid receptor modulates N-type Ca2+ channels in a neuronal expression system. Molecular Pharmacology 49, 707-14.

Partlow, E. A., Cannon, K. S., Hollopeter, G., Baker, R. W., 2022. Structural basis of an endocytic checkpoint that primes the AP2 clathrin adaptor for cargo internalization. Nature Structural & Molecular Biology 29, 339-+. https://doi.org/10.1038/s41594-022-00749-z

Pertwee, R. G., 2001. Cannabinoid receptors and pain. Progress in Neurobiology 63, 569-611. https://doi.org/10.1016/S0301-0082(00)00031-9

Pertwee, R. G., 2008. Ligands that target cannabinoid receptors in the brain: from THC to anandamide and beyond. Addiction Biology 13, 147-59. https://doi.org/10.1111/j.1369-1600.2008.00108.x

Pharmacology, International Union of, Girdlestone, D., 2000. *The IUPHAR Compendium of Receptor Characterization and Classification* (IUPHAR Media).

Piscura, M. K., Sepulveda, D. E., Maulik, M., Guindon, J., Henderson-Redmond, A. N., Morgan, D. J., 2023. Cannabinoid tolerance in S426A/S430A x beta-arrestin 2 knock-out double mutant mice. Journal of Pharmacology and Experimental Therapeutics. https://doi.org/10.1124/jpet.122.001367

Radwan, M. M., Chandra, S., Gul, S., ElSohly, M. A., 2021. Cannabinoids, Phenolics, Terpenes and Alkaloids of Cannabis. Molecules 26. https://doi.org/10.3390/molecules26092774

Rappsilber, J., Mann, M., Ishihama, Y., 2007. Protocol for micro-purification, enrichment, pre-fractionation and storage of peptides for proteomics using StageTips. Nature Protocols 2, 1896-906. https://doi.org/10.1038/nprot.2007.261

Reeves, K. C., Shah, N. K., Munoz, B., Atwood, B. K., 2022. Opioid Receptor-Mediated Regulation of Neurotransmission in the Brain. Frontiers in Molecular Neuroscience 15. https://doi.org/10.3389/fnmol.2022.919773

Reggio, P. H., Greer, K. V., Cox, S. M., 1989. The Importance of the Orientation of the C9 Substituent to Cannabinoid Activity. Journal of Medicinal Chemistry 32, 1630-35. https://doi.org/10.1021/jm00127a038

Reider, A., Barker, S. L., Mishra, S. K., Im, Y. J., Maldonado-Baez, L., Hurley, J. H., Traub, L. M., Wendland, B., 2009. Syp1 is a conserved endocytic adaptor that contains domains involved in cargo selection and membrane tubulation. Embo Journal 28, 3103-16. https://doi.org/10.1038/emboj.2009.248

Ribrault, C., Sekimoto, K., Triller, A., 2011. From the stochasticity of molecular processes to the variability of synaptic transmission. Nature Reviews Neuroscience 12, 375-87. https://doi.org/10.1038/nrn3025

Rinaldi-Carmona, M., Le Duigou, A., Oustric, D., Barth, F., Bouaboula, M., Carayon, P., Casellas, P., Le Fur, G., 1998. Modulation of CB1 cannabinoid receptor functions after a long-term exposure to agonist or inverse agonist in the Chinese hamster ovary cell expression system. Journal of Pharmacology and Experimental Therapeutics 287, 1038-47.

Robinson, M. S., 2015. Forty Years of Clathrin-coated Vesicles. Traffic 16, 1210-38. https://doi.org/10.1111/tra.12335

Robledo, P., Berrendero, F., Ozaita, A., Maldonado, R., 2008. Advances in the field of cannabinoid-opioid cross-talk. Addiction Biology 13, 213-24. https://doi.org/10.1111/j.1369-1600.2008.00107.x

Rozenfeld, R., Devi, L. A., 2008. Regulation of CB1 cannabinoid receptor trafficking by the adaptor protein AP-3. Faseb Journal 22, 2311-22. https://doi.org/10.1096/fj.07-102731

Rueda, D., Galve-Roperh, I., Haro, A., Guzman, M., 2000. The CB1 cannabinoid receptor is coupled to the activation of c-Jun N-terminal kinase. Molecular Pharmacology 58, 814-20. https://doi.org/10.1124/mol.58.4.814

Russo, F., Vandelli, M. A., Biagini, G., Schmid, M., Luongo, L., Perrone, M., Ricciardi, F., Maione, S., Lagana, A., Capriotti, A. L., Gallo, A., Carbone, L., Perrone, E., Gigli, G., Cannazza, G., Citti, C., 2023. Synthesis and pharmacological activity of the epimers of hexahydrocannabinol (HHC). Scientific Reports 13, 11061. https://doi.org/10.1038/s41598-023-38188-5

Saeedimasine, M., Montanino, A., Kleiven, S., Villa, A., 2019. Role of lipid composition on the structural and mechanical features of axonal membranes: a molecular simulation study. Scientific Reports 9. https://doi.org/10.1038/s41598-019-44318-9

Saez, T. M. M., Bessone, I. F., Rodriguez, M. S., Alloatti, M., Otero, M. G., Cromberg, L. E., Devoto, V. M. P., Oubina, G., Sosa, L., Buffone, M. G., Gelman, D. M., Falzone, T. L., 2020. Kinesin-1-mediated axonal transport of CB1 receptors is required for cannabinoid-dependent axonal growth and guidance. Development 147. https://doi.org/10.1242/dev.184069

Schindelin, J., Arganda-Carreras, I., Frise, E., Kaynig, V., Longair, M., Pietzsch, T., Preibisch, S., Rueden, C., Saalfeld, S., Schmid, B., Tinevez, J. Y., White, D. J., Hartenstein, V., Eliceiri, K., Tomancak, P., Cardona, A., 2012. Fiji: an open-source platform for biological-image analysis. Nature Methods 9, 676-82. https://doi.org/10.1038/nmeth.2019

Schlicker, E., Feuerstein, T., 2017. Human presynaptic receptors. Pharmacology & Therapeutics 172, 1-21. https://doi.org/10.1016/j.pharmthera.2016.11.005

Schreiner, D., Nguyen, T. M., Russo, G., Heber, S., Patrignani, A., Ahrne, E., Scheiffele, P., 2014. Targeted Combinatorial Alternative Splicing Generates Brain Region-Specific Repertoires of Neurexins. Neuron 84, 386-98. https://doi.org/10.1016/j.neuron.2014.09.011

Shenoy, S. K., Lefkowitz, R. J., 2011. beta-arrestin-mediated receptor trafficking and signal transduction. Trends in Pharmacological Sciences 32, 521-33. https://doi.org/10.1016/j.tips.2011.05.002

Shonesy, B. C., Bluett, R. J., Ramikie, T. S., Baldi, R., Hermanson, D. J., Kingsley, P. J., Marnett, L. J., Winder, D. G., Colbran, R. J., Patel, S., 2014. Genetic Disruption of 2-Arachidonoylglycerol Synthesis Reveals a Key Role for Endocannabinoid Signaling in Anxiety Modulation. Cell Reports 9, 1644-53. https://doi.org/10.1016/j.celrep.2014.11.001

Simon, A. C., Loverdo, C., Gaffuri, A. L., Urbanski, M., Ladarre, D., Carrel, D., Rivals, I., Leterrier, C., Benichou, O., Dournaud, P., Szabo, B., Voituriez, R., Lenkei, Z., 2013. Activation-dependent plasticity of polarized GPCR distribution on the neuronal surface. Journal of Molecular Cell Biology 5, 250-65. https://doi.org/10.1093/jmcb/mjt014

Smith, S. M., Baker, M., Halebian, M., Smith, C. J., 2017. Weak Molecular Interactions in Clathrin-Mediated Endocytosis. Frontiers in Molecular Biosciences 4, 11. https://doi.org/10.3389/fmolb.2017.00072

Smith, T. H., Blume, L. C., Straiker, A., Cox, J. O., David, B. G., Mcvoy, J. R. S., Sayers, K. W., Poklis, J. L., Abdullah, R. A., Egertova, M., Chen, C. K., Mackie, K., Elphick, M. R., Howlett, A. C., Selley, D. E., 2015. Cannabinoid Receptor-Interacting Protein 1a Modulates CB1 Receptor Signaling and Regulation. Molecular Pharmacology 87, 747-65. https://doi.org/10.1124/mol.114.096495

Sobczak, M., Salaga, M., Storr, M. A., Fichna, J., 2014. Physiology, signaling, and pharmacology of opioid receptors and their ligands in the gastrointestinal tract: current concepts and future perspectives. Journal of Gastroenterology 49, 24-45. https://doi.org/10.1007/s00535-013-0753-x

Soltesz, I., Alger, B. E., Kano, M., Lee, S. H., Lovinger, D. M., Ohno-Shosaku, T., Watanabe, M., 2015. Weeding out bad waves: towards selective cannabinoid circuit control in epilepsy. Nature Reviews Neuroscience 16, 264-77. https://doi.org/10.1038/nrn3937

Stanishneva-Konovalova, T. B., Derkacheva, N. I., Polevova, S. V., Sokolova, O. S., 2016. The Role of BAR Domain Proteins in the Regulation of Membrane Dynamics. Acta Naturae 8, 60-69. https://doi.org/10.32607/20758251-2016-8-4-60-69

Starowicz, K., Malek, N., Przewlocka, B., 2013. Cannabinoid receptors and pain. Wiley Interdisciplinary Reviews: Membrane Transport and Signaling 2, 121-32. https://doi.org/https://doi.org/10.1002/wmts.83

Stella, N., Schweitzer, P., Piomelli, D., 1997. A second endogenous cannabinoid that modulates long-term potentiation. Nature 388, 773-78. https://doi.org/10.1038/42015

Straiker, A., Mackie, K., 2005. Depolarization-induced suppression of excitation in murine autaptic hippocampal neurones. Journal of Physiology-London 569, 501-17. https://doi.org/10.1113/jphysiol.2005.091918

Straiker, A., Wager-Miller, J., Mackie, K., 2012. The CB1 cannabinoid receptor C-terminus regulates receptor desensitization in autaptic hippocampal neurones. British Journal of Pharmacology 165, 2652-59. https://doi.org/10.1111/j.1476-5381.2011.01743.x

Tabrizi, M. A., Baraldi, P. G., 2017. Chemistry of Cannabinoid Receptor Agonists. Handbook of Cannabis and Related Pathologies: Biology, Pharmacology, Diagnosis, and Treatment, 592-605. https://doi.org/10.1016/B978-0-12-800756-3.00072-7

Tanaka, R., Kikura-Hanajiri, R., 2023. Identification of hexahydrocannabinol (HHC), dihydro-iso-tetrahydrocannabinol (dihydro-iso-THC) and hexahydrocannabiphorol (HHCP) in electronic cigarette cartridge products. Forensic Toxicology. https://doi.org/10.1007/s11419-023-00667-9

Tollervey, J. R., Wang, Z., Hortobagyi, T., Witten, J. T., Zarnack, K., Kayikci, M., Clark, T. A., Schweitzer, A. C., Rot, G., Curk, T., Zupan, B., Rogelj, B., Shaw, C. E., Ule, J., 2011. Analysis of alternative splicing associated with aging and neurodegeneration in the human brain. Genome Research 21, 1572-82. https://doi.org/10.1101/gr.122226.111

Trabzuni, D., Ramasamy, A., Imran, S., Walker, R., Smith, C., Weale, M. E., Hardy, J., Ryten, M., Expression, North Amer Brain, 2013. Widespread sex differences in gene expression and splicing in the adult human brain. Nature Communications 4. https://doi.org/10.1038/ncomms3771

Treede, R. D., Rief, W., Barke, A., Aziz, Q., Bennett, M. I., Benoliel, R., Cohen, M., Evers, S., Finnerup, N. B., First, M. B., Giamberardino, M. A., Kaasa, S., Kosek, E., Lavand'homme, P., Nicholas, M., Perrot, S., Scholz, J., Schug, S., Smith, B. H., Svensson, P., Vlaeyen, J. W. S., Wang, S. J., 2015. A classification of chronic pain for ICD-11. Pain 156, 1003-07. https://doi.org/10.1097/j.pain.0000000000000160

Trevaskis, J., Walder, K., Foletta, V., Kerr-Bayles, L., McMillan, J., Cooper, A., Lee, S., Bolton, K., Prior, M., Fahey, R., Whitecross, K., Morton, G. J., Schwartz, M. W., Collier, G. R., 2005. Src homology 3-domain growth factor receptor-bound 2-like (endophilin) interacting protein 1, a novel neuronal protein that regulates energy balance. Endocrinology 146, 3757-64. https://doi.org/10.1210/en.2005-0282

Trillou, C. R., Delgorge, C., Menet, C., Arnone, M., Soubrie, P., 2004. CB1 cannabinoid receptor knockout in mice leads to leanness, resistance to diet-induced obesity and enhanced leptin sensitivity. International Journal of Obesity 28, 640-48. https://doi.org/10.1038/sj.ijo.0802583

Turner, C. E., Hadley, K. W., Fetterman, P. S., Doorenbos, N. J., Quimby, M. W., Waller, C., 1973. CONSTITUENTS OF CANNABIS-SATIVA L .4. STABILITY OF CANNABINOIDS IN STORED PLANT MATERIAL. Journal of Pharmaceutical Sciences 62, 1601-05. https://doi.org/10.1002/jps.2600621005

Turu, G., Hunyady, L., 2010. Signal transduction of the CB1 cannabinoid receptor. Journal of Molecular Endocrinology 44, 75-85. https://doi.org/10.1677/Jme-08-0190

Twitchell, W., Brown, S., Mackie, K., 1997. Cannabinoids inhibit N- and P/Q-type calcium channels in cultured rat hippocampal neurons. Journal of Neurophysiology 78, 43-50. https://doi.org/10.1152/jn.1997.78.1.43

Uezu, A., Horiuchi, A., Kanda, K., Kikuchi, N., Umeda, K., Tsujita, K., Suetsugu, S., Araki, N., Yamamoto, H., Takenawa, T., Nakanishi, H., 2007. SGIP1 alpha is an endocytic protein that directly interacts with phospholipids and Eps15. Journal of Biological Chemistry 282. https://doi.org/10.1074/jbc.M703815200

Uezu, A., Umeda, K., Tsujita, K., Suetsugu, S., Takenawa, T., Nakanishi, H., 2011. Characterization of the EFC/F-BAR domain protein, FCHO2. Genes to Cells 16, 868-78. https://doi.org/10.1111/j.1365-2443.2011.01536.x

Ujvary, I., 2023. Hexahydrocannabinol and closely related semi-synthetic cannabinoids: A comprehensive review. Drug Testing and Analysis. https://doi.org/10.1002/dta.3519

Ujvary, I., Evans-Brown, M., Gallegos, A., Planchuelo, G., de Morais, J., Christie, R., Jorge, R., Sedefov, R., 2023. Hexahydrocannabinol (HHC) and related substances. TECHNICAL REPORT, 1-106. https://doi.org/10.2810/852912

van der Stelt, M., Di Marzo, V., 2004. Endovanilloids - Putative endogenous ligands of transient receptor potential vanilloid 1 channels. European Journal of Biochemistry 271, 1827-34. https://doi.org/10.1111/j.1432-1033.2004.04081.x

Van Gaal, L. F., Rissanen, A. M., Scheen, A. J., Ziegler, O., Rossner, S., Grp, RIO-Europe Study, 2005. Effects of the cannabinoid-1 receptor blocker rimonabant on weight

reduction and cardiovascular risk factors in overweight patients: 1-year experience from the RIO-Europe study. Lancet 365, 1389-97. https://doi.org/10.1016/S0140-6736(05)66374-X

Vanegas, H., Vazquez, E., Tortorici, V., 2010. NSAIDs, Opioids, Cannabinoids and the Control of Pain by the Central Nervous System. Pharmaceuticals 3, 1335-47. https://doi.org/10.3390/ph3051335

Viveros, M. P., Marco, E. M., File, S. E., 2005. Endocannabinoid system and stress and anxiety responses. Pharmacology Biochemistry and Behavior 81, 331-42. https://doi.org/10.1016/j.pbb.2005.01.029

Vuckovic, S., Srebro, D., Vujovic, K. S., Vucetic, C., Prostran, M., 2018. Cannabinoids and Pain: New Insights From Old Molecules. Frontiers in Pharmacology 9. https://doi.org/10.3389/fphar.2018.01259

Vuong, C. K., Black, D. L., Zheng, S. K., 2016. The neurogenetics of alternative splicing. Nature Reviews Neuroscience 17, 265-81. https://doi.org/10.1038/nrn.2016.27

Waldman, S. A., 2002. Does potency predict clinical efficacy? Illustration through an antihistamine model. Annals of Allergy Asthma & Immunology 89, 7-11. https://doi.org/10.1016/S1081-1206(10)61904-7

Wang, Y., Liu, J., Huang, B., Xu, Y. M., Li, J., Huang, L. F., Lin, J., Zhang, J., Min, Q. H., Yang, W. M., Wang, X. Z., 2015. Mechanism of alternative splicing and its regulation. Biomedical Reports 3, 152-58. https://doi.org/10.3892/br.2014.407

Wartmann, M., Campbell, D., Subramanian, A., Burstein, S. H., Davis, R. J., 1995. The Map Kinase Signal-Transduction Pathway Is Activated by the Endogenous Cannabinoid Anandamide. Febs Letters 359, 133-36. https://doi.org/10.1016/0014-5793(95)00027-7

Westra, M., Gutierrez, Y., MacGillavry, H. D., 2021. Contribution of Membrane Lipids to Postsynaptic Protein Organization. Frontiers in Synaptic Neuroscience 13. https://doi.org/10.3389/fnsyn.2021.790773

Wettschureck, N., van der Stelt, M., Tsubokawa, H., Krestel, H., Moers, A., Petrosino, S., Schutz, G., Di Marzo, V., Offermanns, S., 2006. Forebrain-specific inactivation of G(q)/G(11) family G proteins results in age-dependent epilepsy and impaired endocannabinoid formation. Molecular and Cellular Biology 26, 5888-94. https://doi.org/10.1128/mcb.00397-06

Wilhelm, B. G., Mandad, S., Truckenbrodt, S., Krohnert, K., Schafer, C., Rammner, B., Koo, S. J., Classen, G. A., Krauss, M., Haucke, V., Urlaub, H., Rizzoli, S. O., 2014. Composition of isolated synaptic boutons reveals the amounts of vesicle trafficking proteins. Science 344, 1023-28. https://doi.org/10.1126/science.1252884

Wobbrock, J. O., Findlater, L., Gergle, D., Higgins, J. J., 2011. The Aligned Rank Transform for Nonparametric Factorial Analyses Using Only ANOVA Procedures. 29th Annual Chi Conference on Human Factors in Computing Systems, 143-46. https://doi.org/10.1145/1978942.1978963

Woodhams, S. G., Chapman, V., Finn, D. P., Hohmann, A. G., Neugebauer, V., 2017. The cannabinoid system and pain. Neuropharmacology 124, 105-20. https://doi.org/10.1016/j.neuropharm.2017.06.015

Yako, Y. Y., Echouffo-Tcheugui, J. B., Balti, E. V., Matsha, T. E., Sobngwi, E., Erasmus, R. T., Kengne, A. P., 2015. Genetic association studies of obesity in Africa: a systematic review. Obesity Reviews 16, 259-72. https://doi.org/10.1111/obr.12260

Yeo, G., Holste, D., Kreiman, G., Burge, C. B., 2004. Variation in alternative splicing across human tissues. Genome Biology 5, 15. https://doi.org/10.1186/gb-2004-5-10-r74

Yu, L. R., Veenstra, T. D., 2021. Characterization of Phosphorylated Proteins Using Mass Spectrometry. Curr Protein Pept Sci 22, 148-57. https://doi.org/10.2174/1389203721999201123200439

Zarrinpar, A., Bhattacharyya, R. P., Lim, W. A., 2003. The Structure and Function of Proline Recognition Domains. Science's STKE 2003, re8-re8. https://doi.org/10.1126/stke.2003.179.re8

Zhu, X., Finlay, D. B., Glass, M., Duffull, S. B., 2019. Model-free and kinetic modelling approaches for characterising non-equilibrium pharmacological pathway activity: Internalisation of cannabinoid CB1 receptors. British Journal of Pharmacology 176, 2593-607. https://doi.org/10.1111/bph.14684

Zimmer, A., Zimmer, A. M., Hohmann, A. G., Herkenham, M., Bonner, T. I., 1999. Increased mortality, hypoactivity, and hypoalgesia in cannabinoid CB1 receptor knockout mice. Proceedings of the National Academy of Sciences of the United States of America 96, 5780-85. https://doi.org/10.1073/pnas.96.10.5780

Zou, S. L., Kumar, U., 2018. Cannabinoid Receptors and the Endocannabinoid System: Signaling and Function in the Central Nervous System. International Journal of Molecular Sciences 19, 23. https://doi.org/10.3390/ijms19030833

9. LIST OF PUBLICATIONS

Publications related to the thesis:

1. **Durydivka O.**, Gazdarica M., Vecerkova K., Radenkovic S., Blahos J. Multiple Sgip1 Splice Variants Inhibit Cannabinoid Receptor 1 Internalization. Gene. **2023** 147851 doi: 10.1016/j.gene.2023.147851 PMID: 37783296. (IF= 3.913)
2. Gazdarica M., Noda J., **Durydivka O.**, Novosadova V., Mackie K., Pin J.-P., Prezeau L., Blahos J. SGIP1 modulates kinetics and interactions of the cannabinoid receptor 1 and G protein-coupled receptor kinase 3 signalosome. Journal of Neurochemistry. **2022** 160:625-642 doi: 10.1111/jnc.15569 PMID: 34970999. (IF= 5.546)
3. **Durydivka O.**, Mackie K., Blahos J. SGIP1 in axons prevents internalization of desensitized CB1R and modifies its function. Frontiers in Neuroscience. **2023** 17:1-11 doi: 10.3389/fnins.2023.1213094 PMID: 37547151. (IF= 5.152)